REDUCTION OF VOLATILE ORGANIC COMPOUNDS IN WOOD PLASTIC COMPOSITES USING FUNCTIONALIZED HALLOYSITE NANOTUBES

by

GIZEM KURTULMUŞ

Submitted to the Graduate School of Engineering and Natural Sciences
in partial fulfilment of
the requirements for the degree of Doctor of Philosophy

Sabancı University

July 2025

ABSTRACT

REDUCTION OF VOLATILE ORGANIC COMPOUNDS IN WOOD PLASTIC COMPOSITES USING FUNCTIONALIZED HALLOYSITE NANOTUBES

GİZEM KURTULMUŞ

Materials Science and Nano Engineering, Ph.D. Dissertation, July 2025

Dissertation Supervisor: Prof. Yusuf Ziya Menceloğlu

Keywords: volatile organic compounds, wood fiber, wood-plastic composites, halloysite nanotube, modified halloysite nanotube

This thesis investigates the formulation of next-generation wood–plastic composites (WPCs) that meet the dual criteria of environmental responsibility and advanced material performance. The starting point of this study is to respond to increasing regulatory demands for eco-conscious material solutions, particularly in indoor environments where volatile organic compound (VOC) emissions generate unpleasant odors that hinder their use in applications such as automotive interiors. This thesis focusses on halloysite nanotubes (HNTs), their functionalized derivatives (Mod-HNTs), and β-cyclodextrin (β-CD) with regard to the capture of VOCs in WPCs, as well as their capabilities in odor reduction and structural changes. HNTs are naturally obtaining aluminosilicate nanotubes which have a high aspect ratio and being able to modify their internal and external surfaces. To improve their interaction with non-polar polymer matrices and polar VOCs, HNTs were surface-functionalized through aminosilane grafting and termed as Mod-HNT. In parallel, β-CD which has a cyclic oligosaccharide with a toroidal molecular architecture enables the selective inclusion of odor-causing VOCs, particularly aldehydes and aromatic compounds, within its hydrophobic cavity through host–guest complexation. WPCs are produced with high-shear thermo-kinetic mixing, also followed by injection moulding in order to simulate scalable manufacturing processes. The formulations consisted of PP, rPO, PA11 polymers, 30 wt.% wood fiber (WF) and additive concentrations of 2 wt.% and 5 wt.%. A multitude of analytical methods were used to measure the performance of the materials. VOC emissions were quantified via headspace gas chromatography–mass spectrometry (HS-GC-MS), and odor levels were evaluated through sensory Jar testing. Thermal behavior was analyzed through thermogravimetric analysis (TGA) and differential scanning calorimetry (DSC), while interfacial chemistry was investigated by Fourier-transform infrared spectroscopy (FTIR).The morphological properties were analysed by using scanning electron microscopy (SEM), meanwhile mechanical properties were measured with tensile testing.

The experimental results revealed that unmodified HNTs increased stiffness and slightly decreased VOC levels. Mod-HNTs have shown a reduction of up to 96% in VOC emissions in PP-based WPCs and considerably improving fiber–matrix interaction. β-CD revealed selective binding attraction for aromatic and aldehydic compounds, which causes increased ductility, as illustrated by an increase in strain-at-break. The 5 wt.% Mod-HNT and 2 wt.% β-CD generated synergistic effects, improving both environmental and structural results Mechanical analysis suggested increases of up to 12% in tensile strength confirm by SEM imaging that revealed a decrease in interfacial voids and increased nucleation that yields crystallinity. FTIR analysis proved the presence of chemical interactions between the functional additives and the polymer matrices. The effect of matrix polarity on filler dispersion and performance has been discovered in different WPCs formulations. PA11- and rPO-based WPCs displayed distinct fibrillation and dispersion morphologies, which contributed to their unique mechanical profiles. This thesis presents a framework to produce high-performance, low-emission composite materials that comply with the principles of circular economy plans. This study uses functionalized nanofillers with petroleum-based, renewable, and bio-based polymer matrices, providing new insights into the interactions between fillers and matrices. It proposes an efficient strategy for the production of WPCs that suitable for high-performance applications, such as automotive interior, electronic, and building materials.

ÖZET

FONKSİYONLANDIRILMIŞ HALLOYSIT NANOTÜP KULLANILARAK ODUN PLASTIK KOMPOZITLERDEKI UÇUCU ORGANIK BILEŞIKLERIN AZALTILMASI

GİZEM KURTULMUŞ

Malzeme Bilimi ve Nano Mühendislik, Doktora Tezi, Temmuz 2025

Tez Danışmanı: Prof. Dr. Yusuf Ziya Menceloğlu

Anahtar Kelimeler: uçucu organik bileşikler, odun lifi, odun-plastik kompozitler, halloysit nanotüp, modifiye halloysit nanotüp

Bu tez, çevresel sorumluluk ve gelişmiş malzeme performansı gibi iki kriteri karşılayan yeni nesil odun-plastik kompozitlerin (OPK) formülasyonunu araştırmaktadır. Bu çalışmanın başlangıç noktası, özellikle uçucu organik bileşik (VOC) emisyonlarının otomotiv iç mekanları gibi uygulamalarda kullanımını engelleyen hoş olmayan kokulara neden olduğu iç mekan ortamlarında, çevre dostu malzeme çözümlerine yönelik artan yasal taleplere yanıt vermektir. Bu tez, OPK'lerdeki VOC'leri yakalama ve koku azaltma ve yapısal değişikliklerdeki kabiliyetleri açısından halloysit nanotüpler (HNT), bunların fonksiyonelleştirilmiş türevleri (Mod-HNT) ve β-siklodekstrin (β-CD) üzerine odaklanmaktadır. HNT'ler, yüksek en-boy oranına sahip ve iç ve dış yüzeylerini modifiye edilebilen doğal alüminosilikat nanotüplerdir. Polar olmayan polimer matrisler ve polar VOC'lerle etkileşimlerini iyileştirmek için HNT'ler, aminosilan bağlama yoluyla yüzeyleri fonksiyonelleştirilmiş ve Mod-HNT olarak adlandırılmıştır. Buna paralel olarak, halkasal moleküler yapıya sahip halkasal bir oligosakkarit olan β-CD, özellikle aldehitler ve aromatik bileşikler olmak üzere kokuya neden olan uçucu organik bileşiklerin, konuk-misafir kompleksleşmesi yoluyla hidrofobik boşluğuna seçici olarak dahil edilmesini sağlamaktadır. WPC'lerin ölçeklenebilir üretim süreçlerini simüle etmek için enjeksiyon kalıplamanın ardından yüksek kesme kuvvetli termo-kinetik karıştırma ile üretildi. Formülasyonlar, ağırlıkça %30 odun lifi (OL) ve ağırlıkça %2 ve ağırlıkça %5 katkı konsantrasyonlarından oluşmaktadır. Malzemelerin performansını ölçmek için çok sayıda analitik yöntem kullanıldı. Uçucu organik bileşik emisyonları, baş headspace gaz kromatografisi-kütle spektrometrisi (HS-GC-MS) ile nicelendirildi ve koku seviyeleri duyusal (kavanoz) testi ile değerlendirildi. Termal davranış, termogravimetrik analiz (TGA) ve diferansiyel taramalı kalorimetri (DSC) ile analiz edilirken, arayüz kimyası Fourier dönüşümlü kızılötesi spektroskopisi (FTIR) ile incelenmiştir. Morfolojik

özellikler taramalı elektron mikroskobu (SEM) kullanılarak analiz edilmiş, mekanik özellikler ise çekme testi ile ölçülmüştür. Deneysel sonuçlar, modifiye edilmemiş HNT'lerin sertliği artırdığını ve VOC seviyelerini hafifçe azalttığını göstermiştir. Mod-HNT'ler, PP bazlı WPC'lerde VOC emisyonlarında %96'ya varan bir azalma ve lif-matris etkileşimini önemli ölçüde iyileştirme göstermiştir. β-CD, aromatik ve aldehit bileşikler için seçici bağlanma çekiciliği göstermiş ve bu da kopma anındaki gerinimdeki artışla gösterildiği gibi sünekliğin artmasına neden olmuştur. Ağırlıkça %5 Mod-HNT ve ağırlıkça %2 β-CD, hem çevresel hem de yapısal sonuçları iyileştiren sinerjik etkiler oluşturdu. Mekanik analiz, çekme dayanımında %12'ye varan artışlar olduğunu gösterdi; bu, arayüz boşluklarında azalma ve kristalinite sağlayan artan nükleasyon olduğunu gösteren SEM görüntülemesiyle doğrulandı. FTIR analizi, fonksiyonel katkı maddeleri ve polimer matrisleri arasında kimyasal etkileşimlerin varlığını kanıtlamıştır. Matris polaritesinin dolgu maddesi dispersiyonu ve performansı üzerindeki etkisi, farklı WPC formülasyonlarında keşfedilmiştir. PA11 ve rPO bazlı WPC'ler, benzersiz mekanik profillerine katkıda bulunan farklı fibrilasyon ve dispersiyon morfolojileri sergilemiştir.
Bu tez, döngüsel ekonomi planları prensiplerine uygun, yüksek performanslı ve düşük emisyonlu kompozit malzemeler üretmek için bir çerçeve sunmaktadır. Bu çalışma, petrol bazlı, yenilenebilir ve biyo bazlı polimer matrislerle fonksiyonelleştirilmiş nano dolgu maddeleri kullanarak, dolgu maddeleri ve matrisler arasındaki etkileşimlere yeni bakış açıları sunmaktadır. Otomotiv iç mekanı, elektronik ve yapı malzemeleri gibi yüksek performans uygulamalarına uygun WPC'lerin üretimi için verimli bir strateji önermektedir.

ACKNOWLEDGEMENTS

I would like to express my deepest gratitude to my advisor, Prof. Dr. Yusuf Ziya Menceloğlu, for guiding me throughout my Ph.D. journey with his invaluable knowledge and experience. I am deeply grateful for his contributions in developing my scientific thinking and inspiring my research efforts. I sincerely thank him for his patience and understanding through all challenges and for always being there to support me.

I want to sincerely thank the respected jury members; Prof. Dr. Hacer Ayşen Önen, Prof. Dr. Nilgün Kızılcan, Asst. Prof. Dr. Serkan Ünal and Prof. Dr. Fevzi Çakmak Cebeci, for generously contributing their time, expertise, and constructive feedback. Your valuable input has significantly enriched the quality of this work.

I would like to express my sincerest gratitude to Dr. Kaan Bilge for his invaluable support throughout the entire process, which has both accelerated and strengthened my work.

Special thanks go to my friends, Gülayşe Şahin, Meryem Çiğdem UÇAR, Elif Daldal, Mariam Kassem Omar for their unwavering support, encouragement, and shared moments that provided much-needed balance during the demanding phases of this research.

My heartfelt appreciation goes to the past and present members of the YZM Research group, particularly Çağla Girişken, Gizem Semra Arıtürk, Mine Aybike Ersin, Oğuz Alp Kurucu , Armita Safari, Ogeday Rodop, Rana Al-Nakib, Gökmen Şanlı, , İde Ezgi Önal, Ceylin Işıklar, Armita Safari, Gülşah Yıldız, Yeşim Menceloğlu whose collaboration and shared insights have played a pivotal role in the development of this research.

I would also like to acknowledge the support of my colleagues; Büşra Çetiner, Melike Nur Önder, Yelda Yorulmaz, Onur Zırhlı, Nihan Birgün, Sinem Elmas, Sina Khalilvandi Behrouzyar, Ayça Aydurmuş, Nargiz Aliyeva, Kuray Dericiler, İleyna Uvak, Ceren Yıldırım, Aylin Yıldırım, Neslihan Karaca, Emine Ayşe Turhan, Ebru Sarıoğlu, Müge Fidan, Dilara Çelik, Bilge Esenkal, Cansu Yılmaz Baker, Anıl Tez, Burcu Şimşek, Gülşah Balamut, Beste Koçoğlu, Ramazan Çardak and countless others who have contributed to the intellectual vibrancy of our academic community.

Heartfelt gratitude is extended to my mother Ratiye Kurtulmuş, my father Enver Kurtulmuş and my brother Barış Can Kurtulmuş. Throughout my life, they have

supported and provided me with all the opportunities for education and learning, and made their presence always felt by my side.

I would like to acknowledge the Sabancı University Faculty of Engineering and Natural Sciences Conference Travel Grant, for providing support to both of my international conference and congress travels.

Also, I would like to thank the Scientific and Technological Research Council of Turkey (TUBITAK) with project numbers 118C042 and 5230043 and Kastamonu Entegre Wood Industry Co. Inc. (KEAS) for supporting my research and industrial studies.

Finally, I would like to express my deepest respect and gratitude to the great leader Mustafa Kemal Atatürk, who made this work possible with his unwavering commitment to science and education.

Gizem KURTULMUŞ

Dedicated to my mother, father, brother, and me…

TABLE OF CONTENTS

LIST OF TABLES

LIST OF FIGURES

LIST OF ABBREVIATIONS

BET : Brunauer–Emmett–Teller

BJH : Barrett–Joyner–Halenda

CD : Cyclodextrin

DSC : Differential Scanning Calorimetry

DTG : Derivative Thermogravimetry

FESEM : Field Emission Scanning Electron Microscopy

FID : Flame Ionization Detector

FTIR : Fourier Transform Infrared

HH : Hydrazine Hydrate

HNT : Halloysite Nanotube

HS-GC-MS : Headspace Gas Chromatography–Mass Spectrometry

LOD : Limit of Detection

MCA : Monochloroacetic Acid

Mod-HNT : Modified Halloysite Nanotube

NMR : Nuclear Magnetic Resonance

PA11 : Polyamide 11

PP : Polypropylene

RPM : Revolutions Per Minute

rPO : Recycled Polyolefin

SEM : Scanning Electron Microscopy

TGA : Thermogravimetric Analysis

TMPED : N-[3-(Trimethoxysilyl)propyl]ethylenediamine

VOC : Volatile Organic Compound

WF : Wood Fiber

WPC : Wood–Plastic Composite

β-CD : Beta-cyclodextrin

LIST OF SYMBOLS

°C	: Degree Celsius
χ	: Degree of crystallinity
ΔH	: Enthalpy change
ΔHm	: Melting enthalpy
Tm	: Melting temperature
Tc	: Crystallization temperature
Tg	: Glass transition temperature
Td	: Decomposition temperature
σ	: Stress
ε	: Strain
E	: Elastic modulus (Young's modulus)
t	: Time
T	: Temperature
ΔHc	: Crystallization Enthalpy
Xc	: Degree of Crystallinity
$\mathbf{w^F}$	: Weight Fraction of Fiber
$\mathbf{Tm_{onset}}$	: Melting Onset Temperature
$\mathbf{Tm_{endset}}$	: Melting Endset Temperature
ρ	: Density
Φ	: Volume fraction
$\mathbf{P/P_o}$	: Relative Pressure
k	: Thermal conductivity
$\mathbf{C^p}$	: Specific heat capacity

1. INTRODUCTION

In response to growing population and following environmental challenges, governments have introduced regulations to support a circular economy, emphasizing resource efficiency and waste reduction. The European Green Deal, for example, limits plastic use and mandates renewable components in new products—25 % by 2025 and 55 % by 2030 (Packaging waste, 2023). Similarly, the U.S. Environmental Protection Agency (EPA) targets 50 % renewable components (U.S. National Recycling Goal, 2023). So, the demand for sustainable and circular materials has encouraged the use of renewable and recycled resources in polymer composite technologies (Mohanty et al., 2018). Within this context, wood-plastic composites (WPCs), which integrate natural fibers such as wood with thermoplastics, offer an alternative solution to achieving these sustainability goals. In line with this, three types of polymer matrices have become prominent in this context: recycled polyolefin (rPO) for sustainability, biobased polyamide 11 (PA11) for circularity, and virgin polypropylene (PP) for its broad applicability and cost-effectiveness.

Despite their advantages, WPCs face two major limitations that hinder their use, especially in indoor applications (such as automative industry). The first is the undesirable release of odors due to the emission of volatile organic compounds (VOCs) during processing. These VOCs are typically formed through thermal degradation, residual additives, or oxidative reactions of polymer matrix and natural fibers. VOCs include aldehydes (e.g., formaldehyde, acetaldehyde), ketones, alcohol types, furans, and terpenes which may exceed odor thresholds and limit the acceptance of WPCs in indoor applications (Väisänen et al., 2016; Trojanová et al, 2025; Jabbari et al, 2025).

The second challenge that comes with , the incorporation of hydrophilic wood fibers into hydrophobic thermoplastics often leads to poor fiber-matrix interfacial adhesion and increased brittleness, negatively impacting mechanical properties (Teaca et al, 2018; Mitaľová et al, 2024; Ramesh et al, 2022). So, these two interrelated issues (odor release

and reduction of mechanical strength) form the main barriers to broader usage of sustainable WPCs in value-added applications.

To address these limitations, several approaches have been investigated. Process optimization (e.g., controlled degassing, optimized melt temperatures) can partially reduce VOC emissions but often falls short of completely eliminating odors. Therefore, material-based solutions have been examined to provide a more permanent solution, particularly through the use of additives that can physically suppress or chemically adsorb the odors and may also contain the reinforcing ability. So, the effectiveness of additives to reduce odor like zeolites, metal ion-modified materials (like copper-coated silica nanoparticles), activated carbon, carbon nanotubes (CNTs) is investigated (Garofalo et al, 2023; Zhang et al, 2017; Zou et al, 2018). However, they have deficient or disadvantaged characteristics. For instance, zeolites have a microporous structure that adsorbs VOCs, but they are expensive and less mechanically stronger. Copper-coated silica's odor removal effectiveness depends on copper loading (Singh et al, 2010). CNTs are not environmentally friendly and have toxic effect on certain conditions (Poland et al, 2008). While graphene materials are not so cost-effective and safer for humans and the environment and biochar can disrupt biological processes (Theodoropoulou et al, 2023; Dong et al, 2025).

Among these odor reducer additives, more promising solutions are Halloysite Nanotubes (HNTs) and mostly their functionalized derivatives. HNTs are naturally occurring aluminosilicate clays with a unique tubular structure , featuring lumen diameters between 5–150 nm and lengths up to 30 μm, providing a high surface area and dual internal-external functional potential (Wong et al, 2022). Their high aspect ratio and large surface area make them suitable as both nanofillers and adsorbents. Their incorporation into polymer matrices has shown to improve both VOC adsorption and mechanical reinforcement (Aljibori et al, 2024). However, neat HNTs have limited interaction with polar VOCs. Through surface functionalization such as amino-silane modification. Additionally, their adsorption capacity and compatibility with polar VOCs and polymer matrices can be significantly enhanced (Bao et al, 2024).

On the other hand, β-Cyclodextrin, a cyclic oligosaccharide composed of seven glucose units, possesses a toroidal molecular structure that enables it to form inclusion complexes with hydrophobic VOCs. Its inner cavity (diameter 0.60–0.65 nm) allows for selective

adsorption of aromatic hydrocarbons and other odor-active molecules, while its outer hydrophilic surface ensures dispersion compatibility within polymer matrices (Urooj et al, 2024). Although β-CD has been widely studied for environmental and pharmaceutical applications, its integration into WPCs for VOC control remains underexplored (Crini et al, 2021). They are considered safe, non-toxic, and environmentally friendly, making them ideal for sustainable composite development (Musuc, 2024). Thus, due to their similar properties but different structural features with HNT, we compare β-CD with HNT and Modified Halloysite Nanotubes (Mod-HNTs) in this study.

In this context, the study focuses on the production of wood–plastic composites (WPCs) using recycled polypropylene, biobased polyamide 11, and virgin polypropylene, with the incorporation of halloysite nanotubes (HNTs), modified HNTs, and β-cyclodextrin (β-CD) as additives. The main objectives are to reduce volatile organic compounds (VOCs) causing undesirable odors through effective adsorbents (HNT or more efficiently Mod-HNT)) and to enhance mechanical properties by improving fiber–matrix interaction and providing nanoscale reinforcement. The dual functionality of these additives is systematically evaluated through sensory analysis (jar test), instrumental methods (HS-GC-MS, FTIR, TGA, DSC, SEM, NMR, BET), and mechanical testing in this study. This study offers a scalable and cost-effective strategy to simultaneously improve the environmental and mechanical performance of WPCs, thereby contributing to the development of high-performance, odor-controlled composites suitable for indoor applications and supporting the broader goals of sustainable material design within the framework of a circular economy.

This dissertation is composed of five complementary parts, each of them expressing valuable findings with regard to their unique subjects. The introduction offers a thorough outline that defining the problems, spotting the gap in the existing scientific literature, and proposing a solution that highlights novelty of this study.

The second chapter presents a material-centered approach that contributes to the development of more sustainable indoor-use plastics by integrating halloysite nanotubes (HNTs), β-cyclodextrin (βCD), and commercial odor reducer additives into cost-effective and widely used virgin polypropylene (PP) based wood plastic composites (WPCs). Through this integration, the study effectively addresses the dual challenge of reducing odor emissions and enhancing the mechanical performance of the composites. These

WPCs are particularly important for enclosed environments, where emissions of volatile organic compounds (VOCs) from both the polymer matrix and natural fillers can negatively affect air quality, user well-being, and overall material acceptance. Rather than relying on chemical compatibilizers or complex processing techniques, the study adopts a scalable and practical additive-based strategy aimed at improving both environmental and functional performance. HNT and βCD are examined not only for their odor mitigation capabilities but also for their distinct contributions to mechanical and thermal properties. While HNT provides broad-spectrum VOC adsorption through its mesoporous tubular structure, βCD selectively captures polar odor molecules via host–guest inclusion complexation. These complementary effects lead to improved composite performance, making them more suitable for applications in sectors such as automotive interiors, electronics, and household products. Also, the environmentally friendly nature of the additives, coupled with their performance-enhancing properties, supports broader sustainability goals in polymer design. In conclusion, this chapter highlights the potential of multifunctional additive systems in advancing sustainable composite technologies and presents a promising pathway toward the development of high-value, eco-conscious materials.

The third chapter investigates the incorporation of surface-functionalized halloysite nanotubes (HNTs) into recycled polyolefin (rPO) matrices as a strategic approach to simultaneously address odor emission and mechanical performance challenges inherent to recycled thermoplastics. Diverging from the second chapter which examined virgin polypropylene (PP)-based composites, this study deliberately focuses on rPO as a substrate aligned with circular economy principles, aiming to enhance its applicability in high-value, sustainability-oriented domains. The selection of rPO is motivated by the need to develop multifunctional material systems that offer both environmental benefits and improved functional properties. Findings from the previous chapter demonstrated that while unmodified HNTs possess broad-spectrum VOC adsorption capacity, they remain insufficient in capturing certain polar compounds such as aldehydes and specific alcohols. In response, the current work introduces a targeted surface modification strategy utilizing amine-rich silane chemistry to enhance the interaction of HNTs with these polar VOCs. To achieve this, HNTs were functionalized through a sequential three-step process involving N-[3-(trimethoxysilyl)propyl]ethylenediamine (TMPED), monochloroacetic acid (MCA), and hydrazine hydrate (HH), resulting in amine-enriched surfaces with

increased chemical reactivity. The modified HNT obtained at the end of these steps enhances VOC adsorption, particularly for polar compounds that are otherwise poorly retained by unmodified nanotubes. In addition, it improves interfacial compatibility between the filler and the polymer matrix, which contributes to the overall enhancement of thermal and mechanical performance in recycled polyolefin systems. Collectively, this chapter presents a material-focused and scalable strategy to overcome the sensory and structural limitations of recycled plastics, reinforcing their suitability for use in high-value, odor-sensitive applications.

The fourth chapter builds upon the insights gained from the preceding investigation by extending the multifunctional additive approach to a broader material system which is wood–polymer composites (WPCs) through the integration of both petroleum-based and bio-based polymers. Informed by the previous chapter's demonstration of VOC reduction and mechanical enhancement in recycled polyolefin matrices using amino-silane-functionalized halloysite nanotubes (Mod-HNTs), the current study expands the material scope by incorporating polyamide 11 (PA11), a bio-derived polymer, alongside recycled polyolefins, and virgin polypropylene (PP). In doing so, the work not only maintains its focus on sustainability but also embraces the principles of circularity, addressing the full lifecycle potential of WPC materials. WPC formulations containing 30 wt.% wood fiber were prepared with 2 and 5 wt.% of Mod-HNTs and β-cyclodextrin (β-CD). The combination of 5 wt.% Mod-HNTs and 2 wt.% β-CD achieved significant VOC suppression—up to 96% in PP-based systems—while preserving or improving mechanical properties, especially tensile strength. The modified HNTs used in this study not only facilitated effective VOC adsorption but also improved filler–matrix compatibility, resulting in enhanced structural integrity. Collectively, this chapter demonstrates that the integration of functional nanofillers into hybrid WPC systems represents a scalable and circular strategy for overcoming both odor-related and structural limitations in sustainable composite applications.

The final chapter offers a general conclusion to the studies. This thesis addresses a critical gap in the literature by demonstrating the potential of surface-functionalized halloysite nanotubes (Mod-HNTs) and β-cyclodextrin (β-CD) as multifunctional additives for enhancing both odor performance and mechanical properties in sustainable polymer systems. Through the systematic incorporation of these functional additives into recycled

polyolefins, virgin polypropylene, and bio-based polyamide 11 matrices—particularly within wood–polymer composites—this work contributes to the development of advanced materials that align with both sustainability and circularity principles. By overcoming key challenges related to odor emissions and filler–matrix compatibility, the research highlights scalable strategies that enable the use of recycled and bio-based resources without compromising material performance. These findings provide a strong foundation for future studies aimed at optimizing formulation parameters, expanding application areas, and supporting industrial-scale implementation of high-performance, eco-conscious composite technologies. A graphical abstract outlining the full scope and structure of this thesis is presented in Figure 1.

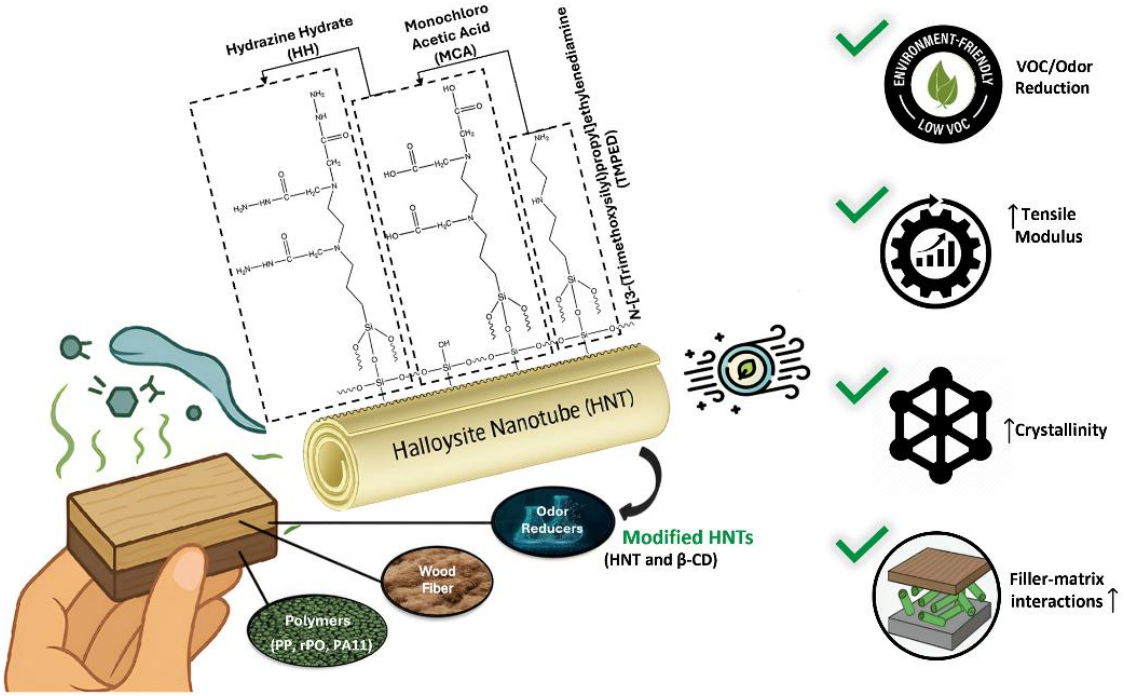

Figure 1. Graphical abstract of the thesis

2. ENHANCING ODOR REDUCTION AND PROPERTIES IN POLYPROPYLENE-BASED WOOD PLASTIC COMPOSITES WITH HALLOYSITE NANOTUBES AND BETA-CYCLODEXTRIN

2.1 Abstract

In this chapter, the effect of halloysite nanotube and beta-cyclodextrin on reducing unwanted odor emission and mechanical properties in polypropylene-based wood plastic composites is investigated. Undesirable odor emissions that originate from polypropylene (PP)-based wood plastic composites (WPCs) caused by volatile organic compounds (VOCs), restrict their indoor applications. This research investigates the effectiveness of halloysite nanotubes (HNT) and beta-cyclodextrin (β-CD) in reducing VOC emissions while simultaneously improving the mechanical and thermal properties of WPCs. Composites are produced by incorporating 2 wt.% and 5 wt.% of HNT, β-CD and are compared to commercial odor-control additives. Odor intensity is tested using sensory (jar) odor and headspace gas chromatography–mass spectrometry (HS GC-MS) methods. Mechanical, thermal, morphological, and structural properties are characterized through tensile testing, thermogravimetric analysis (TGA), differential scanning calorimetry (DSC), scanning electron microscopy (SEM), Fourier-transform infrared spectroscopy (FTIR), and Brunauer–Emmett–Teller (BET) analysis. The odor results show the addition of 5 wt.% HNT and 2 wt.% β-CD causes reduction of VOC peaks by 14% and 35%, respectively. HNT results in a 36.6% reduction of 4-methyl-octane and improves tensile strength and modulus by 6.3 (±0.3) % and 12 (±0.8) %, whereas β-CD advances in toughness. The BET and FTIR analyses confirm distinct adsorption behaviors and interactions within the polypropylene matrix. These results suggest the potential of HNT and β-CD as sustainable additives to improve the indoor applicability of PP-based WPCs.

2.2 Introduction

In light of increasing environmental challenges related to population growth governments globally have implemented regulations with the purpose of creating the evolution towards a circular economy. These regulations points out the importance of resource efficiency and the necessity of reducing plastic waste. In this framework, the European Green Deal outlines the necessity for integrating renewable materials into plastic-based products, directing a minimum of 25% by 2025 and 55% by 2030. The plan intends to decrease dependence on fossil-based resources and lower impacts on the environment ((Packaging waste, 2023). In a parallel manner, the United States Environmental Protection Agency (EPA) aims for a 50% renewable content in plastic production (U.S. National Recycling Goal, 2023). Within this statutes and regulations, wood plastic composites (WPCs), which combine natural fibers such as wood flour with thermoplastics like polypropylene (PP), have gained considerable attention as sustainable material alternatives.

Wood-plastic composites (WPCs) are usually produced with polyethylene and wood fibers have been used for outdoor applications. Conversely, WPCs that consist of polypropylene provide increased mechanical and thermal properties, offering them suitable for indoor applications such as automotive components and consumer products (Wolcott M.P. & Adcock T., 2000). Polypropylene is widely used because of its cost-effectiveness, resistance to moisture, and beneficial chemical stability (Shelesh-Nezhad, 2012). Even so, we want to use the recycled polypropylene it affects substantial challenge regarding odor emissions, especially in indoor environments. The odors observed are mainly caused by volatile organic compounds (VOCs) emitted during the thermal degradation of polypropylene while producing and the decomposition of residual additives and contaminants (Almaie et al, 2022; Canevarolo, 2000; Kang et al, 2020).

The addition of wood fibers to polypropylene further raises odor emissions. Volatile organic compounds (VOCs) originated from wood, which includes formaldehyde, acetaldehyde, and acetic acid, are released during processing, with elevated temperatures intensifying this problem (Fuller et al, 2020; Väisänen et al, 2016; Ahn et al, 2011). These

emissions in disputes adversely influence the acceptability and environmental performance of wood-plastic composites aimed at indoor applications. Thus, the reduction of VOC emissions is essential for improving both the functionality of materials and the acceptance by users.

Despite process-level treatments, involving degassing and adjustments of molding parameters, have been looked into for odor elimination, material-based solutions have shown more effective results (Behraveshet al,2009; Wang & Zhang, 2007; Garofalo et al, 2023). They are the additives, such as zeolites, copper-coated silica, activated carbon, and carbon nanotubes, has been examined for their capacity to adsorb volatile organic compounds (VOCs) (Zhang et al, 2017; Zou et al, 2018). Among these materials, halloysite nanotubes (HNTs) and *β*-cyclodextrin (*β*-CD) have emerged as notably promising candidates, attributed to their distinctive chemical structures and adsorption properties.

β-cyclodextrin is a cyclic oligosaccharide that is formed from seven glucose units. The toroidal molecular structure features a hydrophobic cavity and a hydrophilic outer surface, enabling the formation of stable inclusion complexes with hydrophobic volatile organic compounds, including aromatic hydrocarbons (Da Silva, 2018; Zhao et al, 2007). Halloysite nanotubes are naturally occurring aluminosilicate minerals that characterized by their hollow tubular structures. Their high surface area, dual surface charge, and large aspect ratio characteristics lead to their efficacy as nanofillers and potential adsorbents for VOCs within polymer matrices (Yuan et al, 2015; Wong et al, 2022; Fahimizadeh et al, 2024).

A comparative analysis of HNTs and *β*-CD with other materials reveals significant advantages in terms of performance, safety, and environmental impact. Zeolites, while effective in adsorbing VOCs, are more expensive and mechanically weaker than HNTs, which possess a robust nanoscale tubular structure (Kotova et al, 2022; Kapoor, 2022). *β*-CD, known for its hydrophilic nature, is also effective in VOC adsorption and offers advantages such as chemical stability and aqueous solubility. The odor-removal efficiency of copper-coated silica varies with copper loading, while both HNTs and *β*-CD provide consistent results. HNTs can be converted into carbon nanoflakes for enhanced CO_2 adsorption and supercapacitance, offering a non-toxic alternative to carbon nanotubes (CNTs) (Singh et al, 2010; Ramadass et al, 2020). In polymer composites, HNTs have been shown to improve impact resistance more effectively than CNTs, which

tend to be brittle (Erpek et al, 2015). While graphene offers superior mechanical reinforcement, HNTs and β-CD are more cost-effective and biocompatible. Biochar may interfere with biological systems, whereas β-CD is widely regarded as safe and effective in various applications, including environmental and pharmaceutical uses (Garg et al,2024; Guo et al, 2022).

Even though HNTs and β-CD represent particular potential for the adsorption of VOCs, their specific usage for decreasing odor emissions in polypropylene-based wood-plastic composites (WPCs) remains not properly explored. While β-CD has established the effectiveness in the adsorption of VOCs such as formaldehyde and xylene, and halloysite nanotubes (HNTs) have been highlighted for their ability to improve mechanical strength, there exists an absence of research investigating their individual effects within composite systems intended for odor control by reducing their odorous VOCs (Kadam et al, 2018; Kadam et al, 2020; Jana et al, 2015).

This study investigates the individual effects caused by HNT and β-CD on the VOC emissions, mechanical and other characteristics of polypropylene-based WPCs for addressing this gap. The research proposes to obtain a dual benefits by reducing odor levels and improving the physical performance of WPCs. The uniqueness of this study lies in its comprehensive material approach, which promotes the development of sustainable, functional composites in line with the requirements of the circular economy.

2.3 Materials and experimental

2.3.1 Materials

Polypropylene (PP) HE125MO homopolymer that has a density of 905 kg/m³, melt flow rate (MFR) value 12 g/10 min (230 °C/2.16 kg), and derived in white granule form for injection molding application were supplied by Borealis Compounds, Inc., North Carolina, USA. Wood Fiber with 20-40 micrometer (μm) width 1.5-2.5 mm weighted average length and consists of 70 wt.% oak (Quercus robur) and 30 wt.% pine (Pinus sylvestris) is supplied by Kastamonu Integrated Wood Industry Co. Inc., Gebze/Kocaeli, Türkiye. Halloysite nanotube (HNT) was obtained from Esan Eczacıbaşı Industrial Raw Materials Industry and Trade. Inc., Maltepe, Türkiye. STRUKTOL® RP 53 odor control additive (mask) has an off-white pastille form for compounding PE and PP WPC products

provided by Struktol Company of America, LLC, Ohio, US. TEGO Sorb® PY88TQ is a zinc ricinoleate containing 8.8–10.8% zinc, used as odor absorber in form of pale-yellow pellets. It is used for the production of masterbatches and compounds that are suitable for Polyolefins were supplied by Evonik Nutrition & Care GmbH, Essen, Germany. *β*-Cyclodextrin ≥97 % purity in white powder form with was purchased from Sigma Aldrich, Merck Group, St. Louis, Missouri, USA.

2.3.2 Preparation of PP-WPC Compounds with High Shear Mixing

Wood fiber (WF) and polypropylene (PP) were dried at 80 °C for 24 hours prior to the preparation of wood-plastic composite (WPC) formulations. The base composition consisted of 70 wt.% PP and 30 wt.% WF, with additives incorporated at varying concentrations: 2 wt.% and 5 wt.% Halloysite Nanotubes (HNT), 2 wt.% and 5 wt.% *β*-Cyclodextrin (*β*-CD), and 2 wt.% STRUKTOL® RP 53 and TEGO Sorb® PY 88 TQ. The formulations were processed using a Gelimat GI ultra-high-speed thermokinetic mixer (Draiswerke, USA), which is characterized by high shear forces and short retention times. During mixing, the components were compounded at approximately 4000 rpm, resulting in a chamber temperature of 180 °C. After mixing, the wood-plastic composite was subjected to cooling and granulation using a plastic granulator (Rhong Machinery, China). The granules were subsequently transformed into specimens suitable for mechanical and thermal evaluation through injection molding (Xplore, Sittard, Holland) at a melt temperature of 240 °C, a mold temperature of 35°C, and an injection pressure of 12 bar. The production steps which are compounding in the Gelimat (thermokinetic mixer), crushing process in the crushing machine and molding in the injection machine device orderly are shown in Figure 2. Injection molded samples of all sample are shown in Figure 3.

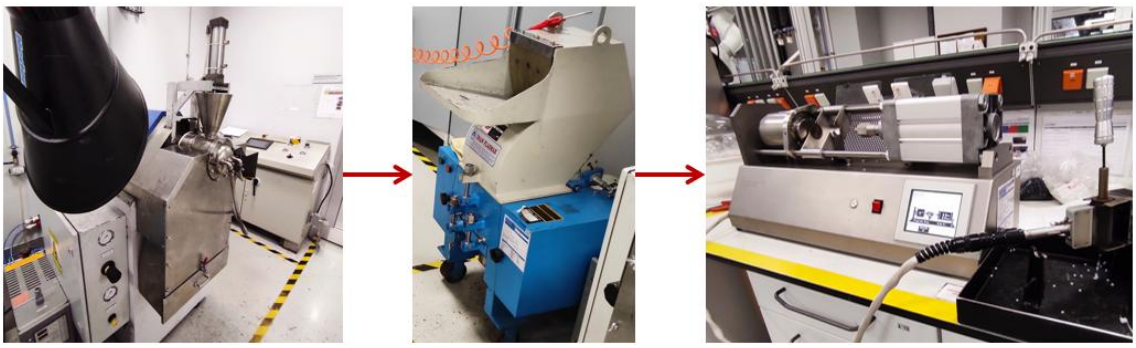

Figure 2. The production steps of WPC formulations

Figure 3. Injection molded samples that composed of 2 wt.% and 5 wt.% HNT, β-CD, and 2 wt.% commercial additives

2.4 Material Characterization

2.4.1 Odor (Jar test) Analysis

The Jar (odor) test was conducted to evaluate the odor intensity of wood–plastic composites (WPCs) formulated with 70 wt.% polypropylene (PP) and 30 wt.% wood flour (WF). The sample set included: (i) a control WPC without additives, (ii) WPCs modified with 2 wt.% and 5 wt.% halloysite nanotubes (HNT), (iii) WPCs containing 2 wt.% and 5 wt.% *β*-CD, and WPCs incorporating 2 wt.% of commercial odor-control additives RP 53 and PY88TQ. As part of the pre-conditioning, all specimens were exposed to ambient laboratory conditions (approximately 23 °C and 50% relative humidity) for a duration of 12 days to simulate environmental aging. Subsequently, the samples were individually placed in 1 L gas-tight glass jars containing 50 mL of distilled water at the base. A stainless-steel wire mesh was positioned above the water to suspend the samples and prevent direct contact. Following sample preparation, all specimens were subjected to three different temperature conditions to simulate various storage and

handling scenarios: (i) 25 °C for 24 hours, (ii) 40 °C for 24 hours, and (iii) 65 °C for 2 hours. After exposure, the odor intensity of each sample was evaluated by a panel of five independent raters. To ensure objective evaluation, the jars were anonymized and randomly labeled from 1 to 7, with no reference to their contents. Odor intensity was rated on a scale from 1 to 6 (1 = imperceptible odor, 6 = Extremely disturbing odor). The average ratings from the panelists are presented in Table 1.

2.4.2 Headspace Gas Chromatography-Mass Spectrometry Analysis

Headspace Gas Chromatography-Mass Spectrometry (HS GC-MS) analyzed for identification of VOCs of samples. Extraction of VOCs was performed using 1 g sample in a 10 mL HS-vial with a PTFE septum. The samples were conditioned and equilibrated at 125 °C with agitation at 250 rpm for headspace enrichment. A HS-20NX Headspace Autosampler (Shimadzu Scientific Instruments, USA) was used for automated sampling. The injection was performed at 200 °C with an injection time of 5 s and a split ratio of 1:20. The analysis was carried out on a GC-MS-QP2010 Ultra system (Shimadzu Scientific Instruments, Carlsbad, CA, USA) equipped with an InertCap Pure-WAX capillary column (60 m × 0.25 mm × 0.25 µm film thickness). Helium was used as a carrier gas at a constant flow rate of 1 mL/min and an average linear velocity of 22 cm/s.

The GC oven was programmed to heat from 50 °C to 200 °C using a multi-rate temperature gradient: 3 °C/min from 50 °C to 100 °C, followed by 12 °C/min to 200 °C. The total running time for each analysis was 30 minutes. The injector temperature was set to 250 °C, and the MS detector was operated in scan mode within a mass range of 30–550 m/z. Blank runs were conducted between samples to prevent cross- contamination.

Identification of VOCs was based on retention times and mass spectra comparison with reference spectra from the WILEY7/NIST mass spectral libraries. For quantification, a seven-point calibration curve was constructed using acetone as the internal standard in 1-butanol at concentrations of 0.1, 0.5, 1, 5, 10, 50, and 100 grams per liter (g/L). A 5 microliter (µL) syringe was used to inject 2 µL of each calibration solution into 10 mL HS vials under identical conditions. The limit of detection (LOD) for VOCs was defined as peaks with heights at least three times the baseline noise and areas exceeding 10% of the acetone peak area at a concentration of 0.5 g/L acetone.

2.4.3 Mechanical Testing

Tensile properties of the polypropylene (PP)-based wood–plastic composites (WPCs) were evaluated in accordance with the ISO 527-2 standard using a universal testing machine (Instron 100 kilonewton (kN) Electromechanical Test System, Massachusetts, USA). A total of five replicates (n = 5) of Type 1A dog-bone specimens, each with a thickness of 2 mm and width of 5 mm in the gauge section, were tested. The experiments were conducted using a 5 kN load cell at a constant crosshead speed of 100 mm/min. An extensometer was employed to accurately record the strain and calculate the percentage elongation at break. This setup enabled the precise determination of tensile strength, modulus of elasticity, and elongation behavior of the composite materials.

2.4.4 Scanning Electron Microscopy

The surface morphologies of samples were characterized using Field Emission Scanning Electron Microscopy (FESEM, CARL ZEISS LEO SUPRA 35VP) operated at an accelerating voltage of 5 kV in secondary electron (SE) mode. Micrographs were acquired at a magnification of 10K X to observe the microstructural features in detail. Fracture surfaces were obtained by mechanically breaking the specimens at room temperature, and imaging was conducted on the fractured cross-sections to evaluate the interfacial adhesion and dispersion of components. Prior to imaging, the sample surfaces were sputter-coated with carbon in three layers to ensure adequate electrical conductivity and minimize charging effects during analysis.

2.4.5 Fourier-transform Infrared Spectroscopy

Fourier-transform infrared (FTIR) spectroscopy analysis of the composites was conducted using a Thermo Scientific Nicolet iS10 FTIR spectrometer (Waltham, Massachusetts, USA), equipped with a diamond Attenuated Total Reflection (ATR) crystal. FTIR spectra were recorded using OMNIC 9.2.98 software (Thermo Fisher Scientific, Gloucester, UK), within the wavelength range of 4000–600 cm^{-1} and a resolution of 4 cm^{-1}. The analysis was performed to identify the presence of functional groups and to investigate interactions among the various components of the composites. A total of 32 scans were collected to enhance the signal-to-noise ratio.

2.4.6 Thermogravimetric Analysis

The thermal stability of the specimens was assessed using thermogravimetric analysis (TGA) conducted on a Mettler Toledo instrument (Giessen, Germany). Alumina crucibles with a volume of 90 µL were utilized for the analysis. Each mass of the samples was approximately 11-12 mg. TGA thermograms were acquired using STAR® SW 16.10 software (Mettler Toledo, Columbus, OH, USA). The tests were performed under a nitrogen atmosphere, spanning a temperature range of 20 to 700 °C, with a heating rate of 10 °C/min.

2.4.7 Differential Scanning Calorimeter

The effect of HNT, β-CD and other additives on the thermal transition temperatures and crystallinity of the PP polymer was analyzed under an inert nitrogen atmosphere with a Differential Scanning Calorimeter (DSC) (Mettler Toledo DSC 3, Giessen, Germany). 100 µl Aluminum crucibles used for testing. The weight of each sample was approximately 10-11 mg. STAR® SW 16.10 software (Mettler Toledo, Columbus, OH, USA) was used to determine the melting enthalpy (ΔHm), melting temperature (Tm), cold crystallization temperature (Tc), and cold crystallization enthalpy (ΔHc). DSC analysis was performed in three cycles. In the first step of the cycle, the samples were heated from room temperature to 200 °C at 10 °C/min and held at 200 °C for 2 minutes to erase their thermal history. In the second cycle, the samples were cooled from 200 °C to -70 °C at a rate of 10 °C/min and held at -70 °C for 2 minutes. The cold crystallization temperatures (Tc) were determined from the maximum points of the peaks in the resulting thermogram. In the third cycle, the samples were reheated from -70 °C to 200 °C at a rate of 10 °C/min, and the melting temperatures (Tm) were derived from the peak maxima observed during this final heating. The degree of crystallinity (Xc) for each sample was calculated using the (Eq. (1)):

$$X_c = [\Delta H_m / \Delta H_m^\circ \times (100 - w^F)] \times 100\% \quad (1)$$

where ΔH_m is the melting enthalpy and ΔH_m° is the melting enthalpy of 100% crystalline polymer and w^F corresponds to the weight percentage of fiber in the composite. The theoretical value of 100% crystalline polypropylene (ΔH_m°) is 207 J/g (Wadi et al, 2020; Gao et al, 2016).

2.4.8 Brunauer–Emmett–Teller (BET) Analysis

The surface area and porosity of HNT and *β*-CD were measured using nitrogen adsorption-desorption at 77 K with the Brunauer–Emmett–Teller (BET) and Barrett–Joyner–Halenda (BJH) methods, employing a high- performance gas adsorption analyzer (Micromeritics 3Flex, Norcross, GA, USA). The specific surface areas of the samples were determined using the BET technique, while the pore size and pore volume were calculated from the desorption isotherm curves using the BJH method and the maximum amount of nitrogen adsorbed at a relative pressure of P/P0 = 0.99. The degassing pressure during the outgassing process reached 1.0 mmHg. All samples were subjected to vacuum outgassing at 80 °C for 24 hours prior to measurement.

2.5 Results and Discussion

2.5.1 Sensory Odor Analysis Result

The odor effect of HNT, *β*-CD and commercial additives (RP53 and PY88TQ) on WPCs have been investigated by Indoor Odor (Jar) test (FORD FLTM BO 131-03 Interior Odor Test standard). The outcomes of were presented in Table 1. Based on that table, the odor reached a “disturbing” level when WPC is formed with the addition of wood fiber and PP. Additionally, the odor level of WPC reduced from 4 (disturbing) to 3 (intense enough to be slightly disturbing) with 2 wt.% HNT. An increase in concentration to 5 wt.% HNT led to a higher reduction in odor levels relative to the 2 wt.% HNT, which lowered the rating from 4 (disturbing) to 2.5 (not disturbing). This effect is attributable to HNTs' unique porous tubular morphology and surface characteristics, which allow for effective VOC adsorption (Duan et al, 2020). In addition, this result was affected by the high surface area and VOC adsorption ability of HNT due to being a nanoparticle. Furthermore, increasing the concentration from 2 to 5 wt.% improved the adsorption capacity of HNT. A similar outcome with the 5 wt.% HNT containing WPC was also achieved by adding 2 wt.% *β*-CD that has adsorption ability due to its porous structure. However, increasing the *β*-CD concentration to 5 wt.% did not yield additional odor reduction, unlike HNT. Considering this, the adsorption capacity of *β*-CD for odor-forming VOCs in WPC was exceeded at this concentration. These results are attributed to the porous structure and high surface area of HNT, which physically adsorbs VOCs, and the host–guest complexation capability of *β*-CD (Yu et al, 2006; Almaie et al, 2022).

Due to the subjective nature of the aforementioned test, it was determined that another supportive and more qualitative test methods were needed such as HS GC-MS.

Table 1. Table of indoor odor (jar) test results

Sample Name	Test Condition	Rating Average	Result
70PP-30WF	1 (25°C, 24 h)	3.0	Very perceptible but not disturbing
	2 (40°C, 24 h)	3.5	Intense enough to be slightly disturbing
	3 (65°C, 2 h)	4.0	Disturbing
68PP-30WF-2HNT	1 (25°C, 24 h)	2.5	Clearly perceptible but not disturbing
	2 (40°C, 24 h)	3.0	Very perceptible but not disturbing
	3 (65°C, 2 h)	3.5	Intense enough to be slightly disturbing
65PP-30WF-5HNT	1 (25°C, 24 h)	1.5	Slightly perceptible
	2 (40°C, 24 h)	2.0	Perceptible, not disturbing
	3 (65°C, 2 h)	2.5	Clearly perceptible but not disturbing
68PP-30WF-2β-CD	1 (25°C, 24 h)	1.5	Slightly perceptible
	2 (40°C, 24 h)	2.0	Perceptible, not disturbing
	3 (65°C, 2 h)	2.5	Clearly perceptible but not disturbing
65P-30WF-5β-CD	1 (25°C, 24 h)	2.0	Perceptible, not disturbing
	2 (40°C, 24 h)	2.5	Clearly perceptible but not disturbing
	3 (65°C, 2 h)	3.0	Very perceptible but not disturbing
68PP-30WF-2RP53	1 (25°C, 24 h)	2.5	Clearly perceptible but not disturbing
	2 (40°C, 24 h)	3.0	Very perceptible but not disturbing
	3 (65°C, 2 h)	3.5	Intense enough to be slightly disturbing
68PP-30WF-PY88TQ	1 (25°C, 24 h)	3.0	Very perceptible but not disturbing
	2 (40°C, 24 h)	3.5	Intense enough to be slightly disturbing
	3 (65°C, 2 h)	4.0	Disturbing

Analytical techniques have been developed to identify VOC emissions and related odors in plastics and their composite materials. Olfactometry is frequently used to detect

and measure the odors produced by VOCs. Samples with intense odors may indicate higher concentrations of VOCs, while mild odors may suggest lower VOC levels. The assessment of odor type and intensity is typically subjective; therefore, involving multiple evaluators help ensure a more accurate evaluation (Fuller et al, 2020). VOCs released from plastics, including Polypropylene (PP), can also be identified using Gas Chromatography (GC) combined with either a Flame Ionization Detector (FID) or Mass Spectrometry (MS), providing more objective results than olfactometry. GC/MS, especially when used with the headspace (HS) technique, allows VOCs to disperse into the gas phase from a solid matrix, offering more accurate and reliable results. Detailed odor characterization often requires a combination of instrumental and sensory analysis techniques (Lomonaco et al, 2020; Prado et al, 2020; Zeng et al, 2023). Therefore, in this study, HS GC-MS and olfactory methods were applied to investigate VOCs responsible for the unpleasant odors of PP-based WPCs.

2.5.2 Characterization of VOCs by HS GC-MS Result

HS GC-MS chromatogram of the volatile compounds from 30 wt.%WF and 70 wt.% PP-based WPC, 2 and 5 wt.% HNT, β-CD, and 2 wt.% RP53, PY88TQ added WPCs are shown in Figure 1. The main peaks of the WPC spectrums are nearly identical to those of other WPCs, indicating that these represent the primary constituent materials. However, there were distinct peaks in Table 2 that could not be attributed to PP or wood materials in WPC. These volatile compounds may result from residual impurities in the raw materials or degradation during processing. Dodecanoic acid (CAS) lauric acid shows up at 19th min in samples containing found in 2 wt.% PY88TQ added WPCs sample as in Figure 4.

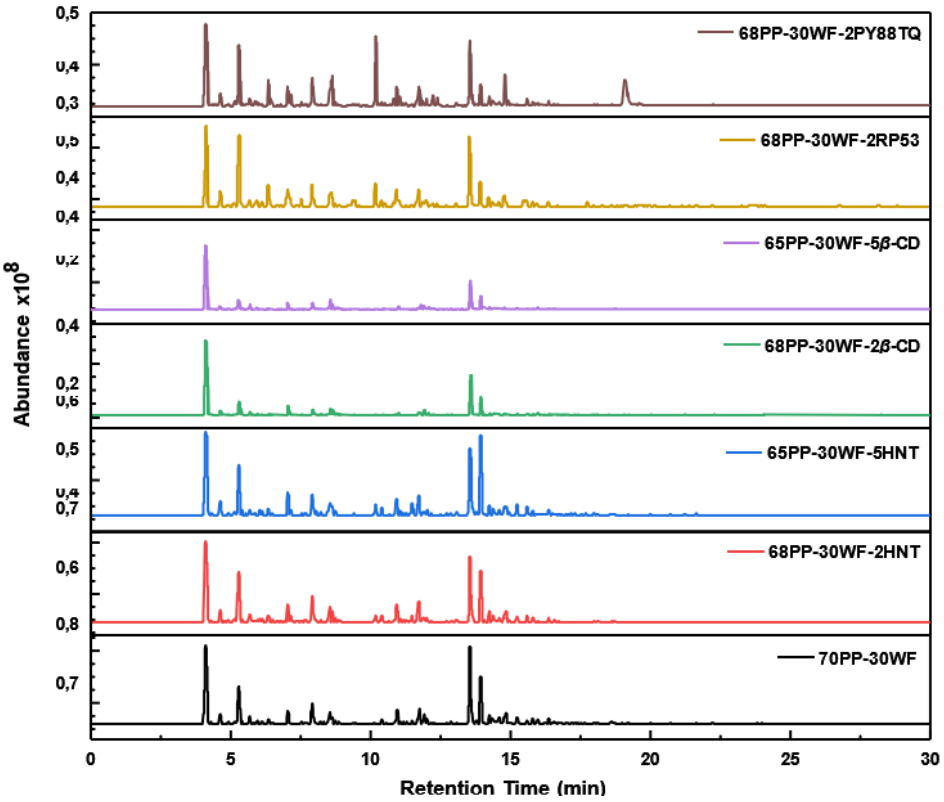

Figure 4. HS GC-MS chromatogram of 30 wt. %WF and 70 wt. %PP based WPC, 2 and 5 wt. % HNT, β-CD, 2 wt. % RP53 and PY88TQ added WPCs

In the analysis, 48 VOCs were identified in PP-based WPC via a reference database matching VOCs by their mass spectra and retention times. By the elimination of peaks lower than 10% of acetone peak height, the number of VOCs decreased to 28 in WPC without additive, 24 with HNT, 23 with PY88TQ, and 18 with *β*-CD as presented in Table 2. The additives reduced VOC peaks by 14 %, 17 %, and 35 %, respectively. HNT was especially effective in lowering the levels of VOCs, such as octane 4-methyl-, acetic acid, and nonane 5- butyl-. Among these, nonane 5-butyl- and octane 4-methyl- were reduced mostly. Additionally, 2,4- Dimethyl-heptane, a compound linked to the pungent plastic odor (Ramesh et al, 2022), disappeared completely when additives like HNT, PY88TQ, or *β*-CD were used. HNT had the biggest impact, reducing 4-methyl-octane—a main odor-causing VOC—by 37 %, likely due to its ability to bind VOC molecules through intermolecular interactions. HNT was also quite efficient in reducing acetic acid VOCs, which are produced by wood fibers in WPC. Compared to PY88TQ, HNT was more feasible at minimizing acetic acid caused by both the wood fibers and the PP in the composite (Fuller et al, 2020; Adamova´ et al, 2020). Moreover, PY88TQ, at a 2 wt.% concentration, was more useful than RP53 and *β*-CD in reducing 2-furancarboxaldehyde

(Furfural), a VOC formed during the breakdown of hemicellulose in wood fibers (Sallem-Idrissi et al, 2016). *β*-CD, on the other hand, was particularly good at reducing peaks of heneicosane 11-(1-ethylpropyl)- and benzaldehyde. These trends align with previous studies showing that HNT can non-selectively adsorb hydrocarbons, while *β*-CD selectively captures polar VOCs via its hydrophobic cavity (Li et al, 2020; Kim et al, 2019).

Table 2. Undesirable odor VOCs identified according to the HS GC-MS chromatogram

Sample Name	**Total VOC peaks numbers***	**Reduction Rate (%**	**Height Decreased VOCs**	**Height Decreasing Rate [%]**
70PP-30WF	28	-	-	-
70PP-30WF-2HNT	24	14	Octane 4-methyl- / Acetic acid / Ammonium Oxalate	1.4 / 17.3 / 6.1
70PP-30WF-5HNT	24	14	Octane, 4-methyl- / Dodecane, 4,6-dimethyl-/ Nonane, 5-butyl- / Acetic acid / 1-Octanol	36.6 / 10.3 / 46.4 / 3.2 /23.3
68PP-30WF-2*β*-CD	18	35	Octane, 4-methyl- / Heneicosane, 11-(1-ethylpropyl)- / 2-Furancarboxaldehyde / Benzaldehyde	9.4 / 43.0 / 21.8 / 36.3
65PP-30WF-5*β*-CD	18	35	Octane, 4-methyl- / Heneicosane, 11-(1-ethylpropyl)- / 2-Furancarboxaldehyde / Benzaldehyde	9.4 / 43.0 / 21.8 / 36.3
68PP-30WF-2RP53	17	39	Acetic acid / 2-Furancarboxaldehyde (Furfural)	9.4 / 48.5
70PP-30WF-2PY88TQ	23	17	Acetic acid/ 2-Furancarboxaldehyde (Furfural)	15.6 / 55.3

*After reducing peaks according to 10% Acetone (control and calibration solution) peak height

2.5.3 Mechanical Test Result

Figure 5 shows the stress-strain curves of all samples as a result of the tensile test. Their data regarding the test analyses are given in Table 3.

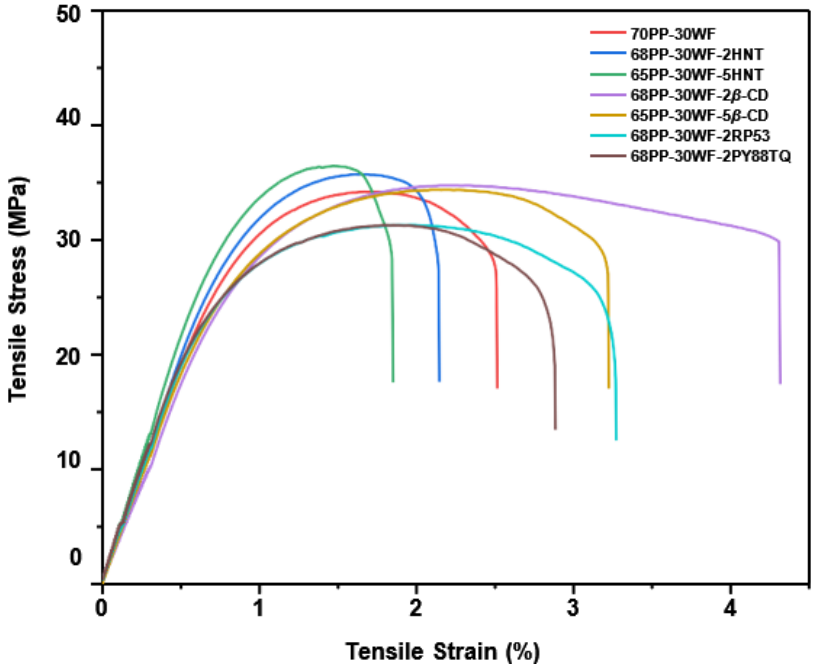

Figure 5. Stress-strain graph of the 30 wt. %WF containing WPC and formulations with the additives

Table 3. Table of tensile test results of the samples

	Tensile Strength (MPa)	Tensile Modulus (MPa)	Tensile Strain at Break (%)	Tensile Strength at Break (MPa)	Yield Stress (MPa)
70PP-30WF	34.2 (±0.3)*	3971.1 (±53.7)	2.5 (±0.1)	28.3 (±0.7)	34.2 (±0.3)
68PP-30WF-2HNT	35.8 (±0.7)	4312.6 (±207.8)	2.1 (±0.1)	29.9 (±1.1)	35.8 (±0.7)
65PP-30WF-5HNT	36.5 (±0.4)	4504.5 (±228.9)	1.8 (±0.1)	29.9 (±2.5)	36.5 (±0.4)
68PP-30WF-2β-CD	34.8 (±0.9)	3458.7 (±58.9)	4.3 (±1.4)	30.0 (±13.7)	34.8 (±0.9)
65PP-30WF-5β-CD	34.4 (±0.5)	3866.1 (±260.2)	3.2 (±1.2)	28.3 (±12.1)	34.4 (±0.5)
68PP-30WF-2RP53	31.3 (±1.0)	4097.8 (±292.7)	3.2 (±0.7)	21.5 (±7.5)	31.3 (±1.0)
68PP-30WF-2PY88TQ	31.3 (±0.9)	4403.1 (±183.3)	2.9 (±0.6)	22.4 (±10.1)	31.3 (±0.9)

*Values in parentheses are standard deviations

The results indicated that the tensile modulus of PP was increased by 63 % by adding 30 wt.% WF. From analysis of the additives on the modulus of WPCs, it can be seen that the tensile modulus increased proportionally with the content of HNT, and the most noticeable increase was observed in the WPC containing 5 wt.% HNT. The enhancement is due to the restriction of movement at molecular chains PP by HNT hence giving more resistance to deformation for the material. The modulus values of WPCs containing 30 wt.% wood fiber were approximately increased by 8 (±0.7) %, 12 (±0.8) %, 3 (±0.8), % and 10 (±0.7) % after the addition of 2 wt.% and 5 wt.% HNT. 2 wt.% RP53, and 2 wt.% PY88TQ, respectively. However, the addition β-CD at concentrations of 2 wt.% and 5 wt.% resulted in a reduction in the modulus of 13 (±0.09) % and 3 (±0.8) %, respectively. This decrease can be explained by the weak binding interactions that exist between the PP polymer and β-CD. During the procedure, the complexing agent may be reduced due to hydrophobic, inactive, and non-adhering polymer. Tensile strength followed a similar trend to tensile modulus for HNT containing WPCs. So, integrating 2 wt.% HNT and 5 wt.% HNT to WPC increased the tensile strength by 4.5 (±0.6) % and 6.3 (±0.3) %, respectively. This can be attributed to improved fiber-matrix interaction, as confirmed by FESEM imaging. HNT likely acts as a rigid filler and nucleating agent, contributing to the stiffness and load-bearing capacity of the composite (Krishnaiah et al, 2020).

The tensile strength of 2 wt.% and 5 wt.% β-CD including WPCs slightly increased 1.7 (±0.7) % and 0.6 (±0.4) %, respectively. Conversely, 2 wt.% β-CD provided the highest strain at break (4.3%), suggesting improved toughness. The reduction in elongation in HNT-reinforced WPCs can be explained by the fact that the increasing HNT content, particularly at 5 wt.%, restricts the movement of polymer chains, preventing them from aligning in the direction of tension. Additionally, HNT aggregation in the PP matrix creates stress concentration points, leading to premature fractures (Tekay et al, 2020).

2.5.4 Morphological Analysis Result

Figure 6 presents FESEM micrographs obtained from the cross-sectional fracture surfaces of specimens broken during tensile testing. Neat polypropylene (PP), was imaged as the control for comparison, as shown in Figure 6a, was imaged as the control for comparison and exhibits a smooth and relatively featureless surface with occasional voids and fiber-like elongations. This morphology is typical of ductile polymers and supports its baseline mechanical behavior, particularly lower stiffness, and higher strain at break. Figure 6b

demonstrates that the addition of 30 wt.% WF results in a less smooth surface and more brittle, fractured fibrous ends. Furthermore, debonding, fiber pull-out, and voids left by broken fibers indicate a distinct interface between the PP matrix and the wood fibers. The weak interfacial bonding between the hydrophilic WF and the hydrophobic PP matrix is a phenomenon also widely documented in natural fiber composites (Joseph et al, 1999). At low HNT content, the FESEM images (Figures 6c and 6d) show homogeneously dispersed nanoparticles and reduced voids, confirming improved interfacial adhesion and stress transfer. These morphological improvements are mirrored in tensile strength as well (Krishnaiah et al, 2020). HNT nanoparticles that have particle sizes under 200 nm within the PP matrix as seen in Figure 6c. The same chromatogram also includes the effect of fibrous structure of PP. Figure 6d illustrates that increasing the HNT content from 2 wt.% to 5 wt.% results in a rougher surface morphology. In the composite containing 2 wt.% HNT, distinct holes are observed, whereas in the 5 wt.% HNT sample, these are replaced by shallower surface cavities. This change suggests improved dispersion and interaction of HNTs within the matrix at higher loading levels, which is consistent with findings reported in similar polymer nanocomposite systems (Li & Shimizu, 2009). Additionally, while thicker wood fibers generally exhibit reduced interfacial adhesion with the polypropylene (PP) matrix, thinner wood fiber enhance matrix-fiber interaction due to their larger specific surface area and improved wettability (Stark & Rowlands, 2003). This improved adhesion, combined with the increased HNT content, contributes to the best reinforcing effect observed in the WPC formulation containing 5 wt.% HNT. As demonstrated in Figure 6e, WPC with the commercial additive RP53 has micro-fractured fibrous ends on the matrix surface. In the WPC prepared with PY88TQ, due to the insufficient bond between the fiber and the matrix, the voids caused by the particles that migrated on the matrix surface and the gap between the fiber were visually revealed with Figure 6f. The addition of 2 wt.% β-CD to WPC, as shown in Figure 6g, results in a uniform and smooth surface, offering the highest toughness among the WPC samples and preventing crack propagation in the wood fibers. Conversely, Figure 6h shows that increasing the β-CD content to 5 wt.% reduces the toughness of the WPC. Additionally, the inclusion of β-CD visibly improves the adhesion between PP and WF.

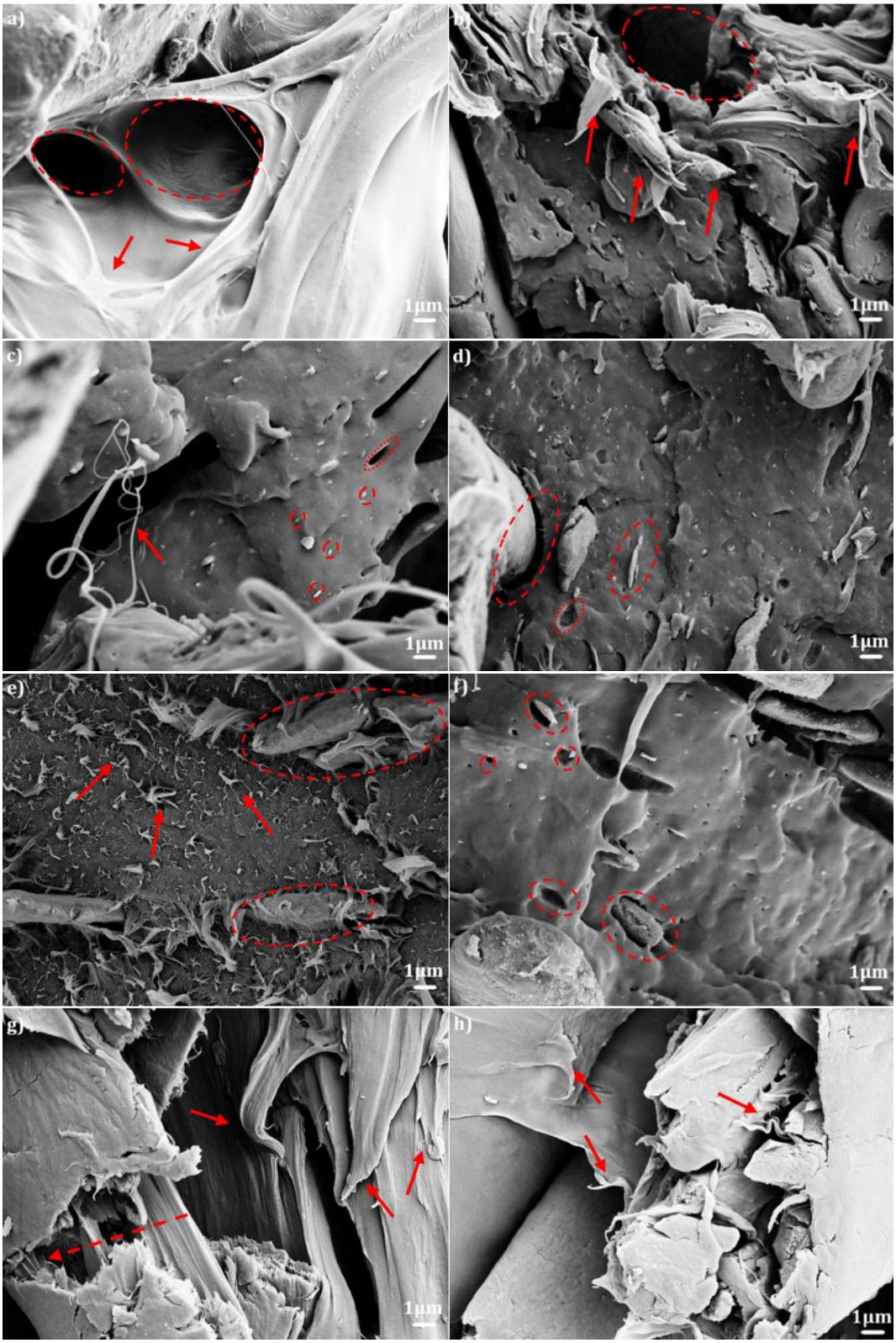

Figure 6. FESEM micrographs of the specimens: (a) neat PP (b) 70PP-30WF, and (c) 68PP-30WF-2HNT (d) 65PP-30WF-5HNT (e) 68PP-30WF-2RP53 (f) 68PP-30WF-2PY88TQ (g) 68PP-30WF-2 β-CD (h) 65PP-30WF-5 β-CD

2.5.5 Fourier-Transform Infrared (FTIR) Spectroscopy Analysis

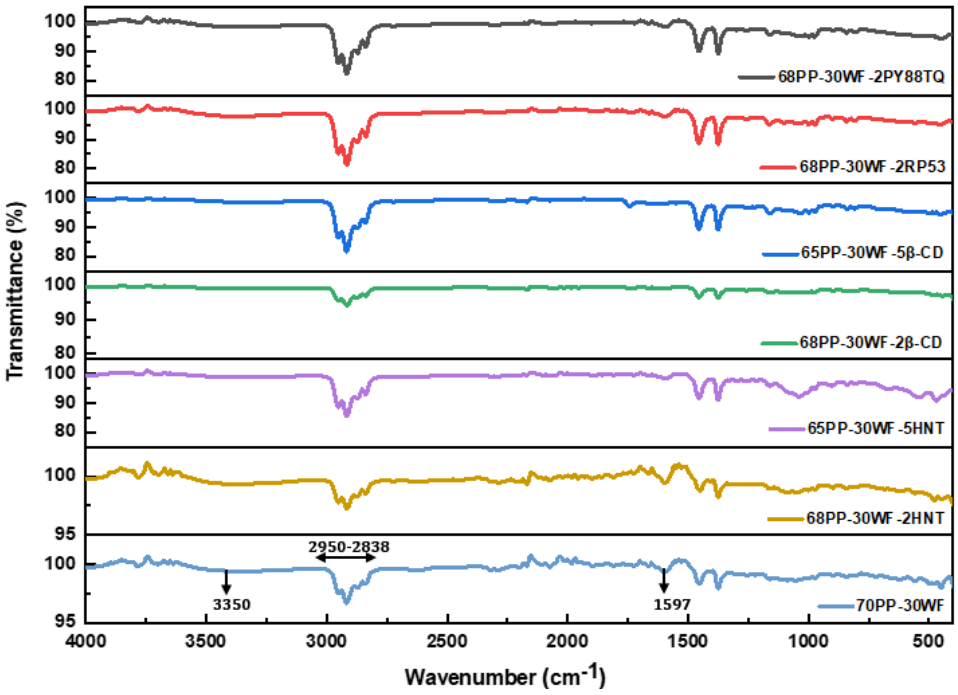

Figure 7. FT-IR spectra of WPC samples composed of PP and 30 wt. % WF

The FT-IR spectra analysis results of WF and PP based WPC composites containing 2 wt.% and 5 wt.% HNT, *β*-CD, and 2 wt.% RP 53 and PY88TQ are presented in Figure 7. The broad absorption peak at 3350 cm−1 corresponds to the O−H stretching of the alcoholic and phenolic hydroxyl groups in WPC belonging to WF. This broadening disappeared especially with the addition of 5 wt.% HNT due to the interaction of their free hydroxyl groups with those in WPC (Lee & Chang, 2012). Additionally, this bonding causes the C-O ether peak at 1052 cm-1 to be more intense than the others. The interaction of 2 wt.% HNT and *β*-CD with WPC resulted in a decrease in the intensity of characteristic peaks of C-H methylene groups (symmetric and asymmetric) and stretching vibration of the alkyl structure of the aliphatic group of PP at 2950, 2918, 2872, and 2838 cm−1. The stretching vibrations of the aliphatic -C=C- bonds appear at 1597 cm−1, with bond breakage spotted in WPC samples containing 2 wt.% and 5 wt.% *β*-CD and 5 wt.% HNT (Kadam et al, 2020). These results support the interaction of HNT, and B-CD with WPCs and their influence on their structural properties.

2.5.6 Thermogravimetric Analysis

The thermal stability of WPC with PP matrix was evaluated through TGA and DTG analyses, as shown in Figure 8, with the results provided in Table 4. All thermograms (weight change vs temperature at the top and derivative of weight change vs temperature

at the bottom) which belong to WPCs in Figure 8 have similar trends. The thermal degradation of all WPCs was comprised of two stages. It is based on the fact that heterogeneity occurs in the polymer matrix in which the wood fiber is incorporated (Mohanty et al, 2002). Results table and thermograms show that the first degradation observed in WPCs occurs at 361 °C by 5 wt.% β-CD and HNT added WPC which is close to the WPC without additive. While other additives have slightly higher degradation temperature, the highest one belongs to the commercial additives and 2 wt.% HNT added WPCs with 364 °C and 363 °C. The ability HNTs which of relatively well-dispersed in PP matrix to trap VOCs occurring during thermal degradation and limit polymer molecule mobility is responsible for the improved thermal stability (Guo et al, 2010; Wang & Huang, 2013). The same phenomenon was observed at the second decomposition stage. The curves in this stage started around 406 °C are not so similar as in the first step with highest weight loss which belongs to 2wt.% β-CD added WPC (Esmizadeh et al, 2020). However, the maximum peak decomposition temperature around 472°C was observed in the 2 and 5 wt.% HNT containing WPC, which exhibited the lowest weight loss of WPC with 2 wt.% HNT approximately 66% in this stage. The residue remaining at the end of the analysis was higher for HNT added WPCs due to high thermal stability of HNT which resulted in higher degradation temperature. This phenomenon can be attributed to the high barrier effect of HNT that covers the surface, distributes heat, and delays the combustion. Notably, HNT is significantly reduced by the rate of degradation as seen in Figure 5.

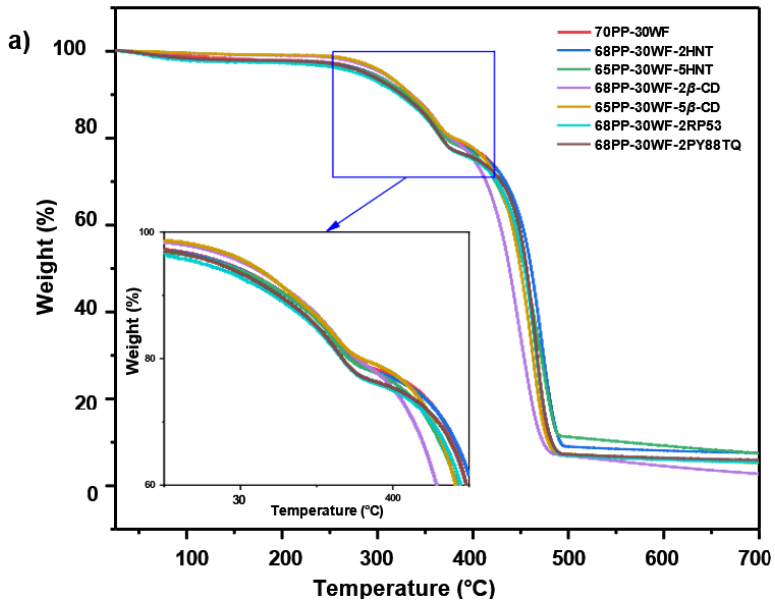

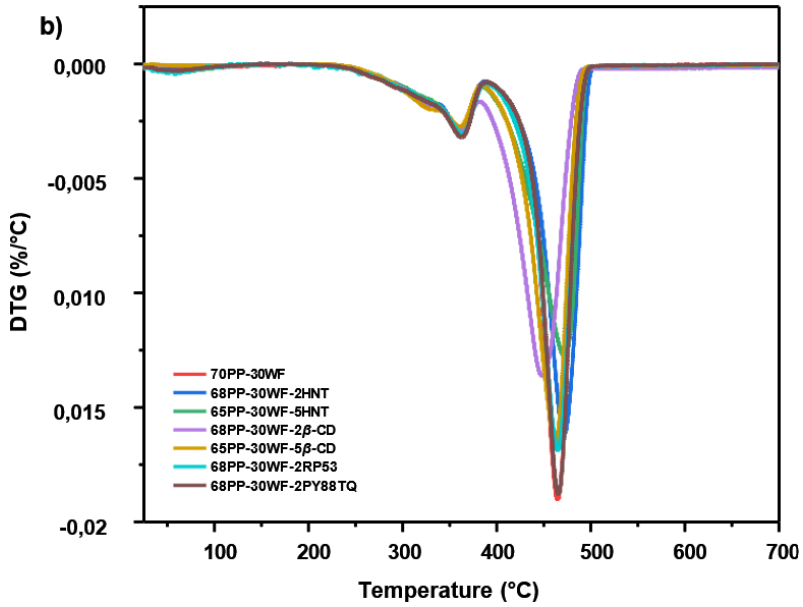

Figure 8. TGA thermograms of all PP and 30 wt. %WF added WPC samples

Table 4. Degradation temperatures, weight loss and residue (%) of WPCs

	1st degradation		2nd degradation		
	Peak (°C)	**Weight Loss (%)**	**Peak (°C)**	**Weight Loss (%)**	**Residue@ 700 °C (%)**
70PP-30WF	361.0	21.9	465.0	72.4	5.6
70PP-30WF-2HNT	363.0	26.2	471.0	66.0	7.4
65PP-30WF-5HNT	361.0	21.5	472.0	70.8	7.5
68PP-30WF-2*β*-CD	362.0	19.7	449.0	76.4	2.7
65PP-30WF-5*β*-CD	361.0	21.3	463.0	73.4	5.3
68PP-30WF-2RP53	364.0	24.4	465.0	70.4	5.3
68PP-30WF-2PY88TQ	363.0	23.9	466.0	69.9	5.9

2.5.7 DSC Analysis

The changes on the thermal transition temperatures of the specimens were examined by DSC analysis. The endothermic melting and exothermic crystallization thermograms obtained from DSC analysis are shown in Figures 9a and 9b below. In addition, melting temperature (Tm), cold crystallization temperature (Tc), melting enthalpy (ΔHm), cold crystallization enthalpy (ΔHc), and crystallinity (Xc) thermograms are given in Table 5. It was found that the melting temperature of PP increased after the 30 wt.% WF addition,

indicating that the crystallization rate of WPC has accelerated. Following this, the temperature and degree of crystallization decreased with the addition of wood fiber content. The explanation for these declines is that wood fibers may hinder the flow of PP polymer and its molecular rearrangement, causing the crystallization process to be retarded. The addition of HNT to WPC led to an increase in melting temperature of about 1.5 % and 7.5 % of crystallization temperatures. Additionally, a decrease in crystallization degree of about 6 % was observed due to interfacial interaction between HNT and PP (Li et al, 2018b). This may be caused by silanol groups on the HNT surface hindering the movement of molecules in the PP polymer chain, preventing molecular packing (Bidsorkhi et al, 2015). Another explanation of this is that HNT causes polymer chains to crystallize more quickly when cooled. HNT functioned as a nucleation agent for PP, reducing the spherulite size and retarding PP crystal growth. Additionally, higher HNT loading (5 wt.% in WPC) yields aggregation in the PP matrix, and aggregated HNTs have lower nucleation capability due to reduced specific surface area, resulting in decreased crystallinity (Liu et al, 2009). The melting and crystallization temperatures in WPC are close to those of 2 wt.% RP53 and PY88TQ. However, PY88TQ has the highest degree of crystallization among other WPCs and is similar to Neat PP. This effect is the inverse of using RP 53 in WPC. The addition of 2 and 5 wt.% β- CD had no significant effect on the melting and crystallization temperature or degree of crystallinity in the WPC.

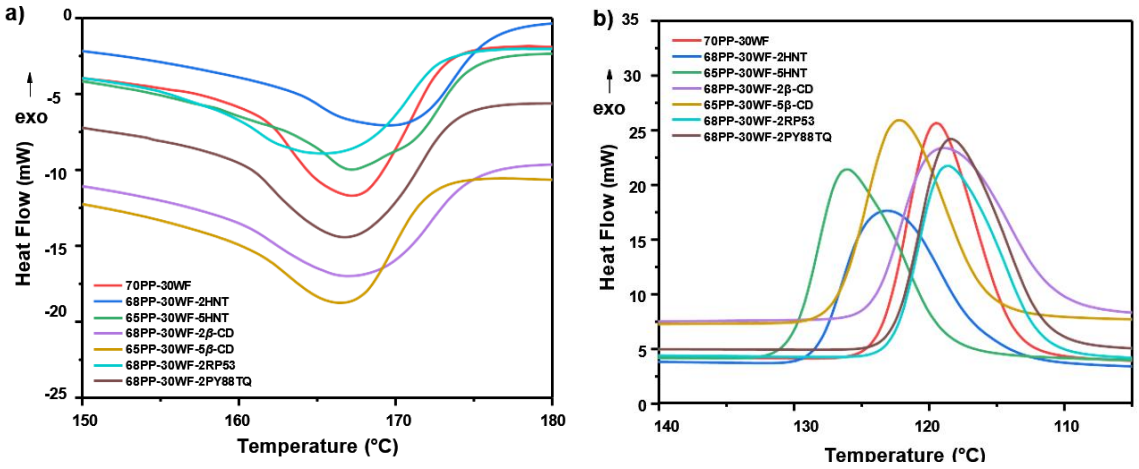

Figure 9. DSC thermograms of PP and 30 wt.%WF added WPC, 2 and 5 wt.% HNT and β-CD added WPCs, and 2 wt.% RP 53 and PY88TQ added WPCs samples : a) melting peaks, b) crystallization peaks

Table 5. DSC Summary of Tm, Tc, ΔHm, ΔHc, and Xc of the WPC with PP matrix samples

Sample Name	Tm (°C)	Tc (°C)	ΔHm (J/g)	ΔHc (J/g)	ΔHm° (J/g)	Xc (%)
70PP-30WF	166.7	120.4	74.1	71.6	207.0	51.1
70PP-30WF-2HNT	169.2	123.8	69.1	68.9	207.0	47.7
65PP-30WF-5HNT	166.8	130.2	69.7	68.6	207.0	48.1
68PP-30WF-2*β*-CD	166.1	119.8	73.8	73.6	207.0	50.9
65PP-30WF-5*β*-CD	165.7	123.1	71.9	70.5	207.0	49.6
68PP-30WF-2RP53	164.9	119.3	70.4	72.5	207.0	48.6
68PP-30WF-2PY88TQ	166.2	119.2	78.7	73.6	207.0	54.3

2.5.8 Brunauer–Emmett–Teller (BET) Analysis

To better understand the adsorption behaviors of the HNTs and *β*-CD, the surface area and porosity characteristics of them were evaluated using nitrogen adsorption–desorption isotherms and Brunauer–Emmett–Teller (BET) analysis. The corresponding isotherms and pore size distributions are presented in Figure 10, and the key parameters are summarized in Table 6.

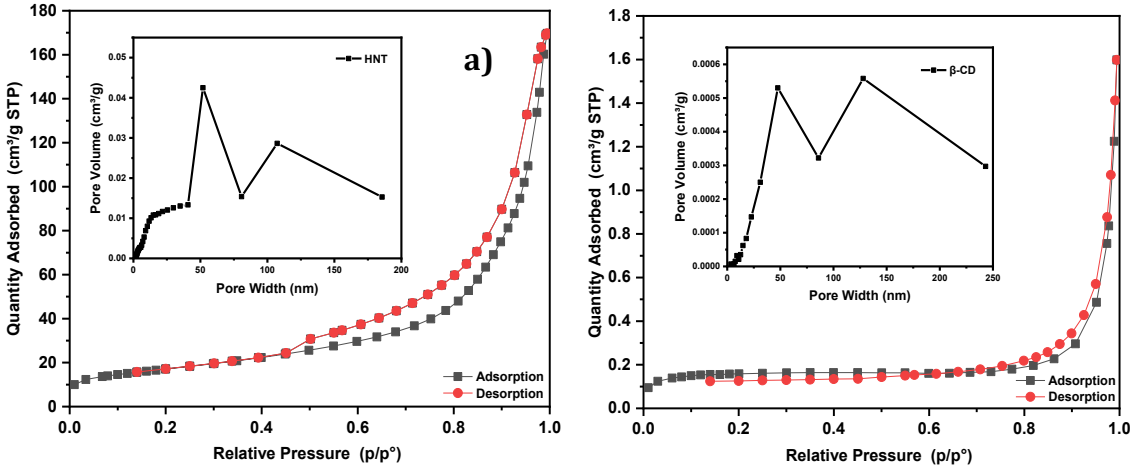

Figure 10. BET adsorption–desorption isotherms and pore size distribution graphs for (a) HNTs and (b) β-CD

Table 6. Tabulated values (bottom) for surface area and pore volume for HNTs and β-CD

Sample Name	BET Surface Area [m^2/g]	Total Pore Volume [cm^3/g]	Average pore diameter [nm]
HNT	60.71	0.1622	10.69
β-CD	0.52	0.000737	5.65

The distinct adsorption behaviors of HNTs and *β*-CD observed as VOC reduction in WPCs can be explained through their nitrogen adsorption–desorption isotherms and corresponding pore size distribution. BET analysis demonstrated the contrasting adsorption behaviors of HNT and *β*-CD. As shown in Figure 10a, the isotherm for HNTs displays a typical type IV behavior with a pronounced H3-type hysteresis loop, indicative of mesoporous structures (Thommes et al, 2015). The characteristics of surface area, total pore volume and average pore diameter that shown in Table 6 point to surface area of 60.71 m^2/g and a mesoporous network (average pore size: 10.69 nm), favoring multilayer adsorption and VOC diffusion. The pore size distribution (in Figure 10a) reveals dominant mesopores around 10–15 nm, further confirming the material's capacity for accommodating relatively large VOC molecules and promoting physical adsorption through increased surface interactions (Lvov & Abdullayev, 2013). In contrast, the adsorption–desorption isotherm of *β*-CD (Figure 7b) exhibits a much flatter profile with a very low total pore volume (0.000737 cm^3/g) and BET surface area (0.52 m^2/g), suggesting limited textural porosity. The average pore diameter, 5.65 nm, aligns with the expected dimensions of *β*-CD's toroidal molecular structure. The pore size distribution (in Figure 10b) confirms a narrow range of mesopores with low volume, reinforcing its relatively low bulk adsorption capacity (Loftsson & Duchêne, 2007). Despite these limitations, *β*-CD's effectiveness in targeting specific VOCs arises from its ability to form host–guest inclusion complexes through its hydrophobic cavity and hydrophilic exterior. This enables selective trapping of small polar VOCs, such as formaldehyde and aromatic compounds and also benzaldehyde, as supported by GC-MS data (You et al, 2021; Crini, 2005; Li et al, 2020; Saenger, 1980). Therefore, while HNTs primarily contribute through high-capacity, non-selective adsorption enabled by their large surface area and mesoporous network, *β*-CD offers selective molecular recognition. These complementary

properties suggest their suitability for tailored WPC applications depending on whether bulk VOC reduction or targeted adsorption is prioritized.

2.6 Conclusions

This study reveals that halloysite nanotubes (HNT) and β-cyclodextrin (β-CD) function as effective additives for enhancing the odor reduction, strength, and thermal resistance of wood plastic composites (WPCs) derived from polypropylene. HNT enabled this through considerable non-selective adsorption due to its mesoporous structure. β-CD, alternatively, efficiently trapped polar VOCs via host–guest inclusion complexation. Both sensory (jar) odor analysis and HS GC-MS tests showed that the formulation containing 5 wt.% HNT and 2 wt.% β-CD significantly reduced most of the VOC emissions, including 4-methyloctane, which is one of the key odorous compounds in WPCs with a polypropylene matrix.

The integration of HNT increased the material's strength and elasticity, whereas the addition of β-CD increased its toughness without compromising its total strength. Thermal and spectroscopic analyses shown that each addition is associated with the polypropylene matrix distinctly. The BET results confirmed their individual adsorption characteristics, illustrating their collaborative functionality in multiple uses.

The usage of each HNT and β-CD effectively produces WPCs that convey restricted odors while functioning successfully in indoor applications. In the future, the investigation of modifying the surfaces of HNT and β-CD to further improve their multifunctionality in composite systems.

3. REDUCTION OF VOLATILE ORGANIC COMPOUNDS WITH HYDRAZINE-, CARBOXYBETAINE- AND AMINOSILANE-FUNCTIONALIZED HALLOYSITE NANOTUBE IN RECYCLED POLYOLEFIN BLENDS

3.1 Abstract

Recycled polyolefin (rPO) is a promising material for sustainable applications, but its use is limited by the release of volatile organic compounds (VOCs), which cause odor and reduce indoor air quality. This study introduces a strategy to address this issue by chemically modifying halloysite nanotubes (HNTs) to improve their VOC adsorption efficiency and multifunctional performance in rPO. HNTs were functionalized through a three-step process involving N-[3-(trimethoxysilyl)propyl]ethylenediamine (TMPED), monochloroacetic acid (MCA), and hydrazine hydrate (HH), producing amine-rich surfaces. Modified HNTs were incorporated into rPO at 2 and 5 wt.% and compared with unmodified HNTs. VOC reduction was assessed using headspace gas chromatography–mass spectrometry (HS GC-MS) and jar testing, while structure and properties were analyzed by FTIR, NMR, TGA, DSC, SEM, BET, and tensile tests. The 5 wt.% TMPED-MCA-HH-HNT composite reduced total VOC intensity by 91%, particularly key odorants such as acetaldehyde and cyclotrisiloxane. This effect is attributed to dual action: physical adsorption in the HNT lumen/mesopores and selective chemisorption via hydrogen bonding and Schiff base formation between amine/hydrazide groups and polar VOCs. Thermal stability, tensile modulus (+25.3%), and crystallinity (73.4%) were also improved. These findings highlight functionalized HNTs as efficient additives for enhancing both mechanical and odor performance of rPO.

3.2 Introduction

Interest in recycling widely used thermoplastic blends like recycled polyolefins has emerged due to the transition to a circular economy. The mechanical strength, chemical durability, and affordability of these materials make them highly valued. The economic and environmental advantages of recycling coexist with limitations on using reclaimed thermoplastics in consumer and indoor products. The primary problem involves the emission of volatile organic compounds (VOCs). The degradation of materials occurs when they break down due to high temperature while processing combined with residual additives and impurities from prior usages (Kang et al., 2020). Occupational exposure studies in small-scale recycling facilities have measured TVOC levels averaging around 1 625 µg/m³ for recycled polypropylene (rPP), compared to approximately 1 190 µg/m³ for recycled polyethylene (rPE) (Lvov & Abdullayev, 2013). These levels are sufficiently high to cause odor issues, challenge regulatory compliance, and affect consumer acceptance, underscoring the urgency for effective VOC mitigation.

To address these challenges, researchers have explored several mitigation strategies, including post-processing stabilization, incorporation of antioxidants, and the use of physical or chemical absorbents. Among these, halloysite nanotubes (HNTs) have attracted particular interest because of their unique structural and chemical features. HNTs are naturally occurring aluminosilicate clays that are characterized by their tubular morphology and high aspect ratio, which provide a large surface area and a lumen structure advantageous for encapsulating small organic molecules (Cavallaro et al., 2017; (Alongi et al., 2012). Prior studies have demonstrated the potential of HNTs in VOC reduction applications; for instance, they have been employed to trap aldehydes released during polymer degradation and to reduce alcohol emissions through adsorption within their lumen structure (Ansar et al., 2021). Such findings underscore their promise as an effective additive compared with other nanofillers that lack internal cavities or tunable surface chemistry. Despite these advantages, the relatively inert surface chemistry of neat HNTs hinders their ability to adsorb polar VOCs, which include aldehydes and alcohols. Different surface modification strategies have been developed to enhance the interaction potential. Functionalization with groups such as amines, carboxyls, or silanes substantially improves chemical affinity for polar VOCs. The addition of amine-containing molecules promotes improved interactions via hydrogen bonding and Schiff

base formation with aldehydic VOCs. Previous studies applying such amine modifications have reported significant enhancements in adsorption efficiency toward polar VOCs. For example, aminated HNTs were shown to reduce formaldehyde and acetaldehyde concentrations by up to 40–60% (Lvov & Abdullayev, 2013b; (Ghaffari et al., 2014), though challenges remain in achieving long-term stability and high adsorption under realistic recycling conditions. These limitations justify the need for further development of more robust modification routes.

The present research employs a novel multi-step chemical modification process to improve the VOC adsorption capacity of HNTs. This process involves the functionalization of HNT by using N-[3-(trimethoxysilyl)propyl]ethylenediamine (TMPED), achieved by a series of reactions with monochloroacetic acid (MCA) and hydrazine hydrate (HH), ending in the formation of TMPED-MCA-HH-HNTs characterized by improved surface polarity and reactivity. TMPED was selected as the modifying agent because of its bifunctional nature: its amine groups provide strong interaction potential with polar VOCs through hydrogen bonding and Schiff base chemistry, while the trimethoxysilane moiety allows for covalent anchoring onto the HNT surface, ensuring stability of the modification. Compared with other silane coupling agents, TMPED offers both enhanced reactivity and improved compatibility with polar organic species, making it particularly suitable for odor reduction in recycled polyolefins (Fitri et al., 2021).

The modified HNTs were added to recycled polyolefin at levels of 2 wt.% and 5 wt.%, and their effectiveness was evaluated using unmodified HNTs. VOC emissions were analyzed via headspace gas chromatography–mass spectrometry (HS GC-MS) and analyzed by using sensory jar tests. Additionally, the mechanical, thermal, morphological, and interfacial characteristics of the composites were examined through tensile testing, thermogravimetric analysis (TGA), differential scanning calorimetry (DSC), scanning electron microscopy (SEM), Fourier-transform infrared spectroscopy (FTIR), and BET surface area measurements.

Overall, this study aims to develop and test an amine-functional silane modification strategy for halloysite nanotubes to enhance their ability to capture odor-causing VOCs in recycled polyolefins. By introducing amine-based groups, the modified nanotubes are expected to interact more effectively with polar VOCs while maintaining stable integration into the polymer matrix. The objective is to evaluate whether this approach

can reduce odor emissions while preserving the mechanical performance of rPO, thereby supporting its use in higher-value applications.

Interest in recycling widely used thermoplastic blends like recycled polyolefins has emerged due to the transition to a circular economy. The mechanical strength, chemical durability, and affordability of these materials make them highly valued. The economic and environmental advantages of recycling coexist with limitations on using reclaimed thermoplastics in consumer and indoor products. The primary problem involves the emission of volatile organic compounds (VOCs). The degradation of materials occurs when they break down due to high temperature while processing combined with residual additives and impurities from prior usages (Kang et al, 2020c).

These VOCs can produce unpleasant odors and bring issues for regulatory compliance and product acceptance. It has been investigated using various approaches, including post-processing stabilization, the addition of antioxidants, and the application of physical or chemical absorbents. Halloysite nanotubes (HNTs) have received considerable attention. HNTs are naturally occurring aluminosilicate clays characterized by their tubular morphology and enhanced aspect ratio, which provide an increased surface area and a lumen structure advantageous for encapsulating small organic molecules (Massaro et al, 2017; Kamble et al, 2012).

Despite these advantages, the relatively inert surface chemistry of neat HNTs hinders their ability in adsorbing polar VOCs, which includes aldehydes and alcohols. Different surface modification strategies have been developed to enhance interaction potential. Functionalization with groups such as amines, carboxyls, or silanes substantially improves chemical affinity for polar VOCs. The addition of amine-containing molecules promotes improved interactions via hydrogen bonding and Schiff base formation with aldehydic VOCs (Massaro et al, 2018; Jin et al, 2019).

The present research employs a novel multi-step chemical modification process to improve the VOC adsorption capacity of HNTs. This process involves the functionalization of HNT by using N-[3-(trimethoxysilyl)propyl]ethylenediamine (TMPED), achieved by a series of reactions with monochloroacetic acid (MCA) and hydrazine hydrate (HH), ending in the formation of TMPED-MCA-HH-HNTs characterized by improved surface polarity and reactivity.

The modified HNTs were added to Recycled polyolefin at levels of 2 wt.% and 5 wt.%, and their effectiveness was evaluated against unmodified HNTs. VOC emissions were

analyzed via headspace gas chromatography–mass spectrometry (HS GC-MS) and analyzed by using sensory jar tests. Additionally, the mechanical, thermal, morphological, and interfacial characteristics of the composites were examined through tensile testing, thermogravimetric analysis (TGA), differential scanning calorimetry (DSC), scanning electron microscopy (SEM), Fourier-transform infrared spectroscopy (FTIR), and BET surface area measurement.

This study provides a scalable and material-efficient solution for decreasing odor emissions in Recycled polyolefin through using chemically modified halloysite nanotube additives, improvement of the performance and applicability of rPO in high-value applications.

3.3 Materials and experimental

3.3.1 Materials

Recycled polyolefin (rPO) polymer, in light green pellet form and consisting of 70 wt.% polyethylene (PE) and 30 wt.% polypropylene (PP), derived from production waste, was supplied by Hayat Kimya (Kocaeli, Türkiye). N-[3-(Trimethoxysilyl)propyl]ethylenediamine (TMPED), monochloroacetic acid (MCA), and toluene were purchased from Sigma-Aldrich (Merck Group, St. Louis, MO, USA). Halloysite nanotubes (HNTs), in white powder form, were obtained from Esan Eczacıbaşı Industrial Raw Materials Industry and Trade Inc. (Maltepe, Türkiye). Hydrazine hydrate (HH) was supplied in liquid form by Sigma-Aldrich Chemie GmbH (Taufkirchen, Germany).

3.3.2 Surface Modification of Halloysite Nanotubes with a Silane Compound Containing Amino Groups

Initially, N-[3-(Trimethoxysilyl)propyl]ethylenediamine (TMPED, 1 mol) was reacted with monochloroacetic acid (MCA, 3 mol) to obtain a difunctional silane intermediate. In this reaction, the chloroacetic acid molecules were covalently bonded to the primary amine groups of TMPED through nucleophilic substitution, resulting in the formation of bis-amide linkages. The resultant compound (TMPED-MCA, or carboxybetaine) was then reacted with hydrazine hydrate (HH) to transform the terminal carboxylic acid groups into hydrazide groups, producing a silane compound abundant in

amino functionalities (TMPED-MCA-HH, or aminosilane). The synthesized amino-functional silane compound was subsequently attached to the surface of halloysite nanotubes (HNTs) by refluxing in toluene at 75 °C for 4 hours. Functionalization was facilitated by the hydrolysis of the methoxy groups followed by condensation with the surface hydroxyl groups of HNTs. The modified nanotubes were recovered via vacuum filtration and dried under vacuum at 25 °C for 15 hours. To investigate the individual effects of each modification step on the final surface properties of the HNTs, additional samples were prepared by modifying the HNTs separately with TMPED and with TMPED-MCA under identical reaction conditions. The extent of surface modification was confirmed qualitatively by the appearance of characteristic absorption bands of functional groups in FTIR spectra and by the additional organic mass loss observed in TGA, which consistently indicated successful stepwise grafting of TMPED, TMPED-MCA, and TMPED-MCA-HH onto the HNTs. A schematic representation of all modification steps is provided in Figure 11.

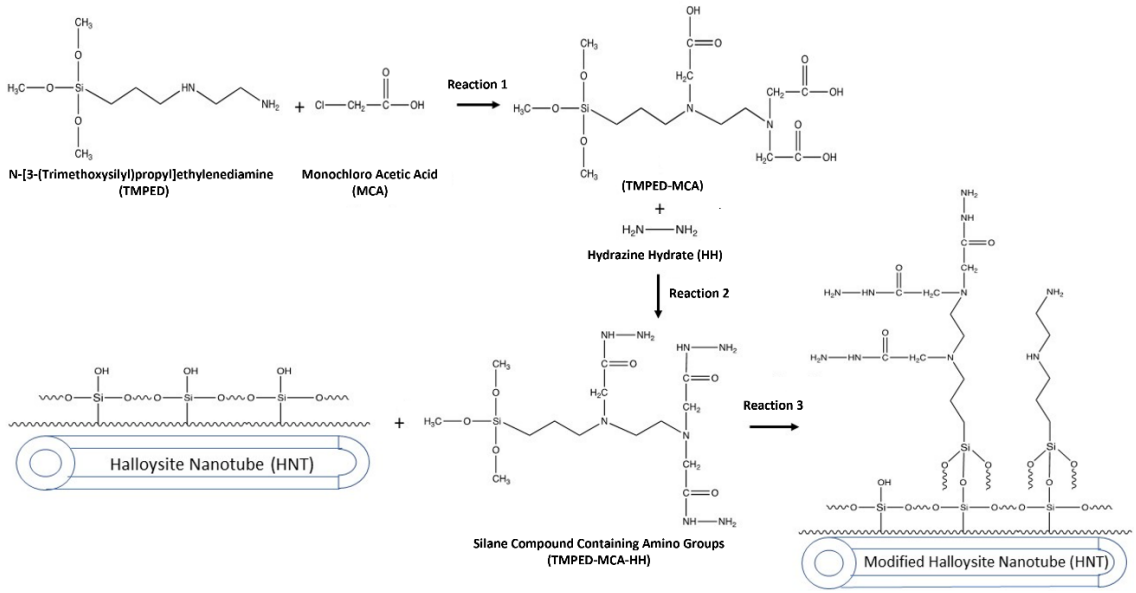

Figure 11. The reaction steps of HNT modification with silane compound containing amino group

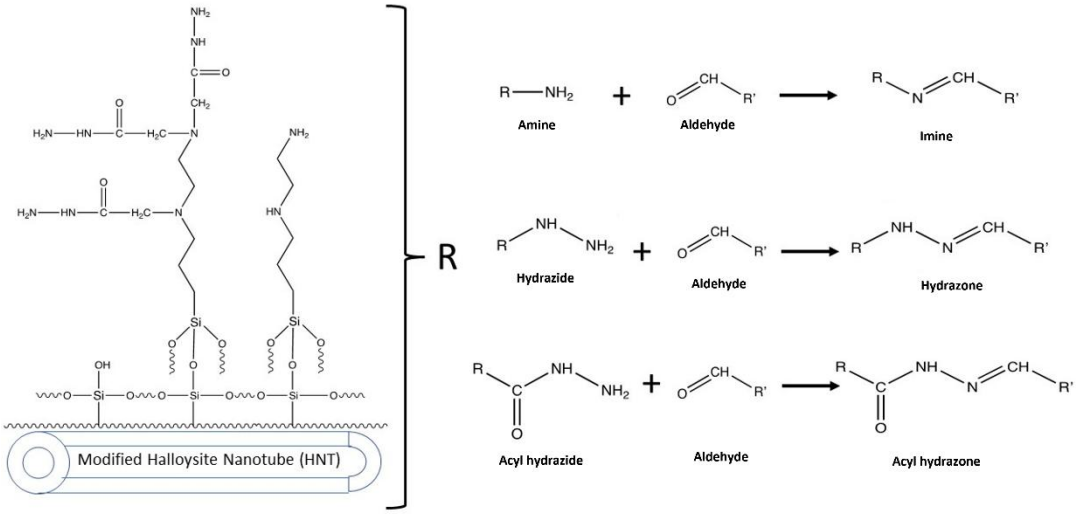

Figure 12. Reactions of functional groups of modified HNT with silane compound containing amino group with aldehydes

The functional end groups of HNT modified with the silane compound containing amino groups are able to bond with aldehydes and form imine, hydrazone, and acyl hydrazone groups, as shown in Figure 12. Therefore, aldehydes and other VOCs that could interact with these functional end groups were captured through chemical reactions with the modified HNT. Also, you can find the modification of HNT steps in Figure 13.

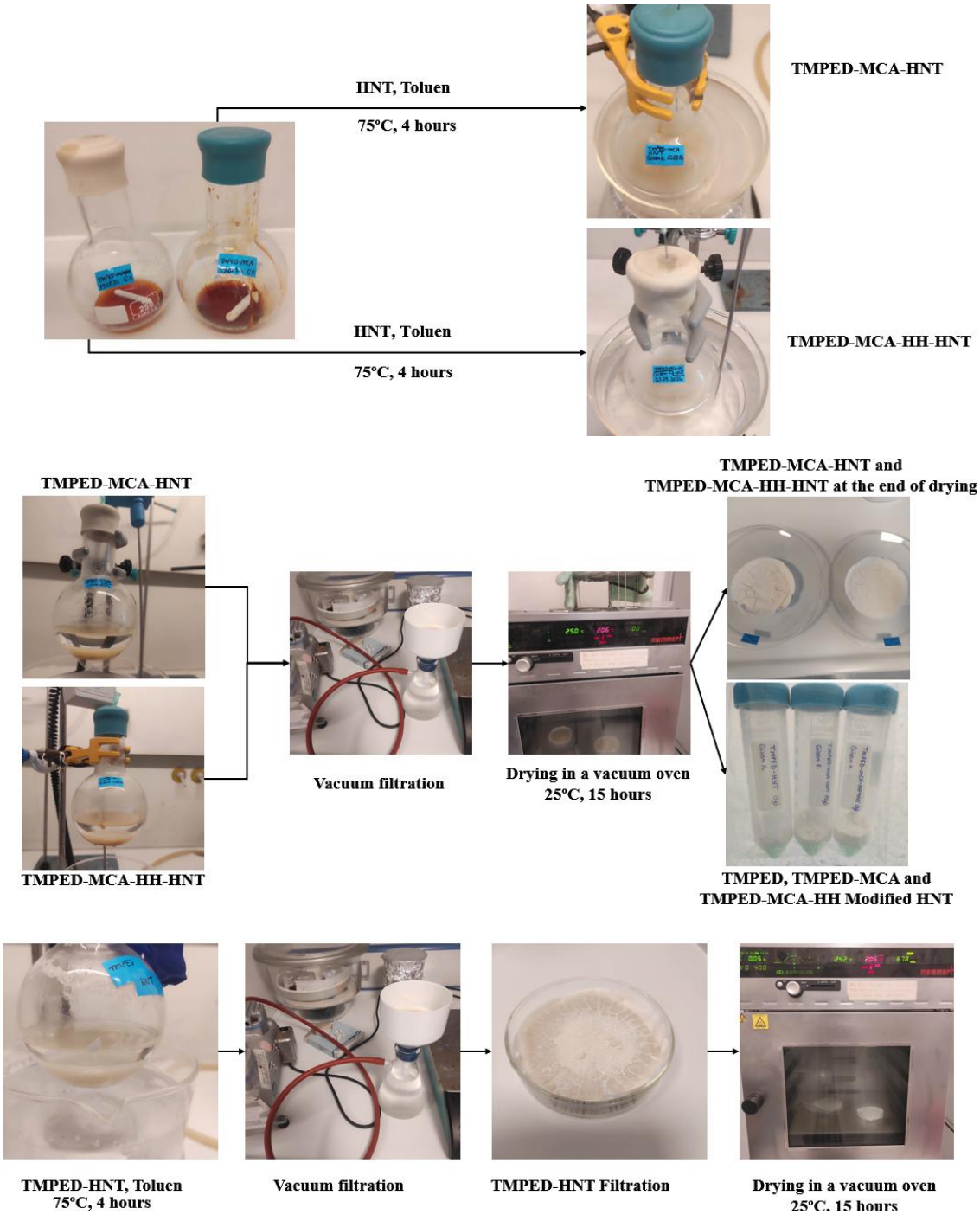

Figure 13. Modification steps of TMPED-MCA and TMPED-MCA-HH Compounds with HNT.

3.3.3 Processing of Recycled Polyolefin/Modified HNT Nanocomposites

The recycled neat polyolefin (rPO), 2 and 5 wt.% HNT, and 5 wt.% HNT modified with N-[3-(Trimethoxysilyl)propyl]ethylenediamine (TMPED) (TMPED-HNT), with the product of the second reaction (TMPED-MCA-HNT), and with the silane compound containing amino groups (TMPED-MCA-HH-HNT) were compounded using an ultra-high-speed thermokinetic mixer, Gelimat GI (Draiswerke, US). After compounding, a plastic granulator (Rhong Machinery, China) was used to crush the materials into granules. The granules were then molded in an injection molding machine (Xplore, Sittard, Holland) to form specimens for tensile testing under the ISO 527 standard using a 100 kN Universal Electromechanical Test Machine (Instron, US). Neat rPO, 2 and 5 wt.% HNT (rPO-2HNT, rPO-5HNT), and 5 wt.% HNT modified with TMPED, TMPED-MCA, and TMPED-MCA-HH (rPO-5TMPED-HNT, rPO-5TMPED-MCA-HNT, rPO-5TMPED-MCA-HH-HNT) were obtained at the end of the production process as in figure 14.

Figure 14. Samples formed by molding the granules in the injection device to be used in the tests: rPO-Neat, rPO-2HNT, rPO-5HNT, rPO-5TMPED-HNT, rPO-5TMPED-MCA-HNT, rPO-5TMPED-MCA-HH-HNT

3.4 Material Characterization

3.4.1 Odor (Jar test) Analysis

The Indoor Odor (Jar) test was performed by evaluating the odor of rPO Neat, rPO-2HNT, rPO-5HNT, rPO-5TMPED-HNT, rPO-5TMPED-MCA-HNT, rPO-5TMPED-MCA-HH-HNT that saved in gas-sealed jars at distinct temperatures and time conditions. As preparation conditions for the test, all samples were exposed to air for 12 days.

Following this, they were placed into gas-tight sealed jars with a stainless-steel wire mesh at the bottom to prevent direct contact with 50 ml of distilled water. The samples were then subjected to three different oven conditions: 25 °C for 24 hours, 40 °C for 24 hours, and 65 °C for 2 hours. At the end of each condition, five independent raters evaluated the odor intensity of each sample using an 11-point scale (1 = imperceptible; 1.5 = slightly perceptible; 2 = perceptible but not disturbing; 2.5 = clearly perceptible but not disturbing; 3 = strongly perceptible but not disturbing; 3.5 = intense enough to be slightly disturbing; 4 = disturbing; 4.5 = strong and disturbing; 5 = definitely disturbing; 5.5 = very strong and disturbing; 6 = extremely disturbing). To minimize subjectivity, all samples were randomly assigned and evaluated in mixed order. The overall mean across all five raters was calculated to generate the final reported odor intensity values. The mean odor intensity results are presented in Table 8.

3.4.2 NMR Analysis

^{1}H-nuclear magnetic resonance spectroscopy (1HNMR / X-Pulse, Oxford Instruments, UK) was employed to conduct a detailed examination of the chemical structure of the reactants and intermediates (MCA, TMPED, TMPED-MCA, TMPED-MCA-HH) associated with the Silane Compound Containing Amino Group. Deuterium oxide (D2O) was used as the solvent.

3.4.3 Brunauer−Emmett−Teller (BET) Analysis

The measurement of porous characteristics was performed applying the Brunauer−Emmett−Teller (BET) method at −196.15°C, using a Micromeritics 3Flex Surface Analyzer. Previous to the analysis, the samples undergo a vacuum-outgassing procedure by using the Micrometrics VacPrep061 equipment for a period of 24 hours at a temperature of 150°C. The specific surface area of the samples was measured with nitrogen adsorption and desorption techniques. Additionally, the pore volume and pore size were evaluated according to a maximum amount of nitrogen adsorbed at a relative pressure of P/P_0=0.99.

3.4.4 Headspace Gas Chromatography-Mass Spectroscopy Analysis

The Headspace Gas Chromatography-Mass Spectrometry (HS GC-MS) analyzed for identification of VOCs of samples. Extraction of VOCs was performed using 1 g sample in a 10 mL HS-vial with a PTFE septum. The samples were conditioned at 125 °C and

exposed to the HS at 125 °C with agitation of 250 rpm. Blanks were run after each sample as a control. A HS-20NX Headspace autosampler from Shimadzu Scientific Instruments (U.S.A) was employed. The compounds were heated from 50 °C at a rate of 3 °C/min to 200 °C at a rate of 12 °C/min temperature program on a GCMS-QP2010 Ultra Gas Chromatography Mass Spectrometry (GCMS) (Shimadzu Scientific Instruments, Carlsbad, CA, USA) which has 250 °C temperature. Injection at 200 C at 5s. The split ratio was 1: 20. Separation was achieved using a InertCap Pure-WAX capillary column (0.25 mm x 60 µm x 0.25 µm) and helium as carrier gas (1 mL/min) with the 22 cm/s average velocity. VOCs were determined by retention time and mass spectra and appear as peaks in the chromatogram by using the National Institute of Standards and Technology standard reference database (WILEY7). For the quantification of VOC's, calibration was carried out using acetone as the calibration solution at seven different concentrations (0.1 / 0.5 /1 / 5 /10 / 50 and 100 g/L) in 1-butanol. A linear calibration curve was established based on these seven calibration points. Calibration measurements were performed using a 5 µL syringe to inject 2 µL of the solution into each 10 ml HS vessels. The detection limit (LOD) for VOC peaks was determined by identifying peaks with heights at least 3 times greater than the baseline noise, and areas exceeding 10% of the acetone peak area, where the acetone concentration in the calibration solution was 0.5 g/L. For the quantification of VOC's, Calibration carried on the Acetone which used as a calibration solution with seven different concentrations (0.1 / 0.5 /1 / 5 /10 / 50 and 100 g) per liter in 1-butanol. The linear line range of calibration curve was obtained from seven points of calibration. The calibration measurement was performed using a 5 µL syringe to inject 2 µL into each 10 ml HS vessels. The detection limit (LOD) of VOC peaks was determined by the election of peaks whose height exceeds the noise of the base line by at least 3 times, and whose area is greater than 10% of the peak for the acetone area, where the concentration in the calibration solution was 0.5 g/L.

3.4.5 Thermogravimetric analysis

Thermal stability was evaluated using thermogravimetric analysis TGA (Mettler Toledo, Giessen, Germany). The study was conducted in the temperature range of 20 to 700 °C at the heating rate of 10 °C/min in nitrogen environment.

3.4.6 Differential Scanning Calorimeter

Thermal stability was evaluated using thermogravimetric analysis TGA (Mettler Toledo, Giessen, Germany). The study was conducted in the temperature range of 20 to 700 °C at the heating rate of 10 °C/min in nitrogen environment. The effect of HNT, modified HNT samples on the thermal transition temperatures and crystallinity of the rPO polymer was analyzed under an inert nitrogen atmosphere with a Differential Scanning Calorimeter (DSC) (Mettler Toledo DSC 3, Giessen, Germany). STAR® SW 16.10 software (Mettler Toledo, Columbus, OH, USA) was used to determine the melting enthalpy (ΔHm), melting temperature (Tm), cold crystallization temperature (Tc), and cold crystallization enthalpy (ΔHc The effect of HNT, modified HNT samples and other additives on the thermal transition temperatures and crystallinity of the rPO based nanocomposites was analyzed under an inert nitrogen atmosphere with a Differential Scanning Calorimeter (DSC) (Mettler Toledo DSC 3, Giessen, Germany). STAR® SW 16.10 software (Mettler Toledo, Columbus, OH, USA) was used to determine the melting enthalpy (ΔHm), melting temperature (Tm), cold crystallization temperature (Tc), and cold crystallization enthalpy (ΔHc). DSC analysis was performed in three cycles. Firstly, the samples were heated from room temperature to 200 °C at 10 °C/min and held at 200 °C for 2 minutes to erase their thermal history. In the second cycle, the samples were cooled from 200 °C to -70 °C at a rate of 10 °C/min and held at -70 °C for 2 minutes. The cold crystallization temperatures (Tc) were determined from the maximum points of the peaks in the resulting thermogram. In the third cycle, the samples were reheated from -70 °C to 200 °C at a rate of 10 °C/min, and the melting temperatures (Tm) were derived from the peak maxima observed during this final heating. The degree of crystallinity (Xc) for each sample was calculated using the Equation (1):

$$X_c = [\Delta H_m / \Delta H_m^{\circ}] \times 100\% \quad (1)$$

where ΔH_m is the melting enthalpy and ΔH_m° is the melting enthalpy of 100% crystalline polymer and w_F corresponds to the weight percentage of fiber in the composite. The theoretical value of 100% crystalline polypropylene ($\Delta H_{m_{PP}}^{\circ}$) is 207 J/g and100% crystalline polyethylene ($\Delta H_{m_{PE}}^{\circ}$) is 293 J/g (Wunderlich, 1990; Gao et al, 2016).

$$X_{c_{\text{Total}}} = X_{c_{\text{PP}}} + X_{c_{\text{PE}}} \quad (2)$$

The rPO material contains 70% PE and 30% PP. The total crystallinity of Recycled polyolefin was calculated by calculating the individual crystallinity contributions of PE

and PP using Equation (1) by dividing them by their respective weight fractions and then summing these values as shown in Equation (2).

3.4.7 Mechanical Testing

The mechanical properties of all rPO nanocomposite samples with 2mm thickness and 5mm width, were analyzed at room temperature using an Instron-100 kN Universal Electromechanical Test Machine (Massachusetts, US) universal testing machine with a capacity of 100 kN and a tensile speed of 1000 mm/min. Also, morphologies of nanocomposites with rPO matrix were examined under 5kV, secondary electron (SE) and also inlens detector mode of Field Emission Scanning Electron Microscopy (FESEM) (CARL ZEISS LEO SUPRA 35VP FESEM). This study was carried out by examining the fracture surfaces from the failure region. Sample surfaces were coated 3 times with carbon before the analysis.

3.4.8 Scanning Electron Microscopy

Morphologies of nanocomposites with rPO matrix were examined under 5kV, secondary electron (SE) and also inlens detector mode of Field Emission Scanning Electron Microscopy (FESEM) (CARL ZEISS LEO SUPRA 35VP FESEM). This study was carried out by examining the fracture surfaces taken from the area where the samples broke. Sample surfaces were coated 3 times with carbon before the analysis.

BET, HS–GC–MS, TGA, DSC, and XRD analyses were conducted as representative single instrumental runs, in line with established practice for these characterization techniques. Consequently, replicate measurements and associated statistical deviations are not customarily reported. In contrast, the odor evaluation (Jar test) was performed in triplicate, and the results are presented as mean ± standard deviation (Table 8).

3.5 Results and Discussion

3.5.1 Modification of HNT

3.5.1.1. NMR Result

The stepwise synthesis of the amine-functional silane compound TMPED-MCA-HH was verified by ^{1}H-NMR spectroscopy, as shown in Figure 15. The 1H-NMR spectrum of monochloroacetic acid (MCA) (Figure 15a) displayed a distinctive singlet at $\delta \approx 4.28$ ppm, associated with the methylene group ($–CH_2Cl$) located next to both the carboxylic

acid and chlorine atoms (Chloroacetic acid(79-11-8) 1H NMR spectrum. (Feb 12, 2024). In the spectrum of N-[3-(Trimethoxysilyl)propyl]ethylenediamine (TMPED) (Figure 15b), multiple signals were detected in the δ ≈ 3.2–3.8 ppm area (peaks 6–9), corresponding to protons from hydroxylated methylene and methine groups. Additionally, signals in the range of δ ≈ 1.0–2.8 ppm (peaks 4–5, 10) suggested the existence of aliphatic CH_2 and CH protons, confirming the anticipated structure of TMPED (N-[3 (Trimethoxysilyl)propyl]ethylenediamine(1760-24-3) ^{1}H NMR spectrum. (Feb 12, 2024). When interacting with MCA, the TMPED-MCA spectrum (Figure 15c) exhibited resonances in the δ ≈ 4.2–4.4 ppm region (peaks 1, 24, 26), which corresponded to the methylene protons originally observed in MCA (Figure 15a) but shifted downfield due to the formation of ester and amide functionalities. Although integration values were not calculated in this study, the signal assignments (e.g., δ ≈ 4.2–4.4 ppm for the methylene protons derived from MCA, δ ≈ 3.2–3.8 ppm for TMPED methylene/methine groups, and δ ≈ 2.5–3.5 ppm for newly formed amide/methylene linkages) are consistent with the expected proton environments, supporting the structural confirmation. The observed downfield shifts relative to the initial materials confirmed the successful reactions of esterification and amidation. Following the amidation with hydrazine hydrate to form TMPED-MCA-HH (Figure 15d), additional spectral complexity was introduced. A sharp singlet was noted at δ ≈ 4.25 ppm, along with broad multiplets in the range of δ ≈ 2.5–3.5 ppm. These traits imply the presence of amide linkages and methylene connections that derived from the diamine unit. The broadening of the signal is associated with the increased molecular weight and the structural flexibility of the resulting multifunctional compound and may also be influenced by exchangeable protons (e.g., –NH) within the structure (Su et al., 2021). These 1H-NMR findings collectively verify the structure and stepwise synthesis of TMPED-MCA-HH. It should be emphasized that the NMR spectra confirm the successful preparation of the free silane intermediates and final TMPED-MCA-HH molecule, but they do not provide direct evidence of the covalent attachment to halloysite nanotubes. The grafting of the silane compound onto the HNT surface was instead demonstrated through complementary solid-state characterization techniques, including FTIR (appearance of Si–O–Si and amide bands), TGA (increased organic mass loss), and SEM observations, which together verified the effective surface functionalization.

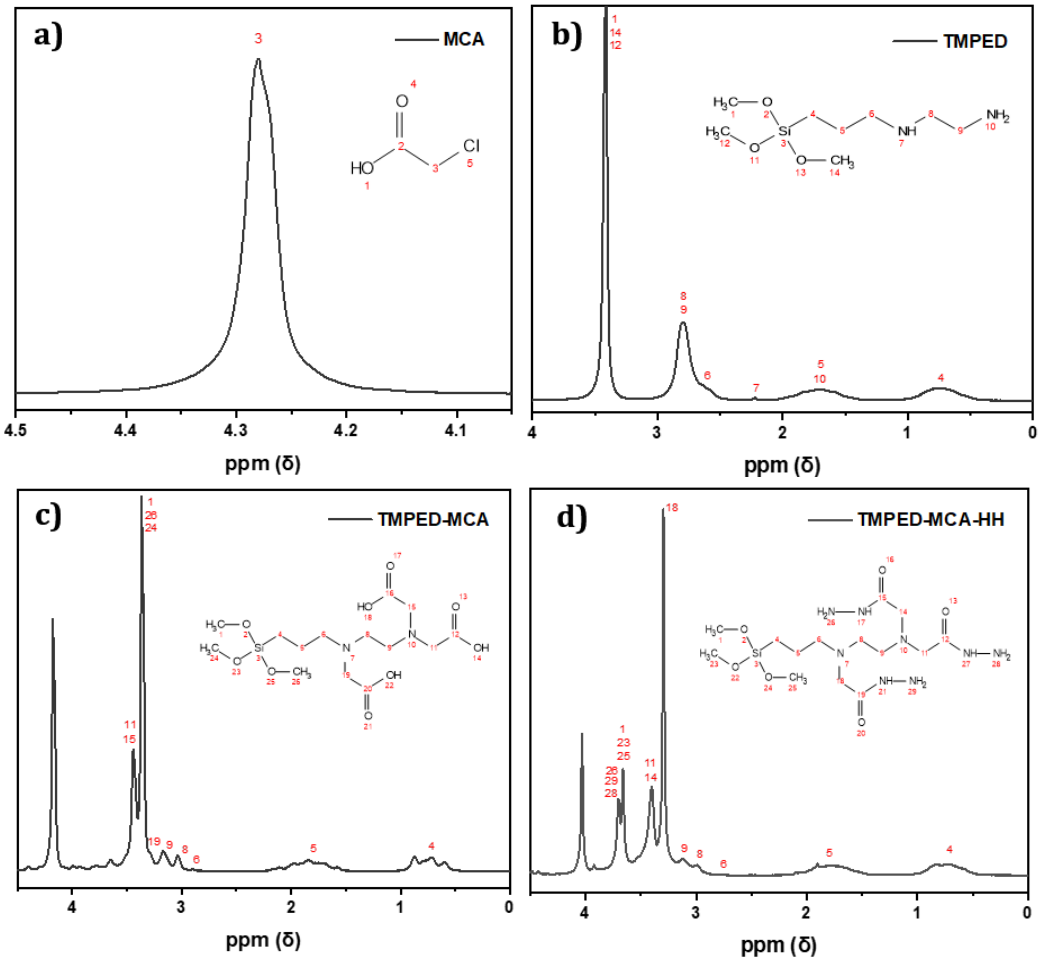

Figure 15. ^{1}H-NMR spectrum of (a) MCA (b) TMPED (c) TMPED-MCA (d) TMPED-MCA-HH

3.5.2 BET Analysis

The surface area and porosity characteristics of HNT, TMPED-HNT, TMPED-MCA-HNT, and TMPED-MCA-HH-HNT were examined through nitrogen adsorption–desorption isotherms and BET analysis to enhance the understanding of their adsorption behaviors. The essential parameters are defined in Table 7, and Figure 16 presents the isotherms along with the corresponding pore size distribution curves for each material.

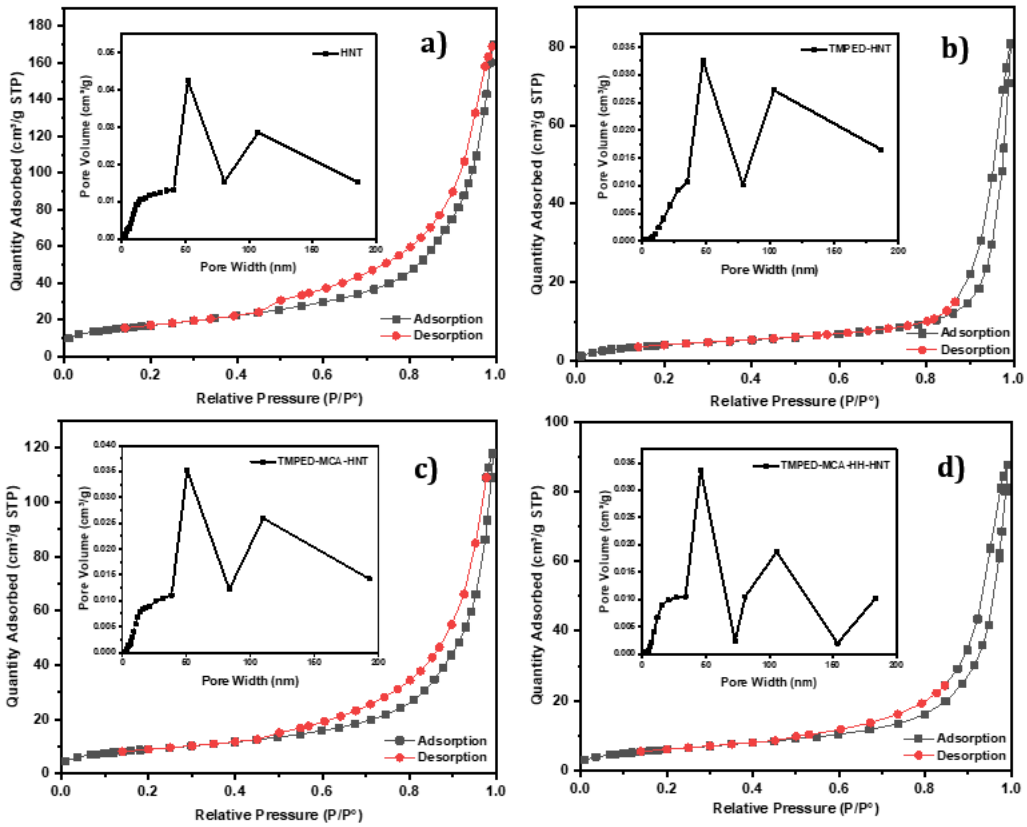

Figure 16. BET adsorption–desorption isotherms and pore size distribution graphs for (a) HNT, (b) TMPED-HNT, (c) TMPED-MCA-HNT and (d) TMPED-MCA-HH-HNT

Table 7. Tabulated values (bottom) for surface area and pore volume for HNT, TMPED-HNT, TMPED-MCA-HNT and TMPED-MCA-HH-HNT

Sample Name	BET Surface Area (m2/g)	Total Pore Volume (cm3/g)	Average pore diameter (nm)
HNT	60.71	0.16	10.69
TMPED-HNT	15.26	0.05	11.98
TMPED-MCA-HNT	32.07	0.09	12.37
TMPED-MCA-HH-HNT	22.30	0.07	11.96

The nitrogen adsorption–desorption isotherm of HNT (Figure 16a) exhibits a classic type IV isotherm, characterized by a distinct H3-type hysteresis loop. This behavior is indicative of mesoporous materials with slit-like pores formed by the aggregation of plate-like particles (Wang et al., 2023). With the increase in HNT content from 2 wt.%

(rPO-2HNT, 35.41 m^2/g) to 5 wt.% (rPO-5HNT, 60.71 m^2/g), the BET surface area increased, and the total pore volume increased from 0.09 to 0.16 cm^3/g, respectively (Table 7). The observed enhancements are due to a majority of mesopores within the 10–15 nm range, which enable multilayer adsorption and promote VOC diffusion. These findings are consistent with the porous morphologies observed in SEM. As shown in Table 1, the surface areas of the modified HNTs decrease after functionalization but do not follow a strict linear trend. This irregularity is attributed to competing effects of surface chemistry and pore accessibility: TMPED grafting blocks part of the pores and lowers surface accessibility, MCA modification partially restores surface exposure through improved dispersion, while the final TMPED-MCA-HH modification enhances crystallinity and densification, leading to further reduction in free volume. Thus, the BET surface area values reflect the balance between pore blockage, structural rearrangement, and chemical functionalization rather than a simple monotonic decrease. The modification with TMPED resulted in a BET surface area of 15.26 m^2/g and a pore volume of 0.05 cm^3/g, implying partial pore blockage and reduced surface accessibility attributed to the grafted silanes (Yang et al., 2017). Concurrently, the average pore diameter exhibited a minor increase to 11.98 nm, most likely related to steric rearrangement on the surface (Table 7, Figure 16b). The functionalization with MCA led to a partial recovery of surface area (32.07 m^2/g) and pore volume (0.09 cm^3/g) (Table 7, Figure 16c), mainly due to improved dispersion and exposure of inner channels (Tharmavaram et al., 2018). The final sample (TMPED-MCA-HH-HNT) demonstrated a reduction in BET surface area to 22.30 m^2/g, followed by a significant reduction in porosity, showing improved densification and decreasing free volume (Figure 16d).

The reduction in BET surface area and pore volume observed after functionalization, despite the relatively unchanged average pore diameter, can be attributed to partial blockage of accessible pores and decreased surface accessibility by the grafted silane groups. The bulky TMPED moieties likely occupied the entrances of mesopores, thereby restricting nitrogen adsorption without altering the intrinsic tubular geometry of HNTs. Additional MCA and HH modifications promoted densification and structural rearrangement, further reducing free volume and limiting adsorption sites. Thus, the observed decrease in surface area and pore volume primarily reflects surface coverage and packing effects rather than changes in the fundamental pore size distribution. This trend corresponds with the crystalline and aggregated morphology, as additionally

supported by SEM (Figure 22d), which supports the interpretation that enhanced crystallinity and tighter packing decrease porosity (Abotaleb et al., 2024). SEM and BET analyses together suggest that pristine HNTs exhibit high porosity and surface area. However, surface modifications, particularly the final TMPED-MCA-HH step, decreased bulk surface accessibility and pore volume (Figures 4d, 6d), while the odor evaluation and HS-GC–MS results confirmed that these modifications enhanced selective adsorption potential toward polar VOCs. The release of VOCs from recycled polyolefins originates from thermo-oxidative degradation of polymer chains, legacy additives, and residual impurities (Kang et al., 2020b; (Brüster et al., 2016).

The incorporation of functionalized HNTs reduced VOC release through a dual mechanism: physical adsorption within the lumen and outer mesoporous surfaces, and selective chemisorption driven by the introduced amine and hydrazide groups. These functional groups interact with polar VOCs through hydrogen bonding, acid–base interactions, and Schiff base condensation with aldehydes and ketones (Lvov & Abdullayev, 2013c; Tekay, 2020), thereby enhancing both the strength and selectivity of adsorption. This dual mechanism is consistent with earlier reports on VOC suppression in polyolefin/HNT systems (Tekay, 2020). Although TMPED-MCA-HNT showed a higher BET surface area than TMPED-MCA-HH-HNT (Table 1), the odor evaluation and HS-GC–MS results (Table 3) revealed that TMPED-MCA-HH-HNT achieved the highest VOC reduction efficiency (91%). This apparent discrepancy demonstrates that surface area alone is not the dominant parameter in VOC adsorption. Instead, the superior performance of TMPED-MCA-HH-HNT arises mainly from the increased density of reactive functional groups (hydrazide moieties) introduced in the final modification step. These groups provide enhanced chemical affinity and stronger specific interactions (hydrogen bonding, Schiff base formation) with polar VOCs such as aldehydes and alcohols. Thus, while surface area contributes to physical adsorption, the decisive factor for selective VOC capture is the improved surface chemistry of TMPED-MCA-HH-HNT.

3.6 Results of Nanocomposites with rPO matrix

3.6.1 Odor Sensory Analysis Result

For investigating the odor effect of HNT and Mod HNTs on WPCs, the Indoor Odor (Jar) test was used. The results are shown in Table 8. The Neat rPO sample has the highest average rating for all test conditions, as seen from the table. That rating corresponds to a "Disturbing" level which indicates the presence of odor-emitting compounds in a very high concentration at the highest testing temperature (65°C). As far as the rPO-2HNT sample containing unmodified HNTs is concerned, it also showed a marked reduction in odor perception as compared with the rPO neat sample. This reduction is attributed to the distinctive porous tubular framework and high surface area of HNTs, which facilitate VOC adsorption (Fahimizadeh et al, 2024).

Increasing the concentration from 2 wt.% to 5 wt.% did not increase HNT's adsorption capacity. In contrast, modified rPO nanocomposites that are named as rPO-5TMPED-MCA-HNT and rPO-5TMPED-MCA-HH-HNT, showed significantly lower rating averages as "Slightly perceptible" and the latter as "Perceptible, not disturbing" even at the highest temperature. This suggests that modification of Halloysite Nanotubes (HNTs) with amino group-containing silane compounds was very effective in reducing odor emission from the rPO. These findings highlight that surface modification enhances the ability of HNTs to capture and remove undesirable VOCs, providing a more efficient odor reduction effect. Given the subjective nature of the jar test, complementary quantitative analysis such as HS-GC–MS was employed to validate these results.

Table 8. Table of indoor odor (jar) test results

Sample Name	Test Condition	Rating Average	Result
rPO Neat	1 (25°C, 24 h)	3.0 (± 0.6)	Very perceptible but not disturbing
	2 (40°C, 24 h)	3.5 (± 0.7)	Intense enough to be slightly disturbing
	3 (65°C, 2 h)	4.0 (± 0.5)	Disturbing
rPO-2HNT	1 (25°C, 24 h)	2.0 (± 0.3)	Perceptible, not disturbing
	2 (40°C, 24 h)	2.5 (± 0.7)	Clearly perceptible but not disturbing
	3 (65°C, 2 h)	3.0 (± 0.6)	Very perceptible but not disturbing
rPO-5HNT	1 (25°C, 24 h)	2.5 (± 0.3)	Clearly perceptible but not disturbing
	2 (40°C, 24 h)	3.0 (± 0.7)	Very perceptible but not disturbing
	3 (65°C, 2 h)	3.5 (± 0.4)	Intense enough to be slightly disturbing
rPO-5TMPED-HNT	1 (25°C, 24 h)	2.0 (± 0.8)	Perceptible, not disturbing
	2 (40°C, 24 h)	2.5 (± 0.5)	Clearly perceptible but not disturbing
	3 (65°C, 2 h)	3.0 (± 0.2)	Very perceptible but not disturbing
rPO-5TMPED-MCA-HNT	1 (25°C, 24 h)	1.5 (± 0.3)	Slightly perceptible
	2 (40°C, 24 h)	2.0 (± 0.6)	Perceptible, not disturbing
	3 (65°C, 2 h)	2.5 (± 0.4)	Clearly perceptible but not disturbing
rPO-5TMPED-MCA-HH-HNT	1 (25°C, 24 h)	1.5 (± 0.5)	Slightly perceptible
	2 (40°C, 24 h)	2.0 (± 0.3)	Perceptible, not disturbing
	3 (65°C, 2 h)	2.5 (± 0.2)	Clearly perceptible but not disturbing

3.6.2 Characterization of VOCs by HS GC-MS Result

Figure 17 shows the HS GC-MS chromatograms of VOCs released by Recycled Polyolefin (rPO Neat), rPO containing 2 and 5 wt.% Halloysite Nanotubes (rPO-2HNT, rPO-5HNT), and rPO containing surface-modified HNTs (rPO-5TMPED-HNT, rPO-5TMPED-MCA-HNT, rPO-5TMPED-MCA-HH-HNT). According to the chromatograms, the neat rPO has a dense number of peaks which are associated with different VOCs like acetaldehyde, propanal, ethanol, and different alcohols, ketones, and ethers. They are conventionally related to thermal degradation of polypropylene during recycling processes and residual additives generated by the earlier product lifecycles. Even though some of the VOC peaks present in the changed samples coincide with neat rPO peaks due to the common polymer matrix, there are also some other new peaks. Such new peaks could originate from raw material impurities or due to secondary degradation reactions resulting from melt processing (Sallem-Idrissi et al, 2016).

Quantitative data from Table 8 indicates a clear trend in VOC suppression. The neat rPO sample exhibited the highest number of VOC peaks at 235, whereas rPO-2HNT and rPO-5HNT exhibited reductions in total VOC peaks to 136 and 108, representing 42% and 54% decreases, respectively. This can be explained by the well-documented adsorption ability of HNTs, which provide a high surface area and internal nanotubular structure conducive to physical entrapment of small organic molecules (Inuwa et al, 2018; Almasri et al, 2019).

The more effective surface functionalization was shown through additional inhibition of VOC peak heights and numbers of HNT samples treated with amino-functional silane. rPO-5TMPED-HNT, rPO-5TMPED-MCA-HNT and rPO-5TMPED-MCA-HH-HNT samples reduced the VOC peak heights to 27, 24 and 22, respectively. These are 88%, 90% and 91% reductions, respectively, indicating that chemical functionalization greatly improved the VOC adsorption capacity of HNTs. This is due to amine groups added using silane coupling agents, which facilitate chemisorption by enabling special interactions with polar VOC molecules like aldehydes and carboxylic acids. In addition to peak count reductions, Table 9 also reports compound-specific peak height reductions. For example, acetaldehyde, propanal, dodecane and acetic acid showed 20–74% suppression with neat HNTs, while cyclotrisiloxane decreased by ~67% in TMPED-HNT and was further suppressed in dual-silane modified HNTs, though still detectable at low intensity. The high suppression ratios (88–91%) observed for functionalized HNT samples are primarily

due to the almost complete elimination of major odorant VOCs such as acetaldehyde, propanal, and benzaldehyde, as well as the strong suppression of cyclotrisiloxane. Although some new oxygenated compounds (e.g., 1-acetoxy-2-propanol, propylene glycol) appeared in the spectra of surface-modified samples, their intensities were negligible compared to the dominant odorants in neat rPO, and thus the overall VOC profile was still markedly reduced. Notably, the rPO-5TMPED-MCA-HH-HNT sample, having two reactive silane groups, seems to gain from synergistic effects and increased density of reactive groups, and suppresses most effectively the key odorants like acetaldehyde, ethanol, and cyclotrisiloxane. These groups are the main contributors to the distinctive odor of recycled polyolefins and are typically hard to remove through conventional physical adsorption (Jin et al, 2019b; Krishnaiah et al, 2020; Zhang et al, 2024).

The VOCs identified in Table 9 reveal that a variety of functional groups such as aldehydes (e.g., nonanal, benzaldehyde), siloxanes, alcohols, esters, and acids were effectively targeted by the surface-modified HNTs. This not only proves that the surface modification strategy enhanced filler-matrix interaction but also selectivity toward environmentally and olfactorily relevant VOCs.

Earlier research has demonstrated comparable enhancements of VOC entrapment with surface-modified nanofillers or molecular adsorbents such as β-cyclodextrin, but while cyclodextrins are generally restricted to entrapment of non-polar volatiles through inclusion complexation (Fahimizadeh et al, 2024). In addition, the peak appearing at ~9.8 min was identified as 1-butanol, originating with acetone from the calibration solution rather than from the rPO samples. By capturing both polar and non-polar compounds through a combination mechanism of physical adsorption (via the HNT lumen and outer surface) and chemical affinity (via amine and hydroxyl groups on the modified surface), the modified HNTs in this study offer broader applicability than those conventional approaches. For complex matrices like recycled plastics, where a wide variety of volatiles are frequently present, this dual-action mechanism is desirable.

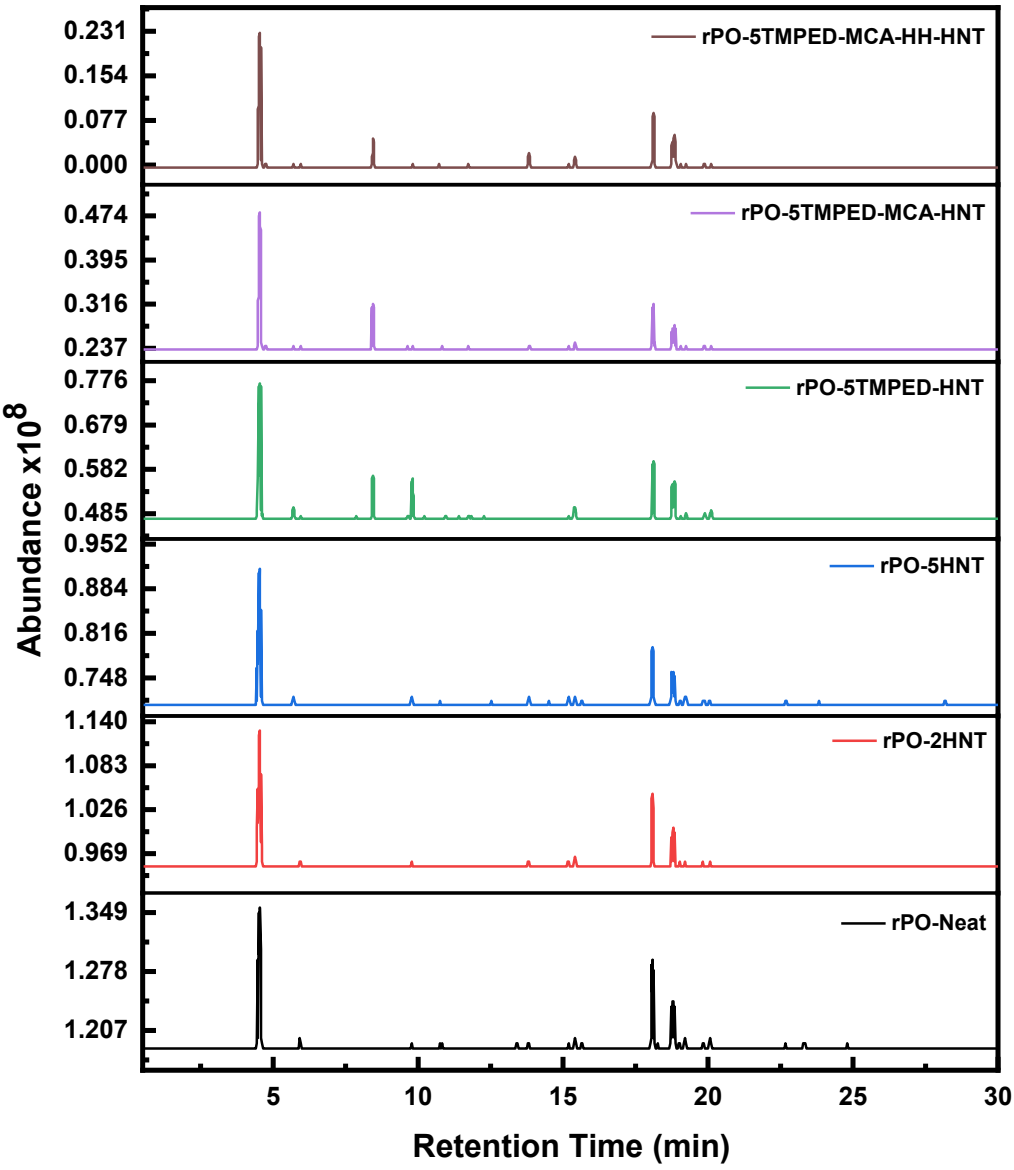

Figure 17. HS GC-MS chromatogram of neat rPO, 2 and 5 wt.% HNT added rPO and rPO-Mod-HNTs

Table 9. Undesirable odor VOCs identified according to the HS GC-MS chromatogram

Sample	Total Number of VOC Peaks	Reduction Rate (%)*	Major Reduced VOCs (with % Peak Height Reduction)	Remarks
rPO Neat	235	–	Acetaldehyde, Ethanol, Propanal, Propionic aldehyde, Cyclotrisiloxane, Dodecane, Acetic acid, Benzaldehyde	High VOC content originating from thermal degradation and legacy additives of previous product cycles
rPO-2HNT	137	42	Propylene carbonate, 2-Propanol derivatives, Phenolic compounds, Crown ether (Crown-5), Dimethylformamide; Acetaldehyde (20.9%), Propanal (53.2%), Cyclotrisiloxane (63.7%), Dodecane (15.4%), Acetic acid (35.4%)	VOC reduction through physical adsorption by HNTs' internal tubular and surface area structure
rPO-5HNT	107	54	Trimethylsilyl compounds, Propionic acid, Pivalic acid, Phenol derivatives; Acetaldehyde (53.8%), Propanal (74.1%), Dodecane (32.9%), Acetic acid (37.4%)	Higher HNT loading results in increased surface area and enhanced adsorption capacity
rPO-5TMPED-HNT	27	88	2-(2-Hydroxypropoxy)-1-propanol, Ethanol, Dimethylformamide; Cyclotrisiloxane (66.8%)	Amino-silane functionalization facilitates chemisorption with polar VOCs
rPO-5TMPED-MCA-HNT	24	90	1-Acetoxy-2-propanol, Propylene glycol, Methoxyethanol, 2-(2-Hydroxypropoxy)-1-propanol	Enhanced selectivity toward oxygenated VOCs
rPO-5TMPED-MCA-HH-HNT	22	91	Tetradecane, Ethanol, Cyclotrisiloxane, 2-Propanol derivatives	Dual-silane functional groups increase reactive group density and synergistically enhance adsorption

*After reducing peaks according to 10% Acetone (control and calibration solution) peak height

3.6.3 TGA Analysis

The thermal stability of nanocomposites with rPO matrix was evaluated through TGA and DTGA analyses, as shown in Figure18a and18b, with the results provided in Table 10. Similar trends can be seen in all of the thermograms that are part of the rPO formulations in Figure 18a and 18b (weight change vs. temperature at the top and derivative of weight change vs. temperature at the bottom). The thermal stability of rPO has been found to be modified by HNT and Mod-HNTs. This enhanced thermal stability is due to the ability of HNTs, which are comparatively uniformly distributed throughout the PP matrix, to limit the mobility of molecules of polymers and trap volatile organic compounds (VOCs) that occur during thermal degradation (Wolfsgruber et al., 2023). All of the samples have a single stage of thermal degradation. The neat rPO sample exhibited the highest weight loss (96.6%), whereas the rPO-5TMPED-MCA-HH-HNT sample exhibited the lowest weight loss (92.2%), as seen in Figure 18a and 18b.

The onset degradation temperature (the temperature at which thermal degradation starts) increases from 434.8 °C in neat rPO to 452.2 °C in rPO-5TMPED-MCA-HH-HNT with the addition of HNT and modified HNT into the rPO systems, meaning an improvement on the thermal stability. Moreover, the peak degradation temperature signifying the highest decomposition rate is higher for rPO-HNT samples (473.5–475.0°C) but shows a slight decrease for rPO-5TMPED-MCA-HH-HNT (469.8°C) due to modifications. The endset temperature, which signals the conclusion of degradation, remains relatively stable for all except for rPO-5TMPED-MCA-HH-HNT, which shows an earlier degradation endpoint (470.6°C). Neat rPO displays the most weight loss (96.6%), and rPO-5TMPED-MCA-HH-HNT displays the least weight loss (92.2%), confirming the excellent improvements in thermal resistance due to modifications. Residue content at 700 °C is significant for char formation or inorganic content remaining after degradation. In this context, the “additivity ratio” corresponds to the theoretical residue calculated from the weighted sum of neat rPO and HNT contributions. Comparison with the experimental TGA results showed that the measured residues were ~1% higher than the calculated values, indicating synergistic stabilization and enhanced char formation provided by functionalized HNTs. In addition, it confirms the modifications in HNT to rPO because with HNT, this residue is increased from 3.4% on neat rPO to 7.8% in rPO-5TMPED-MCA-HH-HNT.

The improved thermal stability can be explained by multiple synergistic mechanisms, since the tubular HNT layers act as physical barriers that delay heat transfer and hinder the diffusion of volatile degradation products. At the same time, the presence of silane-derived organic moieties promotes char formation, which protects the polymer matrix during decomposition. Furthermore, the uniform dispersion of functionalized HNTs creates tortuous diffusion pathways that slow down oxygen and small molecule penetration. Together, these effects limit chain scission reactions and stabilize the polymer during heating. In summary, the rPO thermal stability is enhanced by HNT and its modifications, while rPO-5TMPED-MCA-HH-HNT demonstrates the highest onset temperature rise and residue content increase, indicating the most enhancement.

Table 10. Onset, peak, endset temperatures, % residue of neat rPO, rPO-HNTs and rPO-Mod-HNTs

Sample Name	Onset degradation temperature [°C]	Peak [°C]	Endset degradation temperature [°C]	Weight Loss [%]	Residue@ 700 °C [%]
rPO Neat	434.8	473.7	498.9	96.6	3.4
rPO-2HNT	438.9	473.5	496.8	95.8	4.2
rPO-5HNT	444.7	475.0	499.7	93.1	6.9
rPO-5TMPED-HNT	448.8	473.7	497.2	92.4	7.6
rPO-5TMPED-MCA-HNT	451.2	472.7	497.2	93.2	6.9
rPO-5TMPED-MCA-HH-HNT	452.2	469.8	470.6	92.2	7.8

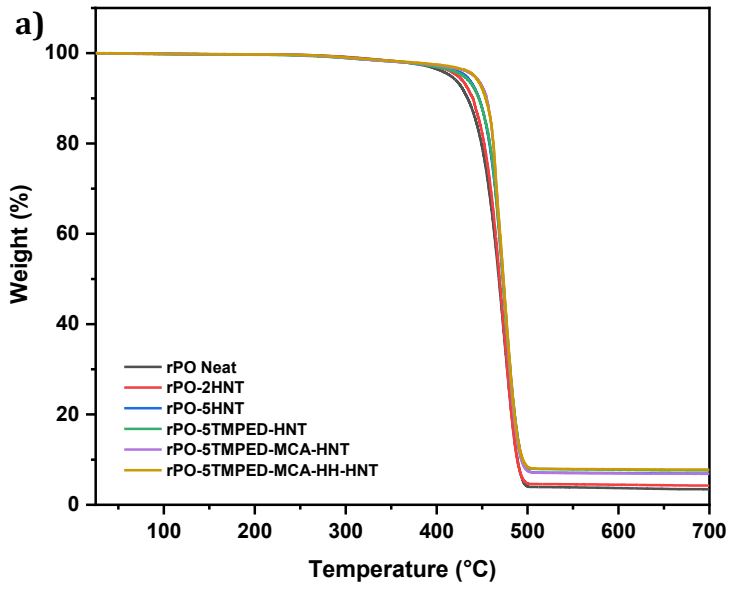

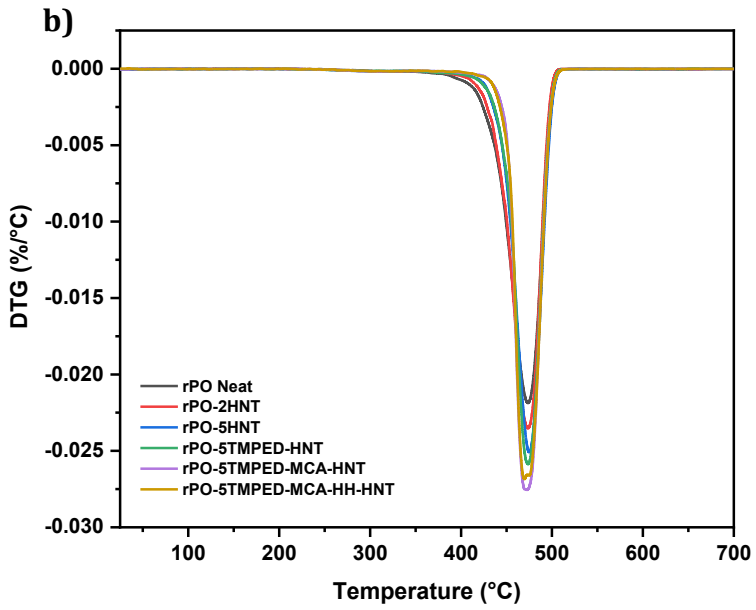

Figure 18. TGA thermograms of all samples: weight change vs temperature at the top and derivative of weight change vs temperature at the bottom

3.2.4. DSC Results

The changes on the thermal transition temperatures of the specimens were examined by DSC analysis. The endothermic melting and exothermic crystallization thermograms obtained from DSC analysis are shown in Figures 19a and 19b below. Thermal behavior and crystallinity of rPO, rPO-HNT, and rPO-Mod-HNT (nanocomposite formulations of rPO) samples, highlighting variations in melting temperature (Tm), crystallization temperature (Tc), enthalpy changes (ΔHm, ΔHc), and crystalline (Xc) are given in Table 11.

Since rPO comprises PE and PP (70/30), there are 2 distinct melting (Tm) and cold crystallization (Tc) peaks. The endothermic and exothermic peaks noted at around 124 °C and 112 °C are linked to the melting and crystallization transitions of the polyethylene (PE) phase, respectively, while the peaks close to 163 °C and 121 °C refer to the melting and crystallization of the polypropylene (PP) phase within the rPO matrix. With the introduction of 2 wt.% and 5 wt.% HNT, minor enhancements in Tm and Tc were noted, indicating that the inclusion of tubular nanofillers may serve as nucleating agents that facilitate the crystallization process (Wolfsgruber et al, 2023). However, the level of crystallinity (Xc) decreased from 83.2% (pure rPO) to 73.5% and 77.3% in the rPO-2HNT and rPO-5HNT samples, respectively, suggesting that the physical interaction

between rPO chains and HNT could restrict chain mobility and consequently decrease the overall crystallization degree (Bidsorkhi et al., 2015; Yin et al., 2017). Additional functionalization of HNTs with the silane coupling agent, including amino groups (TMPED-MCA-HH), resulted in considerable differences in thermal properties. The rPO-5TMPED-HNT, rPO-5TMPED-MCA-HNT, and rPO-5TMPED-MCA-HH-HNT samples revealed a slight rise in Tm (to 127.8 °C) and moderate fluctuations in Tc values. These differences can be associated with improved interfacial compatibility and dispersion of modified HNTs, which impact the crystallization kinetics of the rPO matrix (Patiño-Almanza et al., 2024; Sikora et al., 2019). Out of all the samples, rPO-5TMPED-MCA-HH-HNT had a Tm of 127.8 °C and a crystallinity of 73.4%, proving an improvement over the unmodified HNT-filled rPO. This enhancement can be mechanistically attributed to the presence of functional groups on modified HNTs, which provide heterogeneous nucleation sites and facilitate stronger interfacial interactions with rPO chains. These effects promote more efficient chain alignment and the formation of ordered lamellar crystals, thereby increasing both melting temperature and crystallinity. The results revealed that surface functionalization by TMPED-MCA-HH helps regain crystallinity, whereas HNTs reduce crystallinity slightly by physical constraints. This highlights how modified HNTs can enhance material performance while absorbing VOCs.

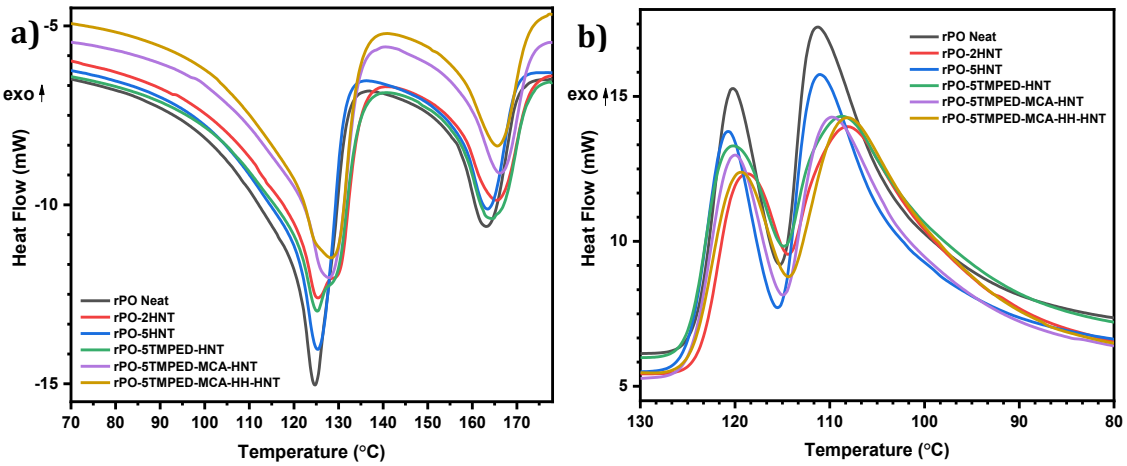

Figure 19. DSC thermograms of Neat rPO, rPO-HNT and rPO-Mod-HNT: a) melting peaks, b) crystallization peaks

Table 11. DSC results of Tm, Tc, ΔHm, ΔHc, and Xc of the neat rPO, rPO-HNT and rPO-Mod-HNT samples

Sample Name	Tm_{PE} (°C)	Tm_{PP} (°C)	Tc_{PE} (°C)	Tc_{PP} (°C)	ΔHc_{PE} (J/g)	ΔHc_{PP} (J/g)	ΔHm_{PE} (J/g)	ΔHm_{PP} (J/g)	$\Delta Hm°_{PE}$ (J/g)	$\Delta Hm°_{PP}$ (J/g)	Xc_{Total} (%)
rPO Neat	124.1	162.7	111.8	120.7	95.5	28.6	84.0	26.2	293.0	207.0	83.2
rPO-2HNT	124.9	165.1	108.6	119.1	87.5	25.7	72.7	23.6	293.0	207.0	73.5
rPO-5HNT	124.8	163.1	111.5	121.2	86.8	26.4	79.8	23.8	293.0	207.0	77.3
rPO-TMPED-HNT	124.7	164.1	109.2	120.6	87.2	28.1	73.5	25.3	293.0	207.0	76.6
rPO-TMPED-MCA-HNT	127.4	165.8	110.3	120.5	83.7	26.0	71.3	23.7	293.0	207.0	73.0
rPO-TMPED-MCA-HH-HNT	127.8	165.3	108.7	119.8	84.1	25.2	74.6	23.0	293.0	207.0	73.4

The transitions and morphological evolution of the crystalline phases noticed in the DSC analysis were also supported by the images obtained using a high-resolution SEM with an in-lens detector at 10KX magnification (Figure 20). Figure 20a shows the formation of lamellar growth within the polypropylene (PP) phase. The rPO matrix has a relatively uniform morphology, without sharply defined crystalline domains, which suggests the typical crystallization behavior of the PP component. Figures 8b and 8c, representing rPO composites containing 2 and 5 wt.% unmodified halloysite nanotubes (HNTs), respectively, show there is no notable alteration in the lamellar morphology of the PP phase. The inclusion of HNTs does not modify the lamellar structure, meaning that HNTs have limited interaction with the PP component. This observation correlates with the interfacial data stated in Table 11. In Figure 8d, which represents rPO with 5 wt.% modified HNTs (TMPED-MCA-HH-HNT), no significant structural change is observed in the PP lamellae compared to unmodified samples (Du et al, 2006; Szpilska et al, 2015; Paul & Robeson, 2008). This indicates that the chemical modification of HNTs does not markedly alter the lamellar crystallization morphology of the PP phase. However, the functional groups introduced via modification enhance compatibility predominantly with the PE domains and at the rPO/HNT interface, as further supported by interfacial and mechanical data.

Overall, the SEM results confirm that both unmodified and modified HNTs do not significantly influence the crystallization morphology of the PP phase, while their enhanced interfacial interactions with the PE phase and the amorphous regions are more decisive for improving composite performance.

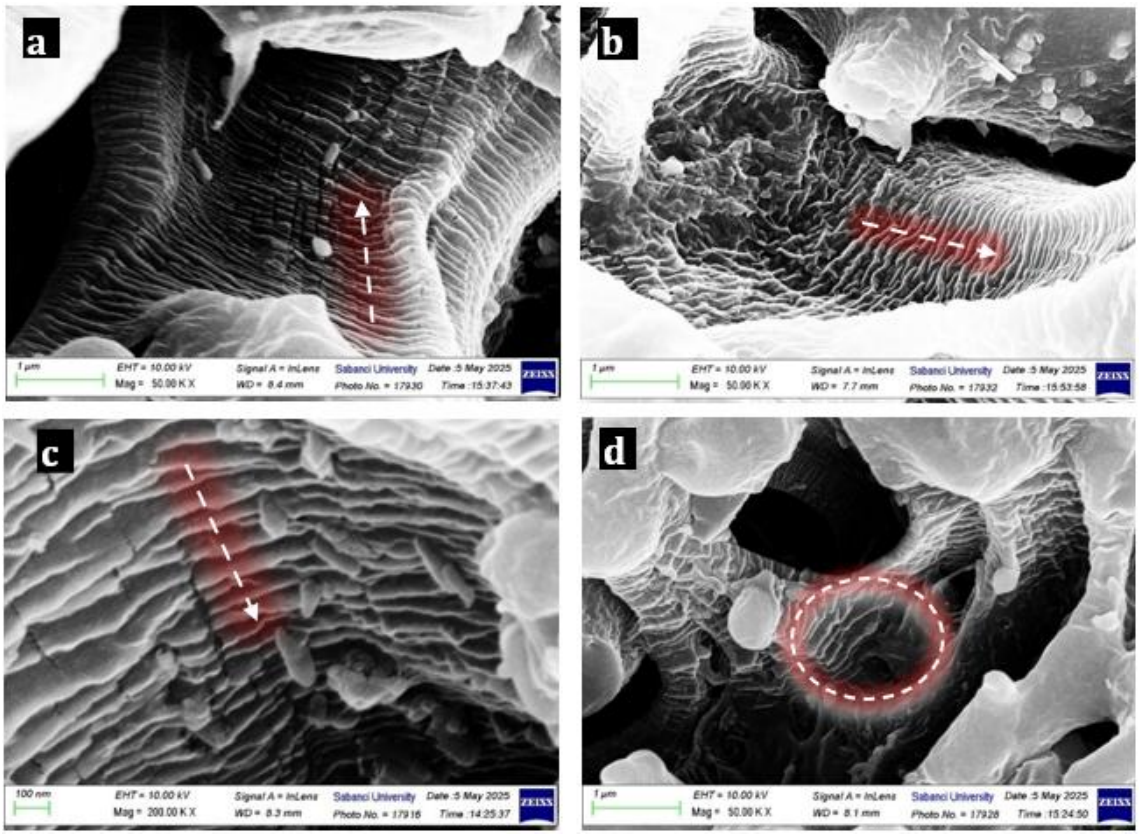

Figure 20. FESEM micrographs of the specimens at 10KX and with inlens detector: (a) rPO Neat (b) rPO-2HNT, and (c) rPO-5HNT (d) rPO-5TMPED-MCA-HH-HNT

3.2.4. Mechanical Test Result

Figure 21 shows the stress-strain curves of all samples as a result of the tensile test. Their data regarding the test analyses is given in Table 12.

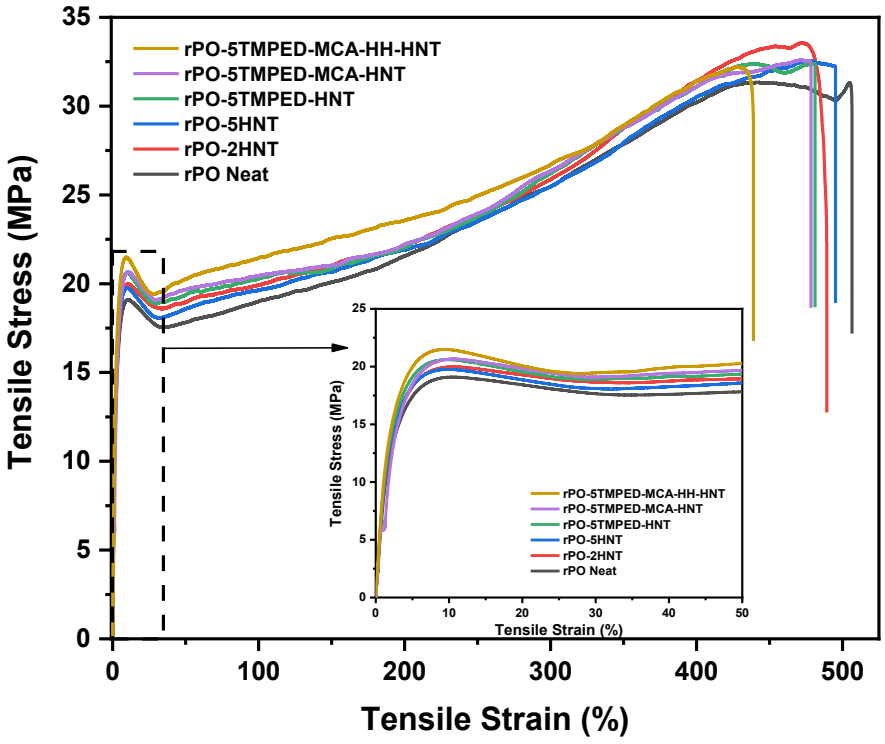

Figure 21. Stress-strain graph of the Neat rPO, rPO-HNTs and rPO-Mod-HNTs

Table 12. Table of tensile test results of the neat rPO, rPO-HNTs and rPO-Mod-HNTs

	rPO Neat	rPO-2HNT	rPO-5HNT	rPO-5TMPED-HNT	rPO-5TMPED-MCA-HNT	rPO-5TMPED-MCA-HH-HNT
Tensile Strength (MPa)	31.3 (±1.5)	33.6 (±1.0)	32.5 (±2.9)	32.4 (±0.9)	32.5 (±3.7)	32.2 (±0.8)
Tensile Modulus (MPa)	815.6 (±41.2)	917.8 (±100.8)	928.9 (±94.5)	934.2 (±48.3)	972.2 (±113.3)	1091.3 (±39.4)
Max Strain (%)	506.5 (±35)	489.2 (±35.5)	495.2 (±41.7)	481.2 (±56.4)	496.5 (±21.65)	439 (±20.7)
Max Strength (MPa)	29.6 (±4.2)	21.4 (±4.4)	32.20 (±8.0)	32.3 (±2.1)	31.9 (±10.4)	28.8 (±8.8)
Yield Stress (MPa)	19.1 (±0.3)	19.9 (±0.5)	19.8 (±1.0)	20.6 (±0.6)	20.1 (±1.2)	21.5 (±0.6)
Yield Strain (%)	10.5 (±0.3)	10.5 (±0.8)	9.8 (±0.8)	9.7 (±0.6)	9.5 (±0.3)	9.3 (±0.6)

*Values in parentheses are standard deviations.

Tensile testing was conducted to evaluate the effect of halloysite nanotubes (HNTs) and their surface functionalization on the mechanical performance of recycled polyolefin

(rPO) composites. The formulation denoted as the Modified Sample (rPO-5TMPED-MCA-HH-HNT) contains 5 wt.% of HNTs functionalized via a sequential process involving TMPED, MCA, and hydrazine hydrate. The addition of of 2 wt.% unmodified HNTs generated an increase in the tensile modulus from 815.6 MPa (neat rPO) to 917.8 MPa. Despite this, an additional increase to 5 wt.% yielded only slight enhancement (928.9 MPa), suggesting decreasing returns possibly due to filler aggregation or lower matrix–filler interfacial efficiency at higher stresses. (Liu et al., 2014). On the other hand, the modified sample has a tensile modulus of 1091.3 MPa, reflecting a 25.3% improvement compared to neat rPO. The enhancement detected can be associated with the increased interfacial adhesion and improved dispersion of nanofillers, which promote more effective stress transfer between the matrix and the nanotubes. Specifically, the introduced amine and hydrazide groups on the HNT surface can form hydrogen bonds and acid–base interactions with oxidized or polar moieties present in rPO, while silane linkages provide anchoring sites that enhance interfacial compatibility. These interactions restrict interfacial slippage and enable stronger load transfer, leading to the observed increase in tensile modulus and yield strength. The introduction of functional groups in surface modification arranges interactions with polymer chains, thus improving mechanical integration and contributing to efficient load distribution. It should be noted that this improvement in stiffness is accompanied by a reduction in ductility, as indicated by the decrease in maximum strain from 506.5% (neat rPO) to 439% in the modified sample. This trade-off highlights that while enhanced interfacial adhesion and filler dispersion contribute to superior modulus, they also restrict chain mobility, leading to embrittlement. In practical terms, the modified rPO composites are particularly promising for applications that demand higher rigidity and dimensional stability, such as automotive components, building materials, or rigid packaging. However, for applications where high ductility and impact resistance are critical, this reduction in strain at break may pose limitations, underscoring the need to balance filler modification strategies with end-use requirements.

A very slight decrease in ductility was observed in the modified sample. The maximum strain decreased from 506.5% to 439%, besides a reduction in yield strain from 10.5% to 9.3%. The seen reduction indicates restricted chain mobility, likely due to the confinement of polymer segments within the interfacial region (Yang et al., 2017c). The modified sample revealed a yield stress of 21.5 MPa, pointing to an 11.2% enhancement relative to

neat rPO, despite a detected reduction in ductility. Tensile failure in rPO is mainly affected by shear yielding of the polyethylene (PE) phase (Wang et al., 2023b). The detected rise in yield stress signifies enhanced plastic resistance due to stronger interfacial bonding within the PE domains (Tekay, 2020b). The simultaneous increase in elastic modulus and yield strength, along with a slight reduction in yield strain, indicates that the mechanical contribution of HNTs is significantly improved through chemical surface modification. Even though the 5 wt.% unmodified HNT sample show the highest crystallinity at 77.3%, the Modified Sample, which offered a slightly lower crystallinity of 73.4%, displayed increased mechanical performance. This suggests that interfacial compatibility contributes an important role rather than crystallinity in determining the mechanical strength of these nanocomposites (Tharmavaram et al., 2018b; F. Yang et al., 2020). In overall, the Modified Sample achieved a desirable balance of stiffness, strength, and flexibility, thereby conveying its suitability for application in performance-critical recycled polyolefins

3.2.5. Morphology, Porosity, and Surface Area Analysis by SEM

The morphological evolution of the nanocomposites was investigated using Field Emission Scanning Electron Microscopy (FESEM), as presented in Figure 22. The low-magnification (2.5KX) SEM images illustrated in Figure 10 reveal the morphological changes in recycled polyolefin (rPO) composites, which consist of both polyethylene (PE) and polypropylene (PP), in relation to the modification with halloysite nanotubes (HNT). SEM micrographs reveal that the darker regions correspond to the polypropylene (PP) phase, while brighter domains are associated with polyethylene (PE)-rich areas.

The neat rPO matrix (in Figure 22a) exhibits a mainly disordered and porous (co-continuous) morphology, inherent to partially miscible polyolefin blends where strong interfacial tension tends to separate the polymer phases (Krishnaiah et al., 2020). The microstructure of the rPO-2HNT (Figure 22b), and rPO-5HNT (Figure 22c), composites exhibited considerable porosity when compared to the unfilled matrix, parallel with the predicted distribution of HNTs and their effects on nucleation and crystal growth. The samples containing 5 wt.% HNT exhibited the highest level of crystallinity, (Xc = 77.3%) and this phenomenon can be explained by the role of unmodified HNTs as highly accessible heterogeneous nucleating agents, which promote crystallite growth while minimally impeding the mobility of polymer chains (Lvov & Abdullayev, 2013d; Bao et

al., 2024). HNT inhibits the crystallinity of PP, and it simultaneously helps to crystallization of PE in their surrounding regions. Following on the TMPED functionalization (Figure 22d), the rPO-5TMPED-HNT sample showed a denser and more compact structure, which suggests enhanced interfacial adhesion and compatibility between the filler and the polymer. Improved homogeneity and decreased porosity on the surface suggested that the intratubular spaces might be partially filled or covered. The additional MCA modifications (rPO-5TMPED-MCA-HNT) (Figure 22e) produced a more homogeneous and continuous surface, most likely due to improved dispersion enabled by hydrogen bonding or dipole–dipole interactions. The final functionalization with HH (rPO-5TMPED-MCA-HH-HNT) resulted in a more consolidated morphology and noticeable reduction in detectable porosity (Figure 22f), showing improved densification and crystallinity. It should be noted that although the final TMPED-MCA-HH functionalization led to a reduction in BET surface area and detectable porosity, this does not necessarily diminish the overall VOC removal efficiency. The reduced number of purely physical adsorption sites is effectively compensated by the presence of hydrazide functional groups, which provide stronger and more selective chemical interactions with polar VOCs. Thus, the balance shifts from physical adsorption to enhanced chemical adsorption, explaining why the TMPED-MCA-HH-HNT sample exhibits the highest removal efficiency despite lower porosity.

Since PP crystallizes at a higher temperature than PE, the observed morphology indicates that PP forms lamellar wall-like crystalline structures near PE domains during cooling. This layered arrangement is commonly associated with improved densification, reduced free volume, and lower porosity. The results support the hypothesis that surface modification results in better matrix packing and molecular-level organization (Abotaleb et al., 2024b; Fahimizadeh et al., 2024). A decrease in porosity and BET surface area measurements has been associated with the structural modifications found by SEM.

The morphological improvements detected also cause an increase in mechanical stiffness and an apparent decrease in the release of volatile organic compounds (VOCs) during processing. The chemical modification of HNTs results in decrease in their specific surface area, thus restricting the diffusion of VOC molecules and allowing their encapsulation within the filler structure. In the framework of polymer processing, the interaction between the modified HNTs and the polyethylene (PE) phase improves the encapsulation mechanism by locally decreasing PE crystallization. This process results in

the formation of additional amorphous regions, that enable more effective trapping of odorant molecules. The inherent mechanical reinforcement conferred by HNTs remains stable, which allows the material to successfully address both mechanical performance and odor suppression challenges in parallel. This multifunctional approach highlights that chemically modified HNTs not only improve stiffness and interfacial interactions but also function as effective VOC adsorbents within recycled polyolefin matrices (Bao et al., 2024b; Kurtulmus & Menceloglu, 2025).

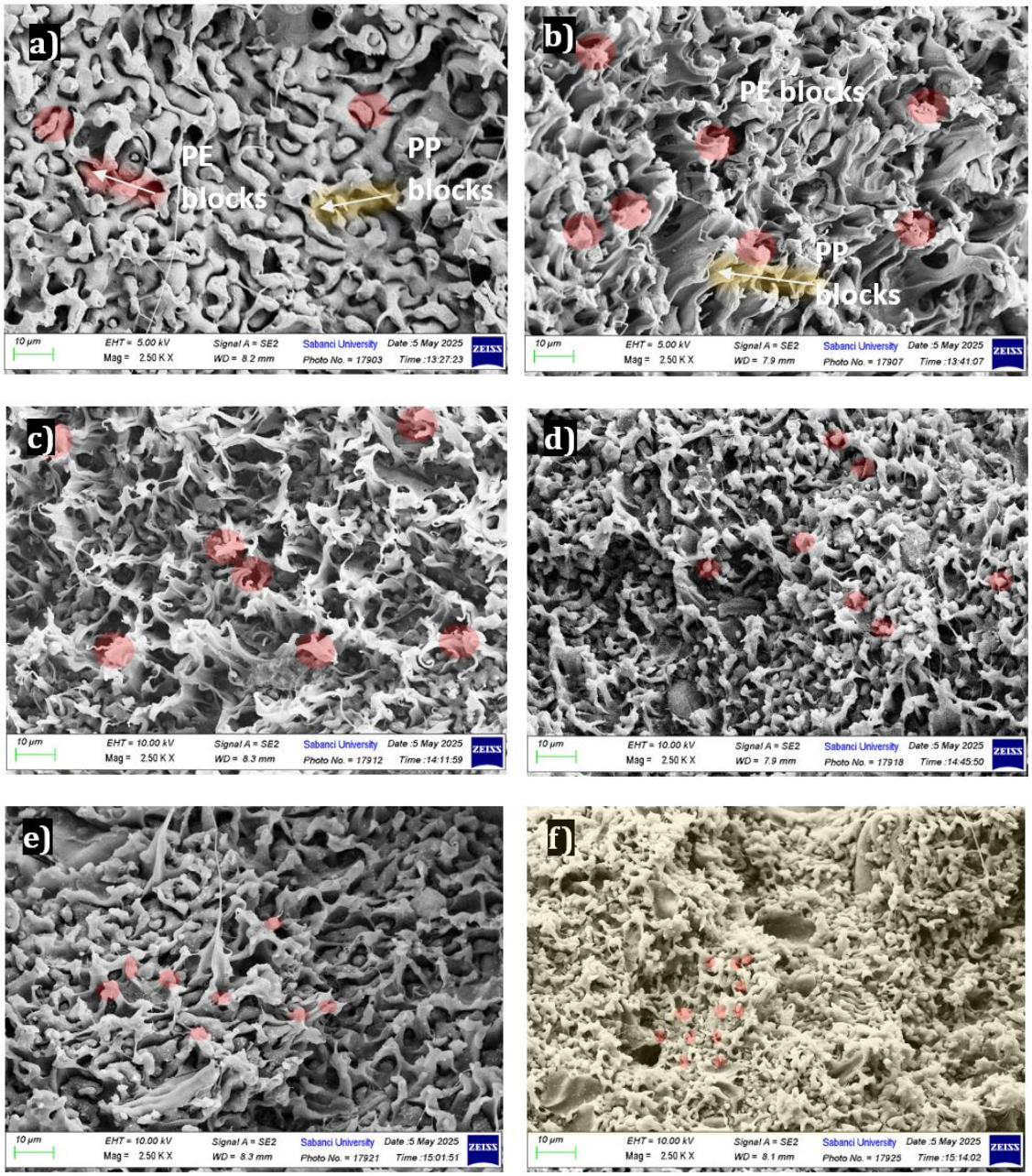

Figure 22. FESEM micrographs of the specimens at 2.5KX, with secondary electron detector: (a) rPO Neat (b) rPO-2HNT, and (c) rPO-5HNT (d) rPO-5TMPED-HNT (e) rPO-5TMPED-MCA-HNT (f) rPO-5TMPED-MCA-HH-HNT

3.7 Conclusion

This research introduces a three-step functionalization of halloysite nanotubes (HNTs) and their impact on decreasing undesirable odor and improving the mechanical performance of recycled polyolefin (rPO) simultaneously. A stepwise amine-based modification was carried out to introduce polar, reactive groups onto the surface of halloysite nanotubes (HNTs). This allowed them to improve their interaction potential with the polymer matrix and to selectively capture of volatile organic compounds (VOCs). The characteristic tubular structure of HNTs faciliated the physical adsorption of relatively small volatile organic compounds (VOCs), whereas the introduced functional groups have an efficient chemical attraction for polar species, including aldehydes, acids, and alcohols.

The addition of 5 wt.% modified HNT into rPO resulted in a 91% decrease in total VOCs, as determined by HS-GC-MS. Relevant reduction has been detected in key odorants, including 4-methyl-octane, acetaldehyde, and cyclotrisiloxane. The results from the odor (jar) testing supported the analytical data, corresponding to a major decrease in perceived odor intensity due to efficient encapsulation of odorant molecules inside chemically modified nanocomposites.

The mechanical characterization resulted in an increasement in a 25.3% in tensile modulus and an 11.2% in yield strength, representing increased stiffness and resistance to permanent deformation. Since elongation exhibited a moderate reduction, flexibility was retained in an acceptable range. The crystallinity, which was initially decreased by the unmodified fillers, increased to 73.4% within the modified composite. Morphological analysis using SEM revealed that notable improvements in dispersion and interfacial adhesion were detected in the sample with TMPED-MCA-HH modified HNTs. This formulation revealed a more compact and homogeneous structure with decreased porosity, suggesting improved matrix packing. In contrast, composites containing unmodified or partially modified HNTs presented limited interaction and no significant changes in lamellar morphology, particularly within the polypropylene (PP) domains. The enhanced morphology in the fully modified samples is associated with the regained crystallinity and improved mechanical performance.

4. IMPACT OF AMINO-SILANE-FUNCTIONALIZED HALLOYSITE NANOTUBES AND B-CYCLODEXTRIN ON ODOR AND MECHANICAL PERFORMANCE IN SUSTAINABLE WOOD–POLYMER COMPOSITES

4.1 Abstract

This chapter analyses the impacts of amino silane functionalized halloysite nanotubes and beta-cyclodextrin on decreasing undesirable odor release. Also, they preserves the mechanical properties of WPCs derived from recycled polyolefin, polypropylene, and polyamide 11 in parallel. WPCs are sustainable materials that combines wood fibers with thermoplastics, providing an appealing solution that coordinates capabilities to improve mechanical properties with sustainability considerations. Even so, the presence of undesirable odor emissions hinders their application in interior spaces. In dealing with this issue, an examination was made within Halloysite Nanotubes (HNT) and Modified Halloysite Nanotubes (Mod-HNT), characterized by their nanoscale size, lumen structure, and absorption and adsorption features, and β-Cyclodextrin (β-CD), which offers a toroidal structure advantageous to the encapsulation of hydrophobic molecules and the adsorption of aromatic hydrocarbons. WPCs containing 30 wt.% WF were produced with 2 wt.% and 5 wt.% of these additives. The examination of odor reduction was performed through the Odor (Jar) test and Headspace Gas Chromatography (HS GC-MS), while the spectroscopic properties were investigated using Fourier Transform Infrared Spectroscopy (FTIR) and the thermal properties were assessed through Thermogravimetric Analysis (TGA) and Differential Scanning Calorimetry (DSC). Odor analyses shows that VOCs such as Nonane, 5-butyl, and Furfural in PP-based WPCs decreased by in excess of 27 percent through the addition of halloysite nanotubes (HNT) and modified HNT (Mod-HNT), and by 96 % with Mod-HNT alone. Tensile tests stated an apparent improvement in tensile strength, particularly in polypropylene-based

composites with Mod-HNTs. The findings offers that Mod-HNT and β-CD effectively improve odor reduction and mechanical performance in sustainable WPCs.

4.2 Introduction

Wood–polymer composites (WPCs) combine thermoplastic matrices with lignocellulosic fillers, like wood fibers, and are gaining growing popularity in structural and semi-structural applications because they are sustainable material properties. The incorporation of neat, recycled, or biobased polymers such as polypropylene (PP), recycled polyolefins, biobased polyamide 11 (PA11), and renewable fibers makes WPCs as environmentally friendly alternatives to traditional plastic-based materials. While WPCs offer certain advantages, they can also release VOCs resulting from the wood components and contaminants found in recycled polymers. The emissions offer major challenges for indoor environments, primarily due to concerns regarding unpleasant odors.

The release of VOCs from wood or plastic materials is an ongoing problem limiting the wider usage of WPCs, particularly in indoor applications. The practical application of WPCs in consumer-facing applications is restricted by these VOCs, which can produce unwanted odors and potentially have a negative impact on the environment and satisfaction of users. Formaldehyde, acetaldehyde, and monoterpenes are just three of the main VOCs released from WPCs that have been observed in studies to contribute to indoor air pollution and sensory dissatisfaction (Väisänen et al, 2016). Other molecules, like cyclohexene, keep on existing even during ongoing ageing periods, despite the fact that emission rates of many VOCs tend to decrease over time. The species of wood, additive composition, processing conditions, and the polymer matrix all have a significant impact on the quantity and types of emissions (Schwarzkopf & Burnard, 2016). With the goal decrease these VOCs while improving overall material's performance, present study is increasingly focused on improving the material composition and surface chemistry of WPCs. This will enable conventional plastics to be considerably replaced in consumer and interior applications.

There are also other researches in materials were studied for overcoming mechanical and sensory limitations by introducing nanostructured additives. However, this study is focusing on improving the strength of polymer matrices while also capturing odor emissions. Halloysite nanotubes (HNTs) are a special additive, consisting of naturally

occurring aluminosilicate clays characterized by their high aspect ratios, tubular forms, and wide surface areas. The unique properties of HNTs enable them to serve multiple functions as mechanical reinforcers and as adsorbents for VOCs applying both their internal lumen and external surface (Cheng et al, 2020; Erdoğan et al, 2014). Despite this, they have challenges for achieving effective interfacial adhesion and uniform dispersion within non-polar polymers, including recycled polyolefins and polypropylene. This incompatibility problem can be solved by chemically modifying the surfaces of HNT using silane coupling agents. These agents enable covalent interactions and hydrogen bonding between the filler and the polymer matrix. The functionalization with amino-silane specifically improves the compatibility at the interface and improves dispersion, which provides the overall mechanical integrity of the composite. Research suggests that silane-treated halloysite nanotubes notably improve tensile strength, Young's modulus, and thermal stability in systems based on poly(butylene terephthalate), polyethylene, and polyamide (Senyel & Dike, 2024). ; Ghosh et al, 2022; Uner, 2022). Furthermore, the modified nanotubes result in a decrease in micro void formation while improving crystallinity, and this results in improved load transfer and more efficient VOC diffusion difficulties (Wieczorek et al, 2024). Their increased polarity and surface activity also improve the performance of VOC adsorption.

In addition to HNTs, β-cyclodextrin (β-CD), which are a toroidal cyclic oligosaccharide, has gained extensive application in polymer systems for the purpose of encapsulating small hydrophobic molecules, including aromatic VOCs. The internal cavity enables the formation of host–guest inclusion complexes, preparing it as a promising additive for decreasing odor intensity in composite materials (Beltrán et al, 2019). While the individual effectiveness of Mod-HNTs and β-CD has been determined for many different kinds of polymer systems, their synergistic application in WPCs has still needs to be thoroughly investigated. It is important to point out that there have been no systematic studies assessing the effects of both of the Mod-HNT and β-CD on mechanical performance and the decreasing of VOCs in WPCs that are formulated with bio-based PA11. Considering the thermal and mechanical strength of PA11, in addition to its biobased origin and increasing significance in industry, exploring its integration into low-odor, high-performance WPCs presents a promising still underexplored area of research. So, this creates specific gap in our knowledge.

This research aims to fill the existing gap by investigating the affects of HNTs, Mod-HNTs, and β-CD on VOC emissions and mechanical performance in WPCs that are separately formulated with rPO, PP, and bio-based PA11 matrices. All composites were produced using 30 wt.% wood fiber and added with 2 wt.% and 5 wt.% of each additive. The analysis of VOCs was conducted through HS GC-MS and odor (jar) tests. Meanwhile, the evaluation of structural and thermal properties was done using FTIR, TGA, DSC, and tensile testing. The results search to support the development of multifunctional WPCs that comply with sustainability, odor control, and mechanical requirements in different polymer applications.

4.3 Materials and experimental

4.3.1 Materials

Biobased semicrystalline Polyamide 11 (PA11) with the Rilsan trade name that has the melt flow rate of 22 g/10 min (at 235°C and 10 kg) in white polymer granules form are derived by Arkema, France. Recycled polyolefin (rPO) polymer derived in light green pellet form which consist of 70% Polyethylene (PE) and 30 wt.% Polypropylene (PP) on production waste from factory were supplied by Hayat Kimya, Kocaeli, Türkiye. Polypropylene (PP) HE125MO homopolymer that has a density of 905 kg/m³, MFR (melt flow rate) value 12 g/10 min (230 °C/2.16 kg), and derived in white granule form for injection molding application were supplied by Borealis Compounds, Inc., North Carolina, USA. Wood Fiber with 20-40 μm width 1.5-2.5mm weighted average length and consists of 70 wt. % oak (Quercus robur) and 30 wt. % pine (Pinus sylvestris). is supplied by Kastamonu Integrated Wood Industry Co. Inc., Gebze/Kocaeli, Türkiye. Halloysite nanotube (HNT) was obtained from Esan Eczacıbaşı Industrial Raw Materials. The components that we synthesized Mod-HNT in previous study which are N-[3-(Trimethoxysilyl) propyl]ethylenediamine (TMPED), Monochloroacetic acid (MCA) and Toluene, are bought from Sigma Aldrich, Merck Group, St. Louis, Missouri, USA and also, Hydrazine hydrate (HH) was supplied in liquid form by Sigma-Aldrich Chemie GmbH - Taufkirchen, Deutschland. *β*-Cyclodextrin ≥97 % purity in white powder form with was obtained by Sigma Aldrich, Merck Group, St. Louis, Missouri, USA.

4.3.2 Production of WPC Composites

Wood fiber (WF) and PP,rPO,PA11 polymers were dried by heat at 80°C for 24 hours. After that, WPC formulations were prepared with same composition for each type of polymer-based WPCs as 70 wt. % polypropylene (PP) and 30 wt.% wood fiber (WF). The formulations were produced using an ultra-high-speed Gelimat GI, thermokinetic mixer (Draiswerke, USA) by high shear forces and short retention times. The components were compounded at high shear forces (approximately 4000 rpm) and short retention times and reaches to melting temperature that allows homogenous mixing. After that, WPC compounds were subjected to cooling and following granulation using a plastic granulator (Rhong Machinery, China). The obtained WPC granules were molded to make specimens suitable for mechanical and thermal evaluation through injection molding (Xplore, Sittard, Holland) at different melt temperatures according to each components processing temperatures. Melting temperature of 240 °C, 220 °C, 230 °C respectively, a mold temperature of 35°C, and an injection pressure of 12 bar used for PP, rPO and PA11 based WPC formulations. Injection molded PP, rPO and PA11 based WPC samples with 2 and 5 wt.% HNT, Mod-HNT and β-CD were shown in Figure 23, Figure 24, and Figure 25.

Figure 23. Injection molded rPO-based WPC samples with HNT, Mod-HNT and β-CD

Figure 24. Injection molded PP-based WPC samples with HNT, Mod-HNT and β-CD

Figure 25. Injection molded PA11-based WPC samples with HNT, Mod-HNT and β-CD

4.4 Material Characterization

4.4.1 Odor (Jar test) Analysis

The Jar (Odor) test consisted of evaluating the odor of samples containing 70 wt. % polymer (PP, rPO, PA11) and 30 wt. % wood fiber (WF), together with WPCs containing 2 and 5 wt. % additives (HNT, Mod-HNT, β-CD). These samples were stored in gas-sealed jars under standard test temperatures and time conditions. All of them were exposed to air contact for a period of 12 days as part of the preparation conditions for the test. Then, the specimens were kept in gas-tight sealed jars that included a stainless-steel wire mesh at the bottom in order to avoid direct contact with 50 ml of distilled water. The samples were then subjected to three different oven conditions: 25°C for 24 hours, 40°C for 24 hours, and 65°C for 2 hours. At the end of the test, five independent raters evaluated the odors according to their intensity of all the jars with samples numbered 1 to 7 in mixed order (so that they could be evaluated objectively without knowing their contents). The average outcomes from their evaluations were presented as a results table.

4.4.2 HS GC-MS Analysis

Headspace Gas Chromatography-Mass Spectrometry (HS GC-MS) were used for identification of VOCs in samples. VOCs were extracted using a 1 g sample in a 10 mL HS-vial equipped with a PTFE septum. The samples undergo conditioned and exposed to HS at 125 °C with an agitation at 250 rpm. Blanks were run after each sample as a control. A HS-20NX Headspace autosampler from Shimadzu Scientific Instruments (U.S.A) was employed. The compounds were heated from 50°C at a rate of 3 °C/min to 200 °C at a rate of 12 °C/min temperature program on a GCMS-QP2010 Ultra Gas Chromatography Mass Spectrometry (GCMS) (Shimadzu Scientific Instruments, Carlsbad, CA, USA) which has 250 °C temperature. Injection at 200 C at 5s. The split ratio was 1: 20. Separation was achieved using a InertCap Pure-WAX capillary column (0.25 mm x 60 µm x 0.25 µm) and helium as carrier gas (1 mL/min) with the 22 cm/s average velocity. VOCs were determined by retention time and mass spectra and appear as peaks in the chromatogram by using the National Institute of Standards and Technology standard reference database (WILEY7). For the quantification of VOC's,

calibration was carried out using acetone as the calibration solution at seven different concentrations (0.1 / 0.5 /1 / 5 /10 / 50 and 100 g/L) in 1-butanol. A linear calibration curve was drawn by using these seven calibration points. Calibration measurements applied a 5 µL syringe to inject 2 µL of the solution into each 10 mL HS vial. The limit of detection (LOD) for VOC peaks was calculated by identifying peaks with heights at least three times greater than the baseline noise and areas higher than 10% of the acetone peak area, with the acetone concentration in the calibration solution set at 0.5 g/L. The images of the samples in the vial, which were placed in the HS unit and tested in the HS GC-MS device, are given in Figure 26 below.

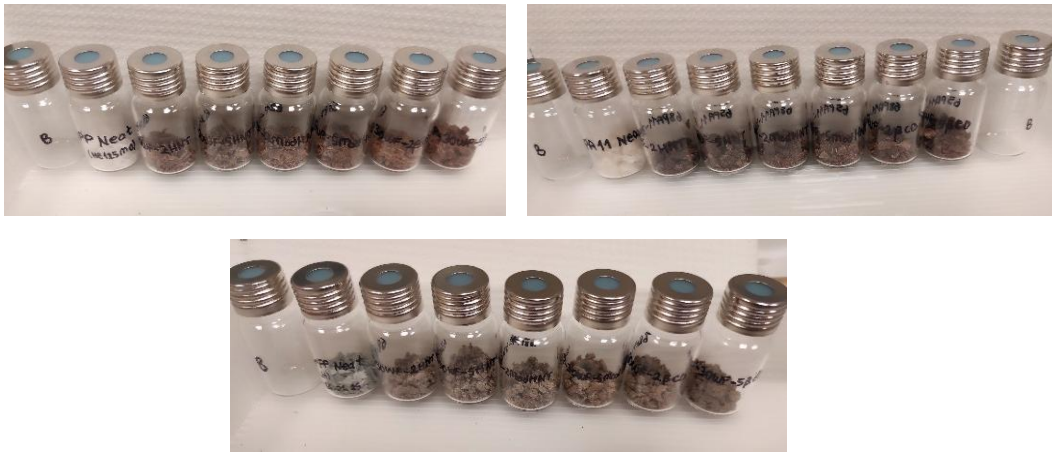

Figure 26. All of the WPC samples in vials that tested by HS GC-MS

4.4.3 Mechanical (Tensile) Testing

Tensile tests were applied for determining mechanical characteristics using a 5982 Static Universal Test Machine at Sabancı University (UTM, Instron, Norwood, MA, USA) at a rate of 2.0 mm/min and a 5 kN load cell, in accordance with ISO 527-2 standards. Tensile testing complying with the ISO 527-2 standard was used to determine the mechanical properties of five dog bone WPC samples with a PP matrix. Each specimen sized 2mm in thickness and 5mm in width. The test was conducted that use a 5 kN load probe and a tensile speed of 1000 mm/min using an Instron-100kN Universal Electromechanical Test Machine (Massachusetts, US), which was equipped with an extensometer for measuring elongation (%).

4.4.4 FTIR Spectroscopy Analysis

The examination of chemical structure of the WPCs was conducted with a Fourier-Transform Infrared Spectrometer (FTIR Thermo Scientific / Nicolet iS10, Waltham, Massachusetts, USA). FTIR spectra were obtained within the wavelength range of 4000–

600 cm-1 at a resolution of 16 cm-1 to identify a presence of functional groups and interactions among the composite components.

4.4.5 TGA analysis

Thermogravimetric analyses of the materials were performed using a TA Q 500 TGA and with Universal Analysis 2000 software. Analyses were performed under a nitrogen atmosphere at a heating rate of 20°C per minute, which ranged from room temperature to 950°C.

The thermal stability of the specimens was determined using thermogravimetric analysis (TGA) from Mettler Toledo, Giessen, Germany. The study was performed within a temperature range of 20 to 700 °C, with a heating rate of 10 °C per minute in a nitrogen atmosphere.

4.4.6 DSC Analysis

The influence of HNT, Mod-HNT, and β-CD additions on the thermal transition temperatures and crystallinity of the WPCs were studied in an inert nitrogen atmosphere with a Differential Scanning Calorimeter (DSC) (Mettler Toledo DSC 3, Giessen, Germany). The STAR® SW 16.10 software (Mettler Toledo, Columbus, OH, USA) was used for determining the melting enthalpy (ΔHm), melting temperature (Tm), cold crystallization temperature (Tc), and cold crystallization enthalpy (ΔHc).

DSC analysis was performed throughout three cycles. In the initial step of the cycle for PP and rPO WPC formulations, the samples were heated from room temperature to 200 °C at a rate of 10 °C/min and then kept at 200 °C for 2 minutes to eliminate their thermal history. Following the second cycle, the samples were cooled from 200 °C to -70 °C at a rate of 10 °C/min before being kept at -70 °C for 2 minutes. The cold crystallization temperatures (Tc) have been calculated from the highest point of the peaks in the resultant thermogram. During the third cycle, the samples were reheated from -70 °C to 200 °C at a rate of 10 °C/min, and the melting temperatures (Tm) were obtained from the maximum of peak viewed in this last heating cycle. Differently, cycle temperatures for PA11 WPC formulations ranged from -70 °C to 300 °C at a rate of 10 °C/min. The crystallinity degree (Xc) for each sample was determined using (Eq. (1)):

$$X_c = [\Delta H_m / \Delta H_m^{\circ}] \times 100\% \quad (1)$$

where ΔH_m is the melting enthalpy and ΔH_m° is the melting enthalpy of 100% crystalline polymer and w_F corresponds to the weight percentage of fiber in the composite. The

theoretical value of melting enthalpy 100% crystalline polypropylene ($\Delta H_{m_{PP}}^{\circ}$) is 207 J/g, for 100% crystalline polyethylene ($\Delta H_{m_{PE}}^{\circ}$) is 293 J/g [88, 89] and for 100% crystalline polyamide 11 ($\Delta H_{m_{PA11}}^{\circ}$) is 189 J/g (Jeziórska et al, 2021).

4.5 Results and Discussion

4.5.1 Sensory Odor Analysis Result

The effect of HNT, Mod-HNT and β-CD on the odor of WPCs has been investigated using the Indoor Odor (Jar) test, according to the FORD FLTM BO 131-03 Interior Odor Test standard. The results were provided in Table 13 below.

The indoor odor performance of wood fiber-reinforced polymer composites combining additives was investigated under three thermal ageing conditions. The findings suggests a distinct association of composition, temperature, and odor intensity. The 70% polymer – 30 wt.% wood fiber (WF) composites (70rPO-30WF, 70PP-30WF, PA11-30WF) had moderate to unpleasant odor level of intensity. At 65 °C, the rPO-based sample released a rating of 5.0 (strongly disturbing), whereas the PP and PA11 based WPCs received ratings of 3.5 (slightly disturbing), implying increased odor in parallel with temperature.

The addition of 5 wt.% ModHNT resulted in an important reduction in odor ratings to 2.5 (clearly perceptible but not disturbing) at 65 °C. This proves that residual contaminants or degradation products in recycled materials show need more responsive odor control strategies and most effective solution was achieved with Mod-HNT additive in rPO based WPCs in this study.

In polypropylene-based composites, the addition of 5 wt.% β-cyclodextrin (β-CD) and 5 wt.% ModHNT successfully decreased odor levels. The additives successfully prevented of odor releasing within all conditions, keeping values between 1.5 and 2.0 (slightly perceptible to not disturbing), even during cases of high temperatures. This clarifies an advantageous interaction between PP matrices and functional additives, which results in stable and sufficient odor performance.

Polyamide 11-based wood-plastic composites displayed preferred odor performance constantly. PA11 formulations, even with unmodified HNT exhibited rather low odor degrees, which were reduced further by the inclusion of 5 wt.% ModHNT or 5 wt.% β-CD. In such situations, odor ratings consistently range from 1.0 to 1.5 (not perceptible to

slightly perceptible) under all ageing conditions, indicating the intrinsic stability of PA11 and the efficacy of the specified odor-controlling additives.

Overall, odor performance in WPCs is considerably impacted by the selection of polymer and additive. Recycled polyolefin-based WPCs have limitations resulting from their complex composition; however, virgin polypropylene and particularly polyamide 11-based systems suggest a positive response to specific additive strategies. ModHNT and β-cyclodextrin stated the highest efficiency, resulting in PA11 based WPCs with the lowest and most thermally stable odor levels. The outcomes approve of the choice of suitable additive–polymer combinations for low-odor biocomposite applications, especially in indoor or odor-sensitive applications.

Considering the subjective nature of the odor (jar) test, it turned out that an additional supportive and more qualitative testing method, such as HS GC-MS, was required.

Table 13. Table of indoor odor (jar) test results of rPO, PP and PA11 based WPCs

Test Conditions	**Samples**		
	rPO Neat	**PP Neat**	**PA11 Neat**
1 (25°C, 24 h)	4,5	3	2
2 (40°C, 24 h)	5	3,5	2
3 (65°C, 2 h)	5,5	3,5	2,5
	70rPO-30WF	70PP-30WF	PA11-30WF
1 (25°C, 24 h)	5	3,5	2
2 (40°C, 24 h)	5	3,5	2,5
3 (65°C, 2 h)	5,5	4	2,5
	68rPO-30WF-2HNT	68PP-30WF-2HNT	68PA11-30WF-2HNT
1 (25°C, 24 h)	4	3	1,5
2 (40°C, 24 h)	4,5	3	1,5
3 (65°C, 2 h)	5	3,5	2
	65rPO-30WF-5HNT	65PP-30WF-5HNT	65PA11-30WF-5HNT
1 (25°C, 24 h)	3,5	2,5	1,5
2 (40°C, 24 h)	3,5	3	2
3 (65°C, 2 h)	4	3	2
	68rPO-30WF-2ModHNT	68PP-30WF-2ModHNT	68PA11-30WF-2ModHNT
1 (25°C, 24 h)	2,5	2,5	1,5
2 (40°C, 24 h)	2,5	2,5	1,5
3 (65°C, 2 h)	3	3	2
	65rPO-30WF-5ModHNT	65PP-30WF-5ModHNT	65 PA11-30WF-5ModHNT
1 (25°C, 24 h)	1,5	2	1,5
2 (40°C, 24 h)	1,5	2,5	1,5
3 (65°C, 2 h)	2	2,5	2

	68rPO-30WF-2β-CD	68PP-30WF-2β-CD	68PA11-30WF-2β-CD
1 (25°C, 24 h)	2	1,5	1
2 (40°C, 24 h)	2,5	1,5	1,5
3 (65°C, 2 h)	3	2	1,5
	65rPO-30WF-5β-CD	65PP-30WF-5β-CD	65PA11-30WF-5β-CD
1 (25°C, 24 h)	3	1,5	1,5
2 (40°C, 24 h)	3	2	1,5
3 (65°C, 2 h)	3,5	2	2

4.5.2 HS GC-MS Result

HS GC-MS chromatogram table of Undesirable odor VOCs from WPC samples are shown in Table 14. The results presented in this section relate very closely with the findings explained in Chapters 2 and 3, that extensively studied the odor and VOC characteristics of WPCs formed from polypropylene and recycled polyolefins. Improvements in the formation and inhibition of odor-causing VOCs have been discovered to be similar as well. The following chapter offers unique outcomes related to PA11-based wood plastic composite formulations that were not previously studied.

The VOC profiles of polyamide 11 (PA11)-based WPCs were investigated using headspace gas chromatography-mass spectrometry (HS GC-MS) to determine the impact of these different types of additives on VOC adsorption. Table 2 reveals that the WPC with 70PA11-30WF formulation released an extensive amount of VOC peaks (144). Thus, it appears that, even though the existing thermal stability of PA11, considerable volatiles can be released as a result of wood fiber degradation along with possible interactions between the matrix and filler during melt processing.

The integration of 2 wt.% and 5 wt.% halloysite nanotubes (HNT) considerably decreased the total number of VOC peaks noticed. The peak number of VOC in 68PA11-30WF-2HNT and 65PA11-30WF-5HNT decreased to 7 and 6, meaning reduction rates of 95% and 96%, respectively. High specific surface area and tubular nanostructure of HNT increase the adsorption of low molecular weight volatiles, such as 2-propanol, acetaldehyde, and heptan-2-one.

Organically modified HNT (Mod-HNT) demonstrated comparable, and in certain instances slightly enhanced, VOC suppression. The samples 68PA11-30WF-2ModHNT and 65PA11-30WF-5ModHNT demonstrated reductions of 95% and 96%, respectively. The formulations exhibited minimal residual VOCs, predominantly consisting of ethanol, acetaldehyde, and trace amounts of ketones. This improved efficiency of Mod-HNT is

achieved by its surface functional groups, which develop interactions with polar VOC species by chemical adsorption functions and physical capture.

Moreover, β-cyclodextrin (β-CD) revealed an interesting ability to reduce VOCs. Samples that includes 2 wt.% and 5 wt.% β-CD revealed VOC reduction rates of 94% and 95%, respectively. The residual compounds in these samples, primarily ethanol and furfural, were found at notably reduced concentrations. β-CD demonstrates notable efficacy in targeting compounds like furfural and benzaldehyde, attributed to its capacity to form host–guest inclusion complexes with hydrophobic volatile molecules.

In summary, all three additives (HNT, Mod-HNT, and β-CD) effectively reduced VOC emissions in PA11-based wood plastic composites. The integration of PA11's natural degradation resistance with the VOC-capturing capabilities of the additives produced a composite system exhibiting superior odor control properties. Mod-HNT and β-CD demonstrated superior efficacy in reducing a broad spectrum of both polar and non-polar VOCs, which is critical for applications requiring low-emission, odor-sensitive materials.

Table 14. Undesirable odor VOCs identified according to the HS GC-MS chromatogram

Sample Names	**Total VOCs peaks***	**VOC reduction Rate (%)**	**Residual VOCs**
70rPO-30WF	162	-	-
68rPO-30WF-2HNT	10	94	Ethanol / Propanoic acid, 2-hydroxy-, ethyl ester, (S)- / Propanoic acid, 2-hydroxy-, butyl ester / Chloromethane / Toluene
65rPO-30WF-5HNT	11	93	Ethanol / Propanoic acid, 2-hydroxy-, ethyl ester, (S)- / Methane, chloro- (CAS) Chloromethane / Toluene
68rPO-30WF-2Mod-HNT	10	94	Ethanol / Propanoic acid, 2-hydroxy-, ethyl ester, (S)- /2,3-Butanedione / Toluene
65rPO-30WF-5Mod-HNT	10	94	2-Propanol / Propanoic acid, 2-hydroxy-, ethyl ester, (S)- / Ethanol / 2,3-Butanedione
68rPO-30WF-2β-CD	12	92	2-Propanol / Propanoic acid, 2-hydroxy-, butyl ester / Ethanol / 2,3-Butanedione / 2-Propanol, 1,1'-oxybis- /
65rPO-30WF-5β-CD	12	92	Dimethylamine / 2-Propanol /Ethanol / 2,3-Butanedione / Propanoic acid, 2-hydroxy-, butyl ester / 2-Propanol, 1,1'-oxybis-

70PP-30WF	30	-	-
68PP-30WF-2HNT	24	20	Octane, 4-methyl- /2,3-Butanedione/ Nonane, 5-butyl- / Dodecane, 4,6-dimethyl- / Acetic acid/ Furfural
65PP-30WF-5HNT	24	20	Octane, 4-methyl- / 2,3-Butanedione / Nonane, 5-butyl- / Dodecane, 4,6-dimethyl-/ Acetic acid / Furfural
68PP-30WF-2Mod-HNT	22	**27**	Octane, 4-methyl-/ Nonane, 5-butyl- / Acetic acid / Furfural
65PP-30WF-5Mod-HNT	22	**27**	Octane, 4-methyl-/ Nonane, 5-butyl- / Acetic acid / Furfural
68PP-30WF-2β-CD	25	17	Octane, 4-methyl-/ Nonane, 5-butyl- / Acetic acid / Furfural
65PP-30WF-5β-CD	26	13	Octane, 4-methyl-/ Nonane, 5-(2-methylpropyl)- / Acetic acid/ Heptadecane / Furfural
70PA11-30WF	144	-	-
68PA11-30WF-2HNT	7	95	Acetaldehyde (CAS) Ethanal, 2-Propanol (CAS) Isopropyl alcohol, 2-Heptanone (CAS) Heptan-2-one. Acetic acid
65PA11-30WF-5HNT	6	96	2-Propanol (CAS) Isopropyl alcohol. 2-Heptanone (CAS) Heptan-2-one. Acetic acid
68PA11-30WF-2Mod-HNT	5	**97**	Acetaldehyde (CAS) Ethanal. Benzene, methyl- (CAS) Toluene, 2-Heptanone (CAS) Heptan-2-one, Acetic acid
65PA11-30WF-5Mod-HNT	6	**96**	Methane, chloro- (CAS) Chloromethane. Acetaldehyde (CAS) Ethanal. Acetic acid, methyl ester (CAS) Methyl acetate, Benzene, methyl- (CAS) Toluene. 2-Heptanone (CAS) Heptan-2-one. Acetic acid. Furfural
68PA11-30WF-2β-CD	9	94	Acetaldehyde (CAS) Ethanal, 2-Propanol (CAS) Isopropyl alcohol, 2-Heptanone, Acetic acid, Furfural
65PA11-30WF-5β-CD	7	95	Acetaldehyde (CAS) Ethanal, 2-Heptanone, l-Limonene, Propanoic acid, 2-hydroxy-, ethyl ester, (S)-, Acetic acid, Furfural

*After reducing peaks according to 10% Acetone (control and calibration solution) peak height

4.5.3 Mechanical Test Result

Mechanical tensile properties of WPCs applying three different types of polymer matrices of recycled polyolefin (rPO), polypropylene (PP), and polyamide 11 (PA11)

were identified and outlined in Tables 15, 16 and 17. The effects of all of the additives, comprising halloysite nanotubes (HNT), surface-modified HNT (Mod HNT), and β-cyclodextrin (β-CD), on tensile strength, modulus, and ductility was analyzed.

Out of all the WPCs, PA11-based composites revealed more efficient mechanical performance. The PA based WPC (70PA11-30WF) showed a tensile strength of 50.7 MPa and a tensile modulus of 2817.8 MPa, significantly going above the test results of both rPO and PP-based WPCs. The highest tensile strength noticed in PP-based WPCs was 37.3 MPa (65PP-30WF-5ModHNT), while rPO-based composites was 22.7 MPa (65rPO-30WF-2ModHNT).

The addition of 5 wt.% Mod HNT resulted in the highest tensile strength of 52.6 MPa and a stiffness of 2948.5 MPa, while keeping the necessary ductility with a yield strain of 3.6% in PA11 WPCs, . The identified developments come from increased interaction between the filler and matrix, resulting from the surface functionalization of HNT, resulting in improved stress transfer efficiency while preserving elongation properties.

In the same way, the addition of β-cyclodextrin at rates of 2 and 5 wt.% generated tensile strengths of 52.3 MPa and 52.8 MPa, respectively, with the 5 wt.% β-CD sample having a modulus of 2976.7 MPa. While displaying a modulus slightly lower than the Mod HNT sample, formulations containing β-CD revealed higher elongation at break, pointing to a more balanced stiffness-ductility relationship.

Significant changes were discovered as well in PP-based WPCs using Mod HNT and β-CD. The greatest yield strength detected as 37.3 MPa in the 5 wt.% Mod HNT sample. It also showed a tensile modulus of 3912.1 MPa that has highest stiffness among all samples. But the increase in stiffness was followed by a decrease in strain values (2.6% yield strain), suggesting it caused brittleness.

rPO-based composites revealed the lowest tensile performance overall, likely is due to chain scission and structural heterogeneity caused by previous life cycles. With the addition of 5 wt.% Mod HNT, the tensile strength obtained was 22.7 MPa, together with a modulus of 2607.1 MPa, and the lowest elongation values noticed within all systems. These results demonstrate the limitations of structure of recycled matrices in mechanical reinforcement.

In overall, PA11-based WPCs suggested improved strength and stiffness in comparison to PP and rPO WPCs, while also demonstrating the most balanced mechanical properties when Integrated with Mod HNT or β-CD. The results suggest

selecting of both the polymer matrix and odor reducer additive plays a significant role in determining the resulting mechanical performance of WPCs. Among the all of them, PA11 with 5 wt.% Mod HNT revealed the highest mechanical durability, indicating significant potential for high-performance biocomposite applications.

Table 15. Table of tensile results of WPCs with rPO matrix

Sample	**70rPO-30WF**	**68rPO-30WF-2HNT**	**65rPO-30WF-5HNT**	**68rPO-30WF-2Mod HNT**	**65rPO-30WF-5Mod HNT**	**68rPO-30WF-2β-CD**	**65rPO-30WF-5β-CD**
Tensile Strength (MPa)	20.8 (±0.3)	20.2 (±0.6)	22.5 (±0.5)	20.9 (±0.1)	22.7 (±0.7)	19.9 (±0.9)	20.0 (±1.1)
Tensile Modulus (MPa)	2403.2 (±50.1)	2323.5 (±74.9)	2672.5 (±58.4)	2460.7 (±166.8)	2699.8 (±42.8)	2496.4 (±82.1)	2334.6 (±99.5)
Max Strain (%)	10.9 (±5.1)	9.2 (±1.7)	5.6 (±0.7)	7.1 (±0.3)	6.1 (±0.6)	10.6 (±0.9)	24.7 (±1.2)
Max Strength (MPa)	2.1 (±1.1)	1.2 (±1.1)	5.8 (±3.7)	3.9 (±1.9)	2.3 (±1.2)	3.3 (±2.2)	0.5 (±0.4)
Yield Stress (MPa)	20.9 (±0.2)	20.9 (±0.1)	22.54 (±0.5)	21.0 (±0.1)	22.1 (±0.7)	10.9 (±0.9)	20.0 (±1.1)
Yield Strain (%)	3.5 (±0.3)	2.5 (±0.1)	2.2 (±0.1)	2.2 (±0.1)	2.3 (±0.2)	3.4 (±0.3)	4.22 (±0.3)

*Values in the parentheses are standard deviations.

Table 16. Table of tensile results of WPCs with PP matrix

Sample	70PP-30WF	68PP-30WF-2HNT	65PP-30WF-5HNT	68PP-30WF-2Mod HNT	65PP-30WF-5Mod HNT	68PP-30WF-2β-CD	65PP-30WF-5β-CD
Tensile Strength (MPa)	35.4 (±1.9)	35.2 (±1.9)	34.2 (±0.6)	34.8 (±0.7)	37.3 (±1.7)	35.1 (±0.8)	34.0 (±0.7)
Tensile Modulus (MPa)	3628.3 (±0.6)	3848.7 (±29.9)	3722.8 (±95.8)	3716.3 (±61.8)	3921.2 (±92.8)	3727.9 (±205.3)	3849.9 (±98.5)
Max Strain (%)	4.3 (±1.9)	2.6 (±0.3)	2.1 (±1.5)	2.6 (±0.3)	2.7 (±1.2)	3.2 (±1.9)	2.4 (±0.3)
Max Strength (MPa)	24.6 (±3.5)	27.8 (±0.8)	29.6 (±11.4)	25.8 (±2.9)	33.2 (±4.6)	26.5 (±1.9)	26.1 (±1.1)
Yield Stress (MPa)	35.4 (±0.6)	35.2 (±0.4)	34.2 (±0.6)	34.8 (±0.7)	37.3 (±1.7)	35.1 (±0.8)	34.0 (±0.7)
Yield Strain (%)	2.2 (±0.3)	1.9 (±0.2)	1.7 (±0.5)	1.9 (±0.6)	2.0 (±0.2)	2.0 (±0.7)	1.9 (±0.3)

*Values in the parentheses are standard deviations.

Table 17. Table of tensile results of WPCs with PA11 matrix

Sample	70PA11-30WF	68PA11-30WF-2HNT	65PA11-30WF-5HNT	68PA11-30WF-2Mod HNT	65PA11-30WF-5Mod HNT	68PA11-30WF-2β-CD	65PA11-30WF-5β-CD
Tensile Strength (MPa)	50.7 (±5.3)	51.6 (±3.1)	52.1 (±0.9)	52.5 (±2.1)	51.4 (±2.5)	52.3 (±0.9)	52.8 (±0.7)
Tensile Modulus (MPa)	2817.8 (±1.2)	2900.4 (±29.9)	2911.2 (±0.9)	2707.4 (±171.0)	2948.5 (±128.9)	2770.7 (±98.1)	2976.7 (±103.7)
Max Strain (%)	4.9 (±0.3)	4.5 (±1.2)	4.9 (±0.9)	5.2 (±0.7)	3.2 (±0.6)	4.7 (±0.6)	3.2 (±0.4)
Max Strength (MPa)	50.3 (±1.4)	51.3 (±2.9)	51.8 (±0.8)	52.2 (±2.0)	51.3 (±2.5)	51.9 (±0.8)	52.7 (±0.5)
Yield Stress (MPa)	50.7 (±1.2)	51.6 (±1.1)	52.1 (±0.9)	52.5 (±2.7)	51.4 (±1.4)	52.3 (±0.9)	52.8 (±0.7)
Yield Strain (%)	4.7 (±0.3)	4.3 (±0.1)	4.8 (±0.6)	4.9 (±0.2)	3.1 (±0.2)	4.4 (±0.3)	3.2 (±0.1)

*Values in the parentheses are standard deviations.

4.5.4 TGA Analysis

Thermogravimetric analysis (TGA) and its first derivative (DTG) were used for determining the thermal degradation information of polypropylene-based wood plastic composites (WPCs) and neat recycled polyolefin (rPO). This chapter analyses the thermal characteristics of PA11-based WPC formulations containing 30 wt.% wood fiber and functional additives such as halloysite nanotubes (HNT), modified HNT (ModHNT), and β-cyclodextrin (β-CD).

Neat PA11 had a single-step decomposition, defined by a peak degradation temperature of 440.3 °C and a minimal char residue of 0.6% (Figure 27, Table 18). This suggests limited thermal resistance and negligible solid residue for the generation in inert atmospheres. The addition of wood fiber caused in a two-stage decomposition process, indicating the heterogeneity found in the polymer matrix into which the wood fiber has been integrated.

The formulation of PA11-based WPC, including 2 wt.% HNT showed the greatest thermal stability among the tested specimens, understanded by a decomposition peak at 458.7 °C and a char residue of 17.7%. The enhancement is due to the barrier properties of the nanotubes and their ability to capture degradation VOCs. In a similar approach, formulations improved with 5 wt.% HNT and ModHNT displayed higher degradation temperatures (between 452 °C and 455.5 °C) and residue formation, which indicates increased thermal stability of the composite structures. The addition of β-CD produced similar char levels; yet it did not significantly affect the degradation onset, probably since of its carbon-rich once thermally less stable structure.

At the end, these findings offers that the integration of these functional additives into PA11 based WPCs considerably improves their thermal performances. These improvements related with previous research on PA-based nanocomposites, in which HNT appeared to improve thermal stability and char yield in systems of comparable structure (Khan et al, 2025).

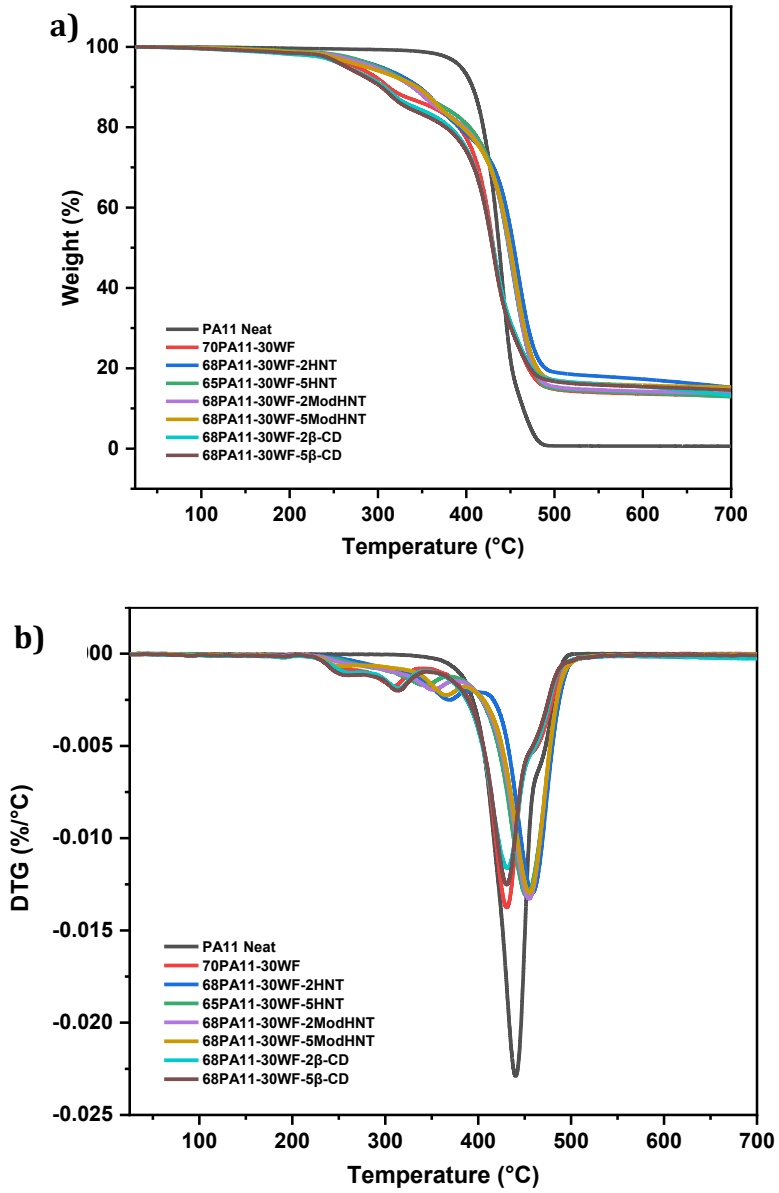

Figure 27. (a) TGA and (b) DTG thermograms of all PP and 30 wt. %WF added WPC samples

Table 18. Onset, peak, endset temperatures, % residue of the neat PA11 and PA11 based WPCs

Sample Name	Peak [PA11] [°C]	Peak [WF] [°C]	Weight Loss [PA11] [%]	Weight Loss [WF] [%]	Residue [PA11] $_{700}$ °C [%]	Residue [WF] $_{@}$ 700 °C [%]
PA11 Neat	440.3	-	99.4	-	0.6	-
70PA11-30WF	430.8	308.3	72.5	13.4	13.99	86.5
68PA11-30WF-2HNT	458.7	367.5	62.3	19.9	17.7	80.0
65PA11-30WF-5HNT	452.5	341.2	71.9	13.8	14.2	86.1
68PA11-30WF-2ModHNT	454.8	350.3	69.3	15.9	14.6	83.9
65PA11-30WF-5ModHNT	455.5	363.8	66.6	17.4	16.1	82.7
68PA11-30WF-2β-CD	431.5	313.7	70.3	13.8	15.9	86.2
65PA11-30WF-5β-CD	430.7	312.8	69.3	14.7	15.9	85.2

4.5.5 DSC Analysis

This section creates onto a previous chapters in this thesis that consist of PP-based WPCs and neat rPO, focusing on the thermal transitions of PA11-based WPCs containing 30 wt.% wood fiber together with functional additives, specifically HNT, ModHNT, and β-CD. The analysis of melting temperature (Tm), crystallization temperature (Tc), and degree of crystallinity (Xc) occurred with differential scanning calorimetry (DSC), given in Table 17 and shown in Figures 28a and 28b.

The neat PA11 presented a melting temperature of 186.9 °C and a crystallization temperature of 162.1 °C, besides a crystallinity of 28.7%. The wood fiber addition resulted in a notable decrease in transition temperatures (Tm = 172.4 °C; Tc = 150.1 °C) and crystallinity (Xc = 21.8%), pointing to that lignocellulosic structures inhibit the orderly configuration of PA11 crystal formation.

Among those the PA11 based-WPC formulations, 2 wt.% ModHNT containing one indicated an improvement in thermal transition performance, as confirmed by an increase in the crystallization temperature (Tc) to 164.3 °C and a

crystallinity (Xc) of 38.2%. It means that ModHNT performs an important function in enabling nucleation and thus improving the process of crystallization. The 5 wt.% ModHNT sample revealed an increase in Tc (163.1 °C) and Xc (25.6%) with respect to the unmodified composite, but to a lower level.

In contrast, the application of β-CD demonstrated minimal advantage. The formulation containing 2 wt.% β-CD exhibited a reduced Tc of 153.6 °C and demonstrated the lowest crystallinity across all samples, with an Xc value of 14.1%. Although the 5 wt.% β-CD variant resulted in a modest increase in Xc to 20.4%, this value remains inferior to that of most other additive systems. This observation shows β-CD may delay, rather than support the formation of ordered crystalline structures in the PA11 matrix.

Results reveal that the thermal transition performance of PA11-based WPCs is considerably effected by the type of additives. ModHNT, especially with a concentration of 2 wt.%, have a significant change in crystallization behavior, suggesting its offering application as a functional reinforcement in biobased composites (Kurtulmus et al, 2025).

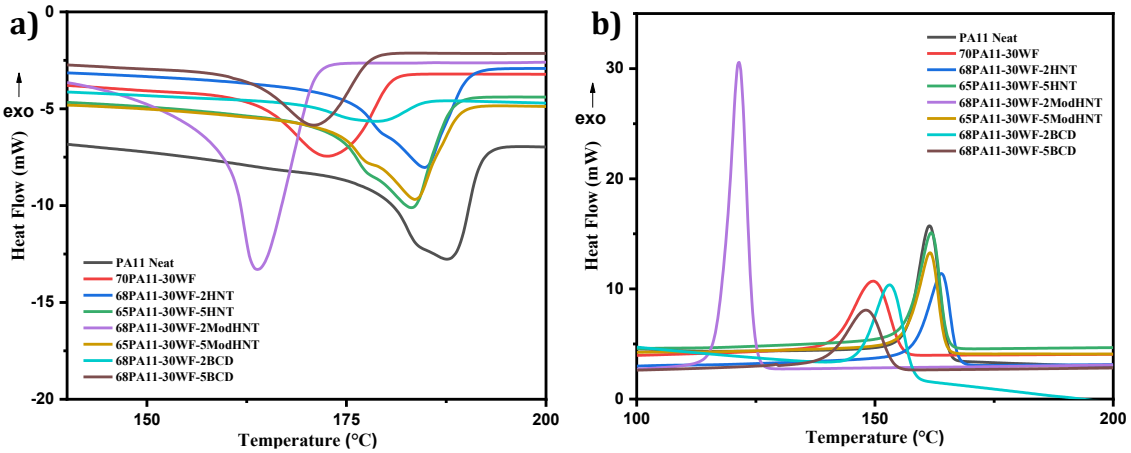

Figure 28. DSC thermograms of WPCs with PA11 matrix: a) melting peaks, b) crystallization peaks

Table 19. DSC results of Tm, Tc, ΔHm, ΔHc, and Xc of the neat PA11 and PA11 based WPC samples

Sample Name	T_{mPA11} (°C)	T_{cPA11} (°C)	ΔH_{mPA11} (J/g)	ΔH_{cPA11} (J/g)	Xc (%)
PA11 Neat	186.9	162.1	54.3	44.1	28.70
70PA11-30WF	172.4	150.1	41.2	40.4	21.82
68PA11-30WF-2HNT	184.5	164.3	40.8	34.1	21.59
65PA11-30WF-5HNT	182.7	162.5	48.5	39.4	25.66
68PA11-30WF-2ModHNT	163.3	122.6	72.1	70.2	38.17
65PA11-30WF-5ModHNT	183.1	162.0	38.9	35.7	20.56
68PA11-30WF-2β-CD	177.5	153.6	26.6	31.2	14.07
65PA11-30WF-5β-CD	170.6	148.5	38.6	35.0	20.42

4.6 Conclusion

This chapter presents an in-depth discussion of the odor performance, volatile organic compound (VOC) emissions, mechanical strength, and thermal characteristics of PA11, PP and rPO based WPCs. The initial focus was on formulations based on biobased WPC formulations with PA11polymer matrix ; but for comparing purposes, WPCs made from PP and recycled polyolefin (rPO), as looked over in Chapters 2 and 3, were also included in the study. Functional additives, involving halloysite nanotubes (HNT), modified HNT (ModHNT), and β-cyclodextrin (β-CD), were added to determine their effect on the performance of the composite.

The results of the odor evaluation revealed that β-CD and ModHNT highly decreased odor intensity at high temperatures, giving ratings that were defined within the slightly perceptible range. The odor results were even further supported by HS GC-MS analysis, which gave results as important reductions in both the amount and intensity of VOC peaks with the use of these additives in WPCs.

PA11-based WPCs showed increased tensile properties, especially for formulations that contained ModHNT, that revealed considerable improvements that were caused by improved interfacial interactions. The performance of these materials exceeded that of their PP-based and rPO-based WPCs, suggesting the potential of PA11 as a bio-based matrix for durable composite applications.

The potential benefits were additionally supported through thermal analysis. The results from TGA displayed that both HNT and ModHNT increased thermal stability and char formation. The DSC analysis found that ModHNT greatly increased crystallinity, hence suggesting its function as an effective nucleating agent within the PA11 matrix.

Overall, this chapter found that aimed additive selection, specifically the use of ModHNT at 2 wt.%, improving the performance of PA11-based WPCs. The outcomes reveal that PA11, when mixed with functional fillers, gives an appealing framework for the production of sustainable and high-performance composite materials.

5. GENERAL CONCLUSION

The growing demand for sustainable, low-emission, and mechanically resilient materials for indoor applications makes WPCs as a beneficial alternative and attracts the focus in the field of material science research. Addressing these requirements requires an extensive method of selecting materials that highlights improved odor management, sustainability in the environment, and overall strength. The studying of them allows the researchers to create specific formulations that can suit regulatory standards while meeting user demands. This thesis aims to offer the findings of an in-depth study focused on the unwanted odor resulting from VOCs, mechanical strength, and thermal properties of WPCs that are formulated by using different polymer matrices and functional additives. These additives, specifically β-CD, HNT, and Mod-HNT, were chosen because of their capabilities in molecular inclusion or adsorption, along with their potential for improving interactions between the matrix and the filler. The selection process to select these additives was driven by their environmental safety, compatibility with bio- or recycled polymers, and their multifunctional properties. This study targets to investigate the performance of these additives compared with each other within different matrices, specifically PP, rPO, and PA11, while keeping a consistent fiber loading of wood fiber (30 wt.%) and complying to specified ageing conditions. Figure 2 presents a summary diagram that illustrates the key problem, materials, functional additives, objectives, and findings of this thesis.

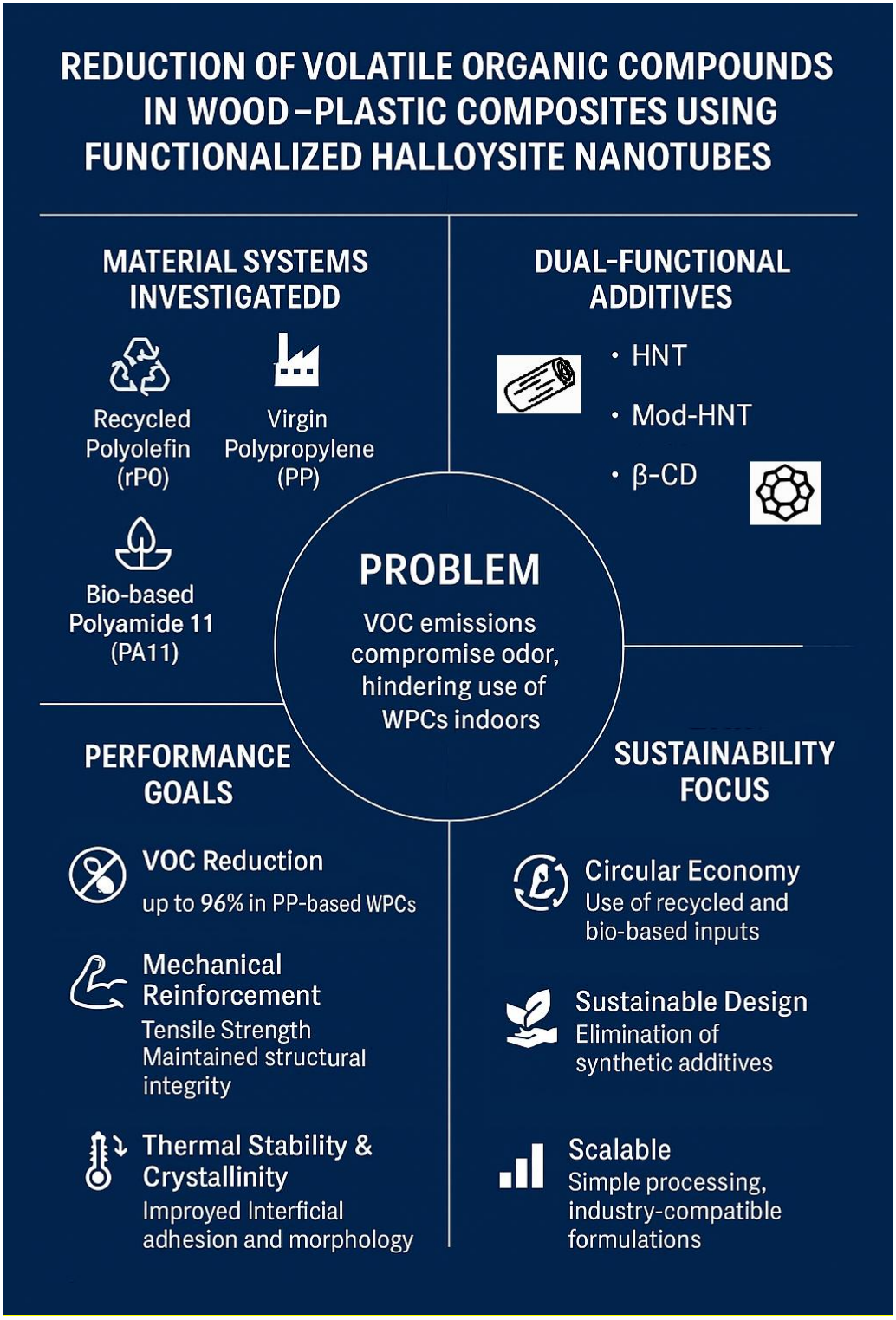

Figure 29. Summary diagram of the thesis

The first chapter presents the study, highlighting the significance of improving odor reduction and environmental safety as one of the key challenges in the producing of WPCs. The importance for indoor applications, using bio-based alternatives, and the role of functional additives are clearly explained. The research questions, scope, and novelty are clearly defined, laying the foundations for upcoming experimental study.

The second chapter aims to improve both odor-related VOCs reduction and mechanical properties in PP based WPCs. The study investigated through different combinations of β-CD and unmodified HNT, and commercial additives and focusing specifically on how they affect odor by releasing VOCs. Each additives played a role in improving outcomes; however, the most notable performance was observed with β-CD at a concentration of 5 wt.%, which resulted in decreased odor intensity with VOC amounts. The results obtained formed a reference point for the effectiveness of additives in pp-based WPCs. They revealed that, even at relatively low initial odor levels, the addition of additives may correspond to considerable improvements in overall performance.

In the third chapter, we succeeded in making the surface modification of HNT with amino-functional silane compounds (Mod-HNTs) to further improve the VOC encapsulation performance discussed in the previous chapter. This section worked on rPO polymer characterized by high odor levels that originate from degradation products resulting from previous usage cycles. The study aimed at developing the absorption of VOCs through the use of halloysite-based additives. The formulations comprised unmodified HNTs at concentrations of 2 and 5 wt.%, and also ModHNTs, namely rPO–5TMPED-HNT, rPO–5TMPED-MCA-HNT, and rPO–5TMPED-MCA-HH-HNT. The modified HNTs revealed an impressive reduction in both the peak intensity and the number of VOCs, reaching up to 91 % reduction when compared to neat rPO, according to results of HS-GC-MS analyses. The improvements in performance seen can be related to higher surface activity and the selective interaction with polar VOCs, which is made possible by the functionalization with amino-silane. This chapter pointed out the considerable advantageous potential of ModHNTs in recycling-based composites, making it possible even in high-emission matrices such as rPO to offer notable adjustments in indoor air compatibility.

In the fourth chapter, the scope of the investigation was broadened with PA11-based WPC formulations. The findings suggest that PA11 WPCs naturally have lesser odor

intensity when compared to PP and rPO WPCs. Among all of the additives, β-CD revealed notable efficacy in selectively targeting specific VOCs that originate from the degradation of wood. However, the addition of 2 wt.% ModHNT offered the most useful performance advantages. The results showed the lowest odor ratings, total amount of VOC peaks and also improved thermal resistance, and tensile strength. Additionally, ModHNT served an important role in increasing the crystallization temperature and the degree of crystallinity, thereby proving its function as both a nucleating and stabilizing agent. This chapter focused on the suitability of PA11 for high-performance, low-emission WPCs and illustrated how the synergistic application of ModHNT can effectively improve its capabilities.

In conclusion, this study clarifies the effects of advanced multifunctional additives in WPCs with bio-based, recycled, or virgin thermoplastic matrices. This integration is needed for developing WPCs that are both environmentally friendly and technically improved for indoor applications. Among all of the additives studied, Mod-HNT has consistently stood out due to its unique multifunctionality. Also, Mod-HNT was synthesized and introduced for the first time in this study and added to the literature as a novel study. It effectively adsorbs odor-causing VOCs, improves the composite structure, and their thermal characteristics. While β-CD offered specific decrease in VOCs and unmodified HNT increased mechanical performance, ModHNT distinctively merged these functionalities. The improvements discovered in both rPO and PA11 matrices point out the significance of surface-modified nanofillers for dealing with the typical problems encountered by WPCS. The impact of additive functionalization in recycled PO-based WPCs was notably worthwhile in terms of VOC adsorption although the mechanical properties and odor results did not seem as notable when compared to PA11. Furthermore, composites based on PA11 that contain 2 wt.% ModHNT suggested the most advantageous integrated final results through all categories, including odor rating, VOC content, mechanical strength, thermal degradation resistance, and crystallinity.

While this thesis study provides meaningful perspectives, further investigation will be so useful to obtain a comprehensive understanding in terms of the long-term performance, scalability of processes, and environmental impact of these advanced WPC formulations. It is important to give priority to real-time ageing tests, recyclability researches, and the optimization of compounding techniques to be able to validate that they are feasible on an industrial scale. In addition, future researches about odor management for WPCs

should consider the analyses of odor production mechanisms, the production of alternative bio-based scavengers like enzymatically modified polysaccharides or lignin derivatives, and the application of encapsulation technologies for extending additive effectiveness. Effective analytical techniques, like two-dimensional gas chromatography-mass spectrometry and predictive odor modelization through machine learning, have the potential to reveal more profound connections between chemical signatures and human sense of smell. In the end the integration of life cycle assessment (LCA) and techno-economic evaluations are going to play an important role in governing the commercial advancement of next-generation WPCs. These findings and insights that achieved from this research may encourage the production of WPCs that are odor-neutral, mechanically resilient, and thermally stable, specifically designed for environmentally friendly indoor settings.

BIBLIOGRAPHY

Abotaleb, A., Gladich, I., Mroue, K., Abounahia, N., Alkhateeb, A., Al-Shammari, A., Tong, Y., Al-Masri, D., & Sinopoli, A. (2024b). Impact of thermal Treatment on halloysite nanotubes: A Combined Experimental-Computational Approach. Heliyon, 10(21), e39952. https://doi.org/10.1016/j.heliyon.2024.e39952

Adamova´, T., Hradecky´, J., & Pa´nek, M. (2020). Volatile Organic Compounds (VOCs) from Wood and Wood-Based Panels: Methods for Evaluation, Potential Health Risks, and Mitigation. Polymers, 12(10), 2289. https://doi.org/10.3390/polym12102289

Ahn, J., Pandey, S. K., & Kim, K. (2011). Comparison of GC-MS calibration properties of volatile organic compounds and relative quantification without calibration standards. Journal of Chromatographic Science, 49(1), 19–28. https://doi.org/10.1093/chrsci/49.1.19

Aljibori, H. S., Al-Amiery, A., & Isahak, W. N. R. W. (2024). Unveiling the Potential of Halloysite Nanotubes: Insights into Their Synthesis, Properties, and Applications in Nanocomposites. Starch - Stärke. https://doi.org/10.1002/star.202400080

Almaie, S., Vatanpour, V., Rasoulifard, M. H., & Koyuncu, I. (2022). Volatile organic compounds (VOCs) removal by photocatalysts: A review. Chemosphere, 306, 135655. https://doi.org/10.1016/j.chemosphere.2022.135655

Almaie, S., Vatanpour, V., Rasoulifard, M. H., & Koyuncu, I. (2022). Volatile organic compounds (VOCs) removal by photocatalysts: A review. Chemosphere, 306, 135655. https://doi.org/10.1016/j.chemosphere.2022.135655

Almasri, D.A., Saleh, N.B., Atieh, M.A. et al. Adsorption of phosphate on iron oxide doped halloysite nanotubes. Sci Rep 9, 3232 (2019). https://doi.org/10.1038/s41598-019-39035-2

Alongi, J., Carosio, F., Frache, A., & Malucelli, G. (2012). Layer by Layer coatings assembled through dipping, vertical or horizontal spray for cotton flame retardancy. *Carbohydrate Polymers*, *92*(1), 114–119. https://doi.org/10.1016/j.carbpol.2012.08.086

Ansar, M. A., et al. (2021). Occupational Exposure to Hazards and Volatile Organic Compounds in Small-Scale Plastic Recycling Plants in Thailand. Journal of Cleaner Production, 329, 129582. https://doi.org/10.1016/j.jclepro.2021.129582

Bao, Z., Yan, Y., & Han, W. (2024). Investigation of Γ-Aminopropyltriethoxysilane

(APTES)-Modified halloysite nanotubes on the reinforcement of Halloysite/Polypropylene (PP) nanocomposites. Polymers, 16(23), 3332. https://doi.org/10.3390/polym16233332

Behravesh, A., Aghdam, A. Z., & Soury, E. (2009). Experimental investigation of injection molding of Wood/Plastics composites. Journal of Reinforced Plastics and Composites, 29(3), 456–465. https://doi.org/10.1177/0731684408099406

Beltrán, F., De La Orden, M., & Urreaga, M. (2018). Amino-modified halloysite nanotubes to reduce polymer degradation and improve the performance of mechanically recycled poly(lactic acid). Journal of Polymers and the Environment, 26(10), 4046–4055. https://doi.org/10.1007/s10924-018-1276-6

Bidsorkhi, H. C., Adelnia, H., Pour, R. H., & Soheilmoghaddam, M. (2015). Preparation and characterization of ethylene-vinyl acetate/halloysite nanotube nanocomposites. Journal of Materials Science, 50(8), 3237–3245. https://doi.org/10.1007/s10853-015-8891-6

Canevarolo, S. V. (2000). Chain scission distribution function for polypropylene degradation during multiple extrusions. Polymer Degradation and Stability, 70(1), 71–76. https://doi.org/10.1016/s0141-3910(00)00090-2

Cavallaro, G., Lazzara, G., Panchal, A., Fakhrullin, R., Stavitskaya, A., Vinokurov, V., & Lvov, Y. (2017). Halloysite Nanotubes: Controlled Access and Release by Smart Gates. Nanomaterials, 7(8), 199. https://doi.org/10.3390/nano7080199

Cheng, C., Song, W., Zhao, Q., & Zhang, H. (2020). Halloysite nanotubes in polymer science: purification, characterization, modification, and applications. Nanotechnology Reviews, 9(1), 323–344. https://doi.org/10.1515/ntrev-2020-0024

Chloroacetic acid(79-11-8) 1H NMR spectrum. (Feb 12, 2024). https://www.chemicalbook.com/SpectrumEN_79-11-8_1HNMR.htm

Crini, G. (2005). Recent developments in polysaccharide-based materials used as adsorbents in wastewater treatment. Progress in Polymer Science, 30(1), 38–70. https://doi.org/10.1016/j.progpolymsci.2004.11.002

Da Silva, A. M. (2018). Room at the Top as well as at the Bottom: Structure of Functional Food Inclusion Compounds. In InTech eBooks. https://doi.org/10.5772/intechopen.74162

Dong, M., Jiang, M., He, L., Zhang, Z., Gustave, W., Vithanage, M., Niazi, N. K., Chen, B., Zhang, X., Wang, H., & He, F. (2025). Challenges in safe environmental applications of biochar: identifying risks and unintended consequence. Biochar, 7(1). https://doi.org/10.1007/s42773-024-00412-4

Du, M., Guo, B., & Jia, D. (2006). Thermal stability and flame-retardant effects of halloysite nanotubes on polypropylene. European Polymer Journal, 42(6), 1362–1369. https://doi.org/10.1016/j.eurpolymj.2005.12.006

Duan, X., Yuan, C., Guo, Q., Niu, S., He, K., & Xia, G. (2020). Preparation of halloysite nanotubes- encapsulated magnetic microspheres for elemental mercury removal from coal-fired flue gas. Journal of Hazardous Materials, 406, 124683. https://doi.org/10.1016/j.jhazmat.2020.124683

Erdoğan, A., Kaygusuz, I., & Kaynak, C. (2014). Influences of aminosilanization of halloysite nanotubes on the mechanical properties of polyamide-6 nanocomposites. Polymer Composites, 35(8), 1350–1361. https://doi.org/10.1002/pc.22787

Erpek, C. E. Y., Ozkoc, G., & Yilmazer, U. (2015). Comparison of natural halloysite with synthetic carbon nanotubes in poly(lactic acid) based composites. Polymer Composites, 38(11), 2337–2346. https://doi.org/10.1002/pc.23816

Esmizadeh, E., Tzoganakis, C., & Mekonnen, T. H. (2020). Degradation Behavior of Polypropylene during Reprocessing and Its Biocomposites: Thermal and Oxidative Degradation Kinetics. Polymers, 12(8), 1627. https://doi.org/10.3390/polym12081627

Fahimizadeh, M., Wong, L. W., Baifa, Z., Sadjadi, S., Auckloo, S. a. B., Palaniandy, K., Pasbakhsh, P., Tan, J. B. L., Singh, R. R., & Yuan, P. (2024). Halloysite clay nanotubes: Innovative applications by smart systems. Applied Clay Science, 251, 107319. https://doi.org/10.1016/j.clay.2024.107319

Fitri, S., Fatimah, I., et al. (2021). Surface Functionalized Halloysite with N-[3-(trimethoxysilyl)propyl]ethylenediamine for Chromium and Nickel Adsorption from Aqueous Solution. Biointerface Research in Applied Chemistry, 11(6), 14794–14808. https://doi.org/10.33263/BRIAC126.72057213

Fuller, J., White, D., Yi, H., Colley, J., Vickery, Z., & Liu, S. (2020). Analysis of volatile compounds causing undesirable odors in a polypropylene-high-density polyethylene recycled plastic resin with solid-phase microextraction. Chemosphere, 260, 127589. https://doi.org/10.1016/j.chemosphere.2020.127589

Gao, X., Li, Q., Cheng, W., Han, G., & Xuan, L. (2016). Optimization of high temperature and pressurized steam modified wood fibers for High-Density Polyethylene Matrix composites using the orthogonal design method. Materials, 9(10), 847. https://doi.org/10.3390/ma9100847

Garg, A., Basu, S., Mahajan, R. L., & Mehta, R. (2024). Enhancement in mechanical properties of GFRP-coal-derived graphene oxide composites by addition of multiwalled carbon nanotubes and halloysite nanotubes: A comparative study. Polymer Composites. https://doi.org/10.1002/pc.28694

Garofalo, E., Taurino, L., Di Maio, L., Neitzert, H. C., & Incarnato, L. (2023). Assessment of Melt Compounding with Zeolites as an Effective Deodorization Strategy for Mixed Plastic Wastes and Comparison with Degassing. Polymers, 15(8), 1858. https://doi.org/10.3390/polym15081858

Ghaffari, M., Naderi, R., & Ehsani, M. (2014). Effect of silane as surface modifier and coupling agent on rheological and protective performance of epoxy/nano-glassflake coating systems. *Iranian Polymer Journal*, *23*(7), 559–567. https://doi.org/10.1007/s13726-014-0250-y

Ghosh, S., Das, T., Ganguly, S., Nath, K., Paul, S., Ganguly, D., & Das, N. (2022). Silane functionalization of sodium montmorillonite and halloysite (HNT) nanoclays by ‘grafting to’ method to improve physico-mechanical and barrier properties of LLDPE/clay nanocomposites. Polymer Bulletin, 80, 4307–4335.

https://doi.org/10.1007/s00289-022-04281-4

Guo, J., Tang, Y., & Xu, Z. (2010). Performance and thermal behavior of wood plastic composite produced by nonmetals of pulverized waste printed circuit boards. Journal of Hazardous Materials, 179(1–3), 203–207. https://doi.org/10.1016/j.jhazmat.2010.02.080

Guo, T., Zhang, R., Wang, X., Kong, L., Xu, J., Xiao, H., & Bedane, A. H. (2022). Porous structure of B-Cyclodextrin for CO2 capture: structural remodeling by thermal activation. Molecules, 27(21), 7375. https://doi.org/10.3390/molecules27217375

Huang, H., Han, B., Wang, L., Miao, N., Mo, H., Zhou, N., Ma, Z., Zhang, J., & Shen, J. (2010). Crystallization kinetics of polypropylene composites filled with nano calcium carbonate modified with maleic anhydride. Journal of Applied Polymer Science, 119(3), 1516–1527. https://doi.org/10.1002/app.32842

Inuwa, I. M., Hassan, A., El-Shekeil, Y. A., Jawaid, M. (2018). Enhancing performance of Recycled Polyolefin composites by incorporating halloysite nanotubes. Polymer Composites, 39(S3), E1472–E1480. https://doi.org/10.1002/pc.24470

Jabbari, S. G., Domínguez, J. F., Sufuentes, S. R., Nyberg, S. O., Vehus, T. S., & Nielsen, H. K. (2025). VOC emissions from commercial wood panels using PTR-MS for indoor air quality evaluation. Frontiers in Built Environment, 11. https://doi.org/10.3389/fbuil.2025.1591669

Jana, S., Das, S., Ghosh, C., Maity, A., & Pradhan, M. (2015). Halloysite Nanotubes capturing isotope selective atmospheric CO2. Scientific Reports, 5(1). https://doi.org/10.1038/srep08711

Jeziórska, R., Szadkowska, A., Studziński, M., & Żubrowska, M. (2021). The use of modified silica to control the morphology of polyamide 11 and poly(phenylene oxide) blends. Polimery, 66(7–8). https://doi.org/10.14314/polimery.2021.7.3

Jin, X., Zhang, R., Su, M., Li, H., Yue, X., Qin, D., & Jiang, Z. (2019). Functionalization of halloysite nanotubes by enlargement and layer-by-layer assembly for controlled release of the fungicide iodopropynyl butylcarbamate. RSC Advances, 9(72), 42062–42070. https://doi.org/10.1039/c9ra07593c

Joseph, P. V., Joseph, K., & Thomas, S. (1999). Effect of processing variables on the mechanical properties of sisal-fiber-reinforced polypropylene composites. Composites Science and Technology, 59(11), 1625–1640. https://doi.org/10.1023/A:1014704223702

Kadam, V., Truong, Y. B., Schutz, J., Kyratzis, I. L., Padhye, R., & Wang, L. (2020). Gelatin/β–Cyclodextrin Bio–Nanofibers as respiratory filter media for filtration of aerosols and volatile organic compounds at low air resistance. Journal of Hazardous Materials, 403, 123841. https://doi.org/10.1016/j.jhazmat.2020.123841

Kamble R, Ghag M, Gaikawad S, Panda BK, Halloysite Nanotubes and Applications: A Review. J Adv Sci Res., 2012; 3(2): 25-29.

Kang, P., Wu, P., Jin, Y., Shi, S., Gao, D., Chen, G., & Li, Q. (2020). Formation and

Emissions of Volatile Organic Compounds from Homo-PP and Co-PP Resins during Manufacturing Process and Accelerated Photoaging Degradation. Molecules, 25(12), 2761. https://doi.org/10.3390/molecules25122761

Kapoor, M. P., Moriwaki, M., Minoura, K., Timm, D., Abe, A., & Kito, K. (2022). Structural Investigation of Hesperetin-7-O-Glucoside Inclusion Complex with β-Cyclodextrin: A Spectroscopic Assessment. Molecules, 27(17), 5395. https://doi.org/10.3390/molecules27175395

Khan, A. M., Achaby, M. E., Hassan, A., & Qaiss, A. (2025). Effect of halloysite nanotubes on thermal and mechanical properties of RPET/PA11/Joncryl® blends. Polymers, 17(11), 1433. https://doi.org/10.3390/polym17111433

Kim, J. H., Lee, J. S., Lee, D. S. (2019). Inclusion complexation of VOCs by β-cyclodextrin. Industrial & Engineering Chemistry Research, 58(1), 135–142. https://doi.org/10.1021/acs.iecr.8b04715

Kotova, O., Sun, S., Kotova, E., Ponariaydov, A., & Brodskaya, R. (2022). Aluminosilicates: interphase boundary interactions and nature engineering of nanostructures. Journal of Physics Conference Series, 2315(1), 012003. https://doi.org/10.1088/1742-6596/2315/1/012003

Krishnaiah, P., Manickam, S., Ratnam, C. T., Raghu, Parashuram, L., Kumar, S. P., & Jeon, B. (2020). Mechanical, thermal, and dynamic-mechanical studies of functionalized halloysite nanotubes reinforced polypropylene composites. Polymers and Polymer Composites, 29(8), 1212–1221. https://doi.org/10.1177/0967391120965115

Kurtulmus, G., & Menceloglu, Y. Z. (2025). Enhancing odor reduction and properties in polypropylene-based wood plastic composites with halloysite nanotubes and beta-cyclodextrin. Journal of Applied Polymer Science. Advance online publication. https://doi.org/10.1002/app.57661

Kurtulmus, G., Bilge, K., & Menceloglu, Y. Z. (2025). Reduction of volatile organic compounds with hydrazine, carboxybetaine and aminosilane functionalized halloysite nanotube in recycled polyolefin blends. Journal of Applied Polymer Science, submitted for publication.

Lee, K., & Chang, Y. (2012). Thermal, mechanical, and rheological properties of poly(ε-caprolactone)/halloysite nanotube nanocomposites. Journal of Applied Polymer Science, 128(5), 2807–2816. https://doi.org/10.1002/app.38457

Li, H., Ma, Q., Wu, J., et al. (2020). Removal of formaldehyde by β-cyclodextrin based electrospun nanofibers. Environmental Science: Nano, 7, 341–349. https://doi.org/10.1039/C9EN00900J

Li, X., Tan, D., Xie, L., Sun, H., Sun, S., Zhong, G., & Ren, P. (2018b). Effect of surface property of halloysite on the crystallization behavior of PBAT. Applied Clay Science, 157, 218–226. https://doi.org/10.1016/j.clay.2018.02.005

Li, Y., & Shimizu, H. (2009). Improvement in toughness of polypropylene by melt compounding with nanoscale silica particles. Polymer, 50, 4669–4679. https://doi.org/10.1016/j.polymer.2009.07.024

Li, Y., Chen, H., Wang, Y. (2020). Efficient removal of VOCs using mesoporous nanomaterials. Journal of Hazardous Materials, 381, 120998.

https://doi.org/10.1016/j.jhazmat.2019.120998

Liu, M., Guo, B., Du, M., Chen, F., & Jia, D. (2009). Halloysite nanotubes as a novel β-nucleating agent for isotactic polypropylene. Polymer, 50(13), 3022–3030. https://doi.org/10.1016/j.polymer.2009.04.052

Liu, M., Jia, Z., Jia, D., & Zhou, C. (2014). Recent advance in research on halloysite nanotubes-polymer nanocomposite. Progress in Polymer Science, 39(8), 1498–1525. https://doi.org/10.1016/j.progpolymsci.2014.04.004

Loftsson, T. & Duchêne, D. (2007). Cyclodextrins and their pharmaceutical applications. International Journal of Pharmaceutics, 329(1–2), 1–11. https://doi.org/10.1016/j.ijpharm.2006.10.044

Lomonaco, T., Manco, E., Corti, A., La Nasa, J., Ghimenti, S., Biagini, D., Di Francesco, F., Modugno, F., Ceccarini, A., Fuoco, R., & Castelvetro, V. (2020). Release of harmful volatile organic compounds (VOCs) from photo-degraded plastic debris: A neglected source of environmental pollution. Journal of Hazardous Materials, 394, 122596. https://doi.org/10.1016/j.jhazmat.2020.122596

Lvov, Y.M. & Abdullayev, E. (2013). Functional polymer–clay nanotube composites with sustained release of chemical agents. Progress in Polymer Science, 38(10–11), 1690–1719. https://doi.org/10.1016/j.progpolymsci.2013.05.009

Massaro, M., Cavallaro, G., Colletti, C. G., Lazzara, G., Milioto, S., Noto, R., & Riela, S. (2018). Chemical modification of halloysite nanotubes for controlled loading and release. Journal of Materials Chemistry B, 6(21), 3415–3433. https://doi.org/10.1039/c8tb00543e

Massaro, M., Lazzara, G., Milioto, S., Noto, R., & Riela, S. (2017). Covalently modified halloysite clay nanotubes: synthesis, properties, biological and medical applications. Journal of Materials Chemistry B, 5(16), 2867–2882. https://doi.org/10.1039/c7tb00316a

Mitaľová, Z., Mitaľ, D., & Berladir, K. (2024). A concise review of the components and properties of Wood–Plastic composites. Polymers, 16(11), 1556. https://doi.org/10.3390/polym16111556

Mohanty, A. K., Vivekanandhan, S., Pin, J., & Misra, M. (2018). Composites from renewable and sustainable resources: Challenges and innovations. Science, 362(6414), 536–542. https://doi.org/10.1126/science.aat9072

Mohanty, A.K., Misra, M. & Drzal, L.T. Sustainable Bio-Composites from Renewable Resources: Opportunities and Challenges in the Green Materials World. Journal of Polymers and the Environment 10, 19–26 (2002). https://doi.org/10.1023/A:1021013921916

Musuc, A. M. (2024). Cyclodextrins: Advances in chemistry, toxicology, and multifaceted applications. Molecules, 29(22), 5319. https://doi.org/10.3390/molecules29225319

N-[3-(Trimethoxysilyl)propyl]ethylenediamine(1760-24-3) 1H NMR spectrum. (Feb 12, 2024). https://www.chemicalbook.com/SpectrumEN_1760-24-3_1HNMR.htm

Packaging waste. (2023, February 22) Environment.

https://environment.ec.europa.eu/topics/waste-and-recycling/packaging-waste_en.

Patiño-Almanza, R., García-Méndez, R. F., Rivera-Armenta, J. L., Strachota, A., & Almendarez-Camarillo, A. (2024). 3D printing polypropylene composites reinforced with functionalized halloysite: Balance between stiffness and impact resistance. Polymer Composites, 45(7), 6439–6452. https://doi.org/10.1002/pc.28208

Paul, D. R., & Robeson, L. M. (2008). Polymer nanotechnology: Nanocomposites. Polymer, 49(15), 3187–3204. https://doi.org/10.1016/j.polymer.2008.04.017

Poland, C. A., Duffin, R., Kinloch, I., Maynard, A., Wallace, W. a. H., Seaton, A., Stone, V., Brown, S., MacNee, W., & Donaldson, K. (2008). Carbon nanotubes introduced into the abdominal cavity of mice show asbestos-like pathogenicity in a pilot study. Nature Nanotechnology, 3(7), 423–428. https://doi.org/10.1038/nnano.2008.111

Prado, K. S., Strangl, M., Pereira, S. R., Tiboni, A. R., Ortner, E., Spinace´, M. A., & Buettner, A. (2020). Odor characterization of post-consumer and recycled automotive polypropylene by different sensory evaluation methods and instrumental analysis. Waste Management, 115, 36–46. https://doi.org/10.1016/j.wasman.2020.07.021

Ramadass, K., Sathish, C. I., MariaRuban, S., Kothandam, G., Joseph, S., Singh, G., Kim, S., Cha, W., Karakoti, A., Belperio, T., Yi, J. B., & Vinu, A. (2020). Carbon Nanoflakes and Nanotubes from Halloysite Nanoclays and their Superior Performance in CO2 Capture and Energy Storage. ACS Applied Materials & Interfaces, 12(10), 11922–11933. https://doi.org/10.1021/acsami.9b21510

Ramesh, M., Rajeshkumar, L., Sasikala, G., Balaji, D., Saravanakumar, A., Bhuvaneswari, V., & Bhoopathi, R. (2022). A Critical Review on Wood-Based Polymer Composites: Processing, Properties, and Prospects. Polymers, 14(3), 589. https://doi.org/10.3390/polym14030589

Saenger, W. (1980). Cyclodextrin inclusion compounds in research and industry. Angewandte Chemie International Edition, 19(5), 344–362. https://doi.org/10.1002/anie.198003441

Sallem-Idrissi, N., Corn, S., Bistac, S. (2016). Investigation of Volatile Organic Compounds (VOCs) emitted from recycled and virgin polypropylene: Comparison and removal strategies. Polymer Degradation and Stability, 134, 76–84. https://doi.org/10.1016/j.polymdegradstab.2016.07.017

Sallem-Idrissi, N., Vanderghem, C., Pacary, T., Richel, A., Debecker, D. P., Devaux, J., & Sclavons, M. (2016). Lignin degradation and stability: Volatile Organic Compounds (VOCs) analysis throughout processing. Polymer Degradation and Stability, 130, 30–37. https://doi.org/10.1016/j.polymdegradstab.2016.05.028

Schwarzkopf, M., & Burnard, M. D. (2016). Volatile organic compound (VOC) emissions from wood-based materials and their impact on indoor air quality. Forest Products Journal, 66(5–6), 123–132. https://doi.org/10.13073/FPJ-D-15-00069

Senyel, M., & Dike, A. (2024). Contribution of silane modification of halloysite

nanotube to its poly(butylene terephthalate)-based nanocomposites: Structural, mechanical, and thermal properties. Polymer Bulletin. https://doi.org/10.1007/s00289-024-05173-5

Shelesh-Nezhad, K., Orang, H., & Motallebi, M. (2012). The Effects of Adding Nano-Calcium Carbonate Particles on the Mechanical and Shrinkage Characteristics and Molding Process Consistency of PP/nano-CaCO3 Nanocomposites. https://doi.org/10.5772/35272.

Sikora, J. W., Gajdoš, I., & Puszka, A. (2019). Polyethylene-matrix composites with halloysite nanotubes with enhanced physical/thermal properties. Polymers, 11(5), 787. https://doi.org/10.3390/polym11050787

Singh, A., Krishna, V., Angerhofer, A., Do, B., MacDonald, G., & Moudgil, B. (2010). Copper coated silica nanoparticles for odor removal. Langmuir, 26(20), 15837– 15844. https://doi.org/10.1021/la100793u

Stark, N. M., & Rowlands, R. E. (2003). Effects of wood fiber characteristics on mechanical properties of wood/polypropylene composites. Wood and Fiber Science, 35(2), 167–174.

Su, R., Liu, G., Sun, H., & Yong, Z. (2021). A new method to measure the three-dimensional solubility parameters of acrylate rubber and predict its oil resistance. Polymer Bulletin, 79(2), 971–984. https://doi.org/10.1007/s00289-020-03516-6

Szpilska, K., Czaja, K., & Kudła, S. (2015). Thermal stability and flammability of polyolefin/halloysite nanotubes composites. Polimery, 60(10), 673–679. https://doi.org/10.14314/polimery.2015.673

Teaca, C., Tanasa, F., and Zanoaga, M. (2018). "Multi-component polymer systems comprising wood as bio-based component and thermoplastic polymer matrices – An overview," BioRes. 13(2). 4728-4769.

Tekay, E. (2020). Halloysit Nanotüp Takviyeli Kopoliester Termoplastik Elastomer Kompozitler: Isıl ve Mekanik Ozelliklerin Incelenmesi. El-Cezeri Fen ve Mühendislik Dergisi. https://doi.org/10.31202/ecjse.764528

Theodoropoulou, A., Gkika, D. A., Alodhayb, A., & Kyzas, G. Z. (2023). A critical evaluation of the safety datasheets of graphene materials. Journal of Nanoparticle Research, 25(5). https://doi.org/10.1007/s11051-023-05753-y

Thommes, M., Kaneko, K., Neimark, A. V., Olivier, J. P., Rodriguez-Reinoso, F., Rouquerol, J., & Sing, K. S. (2015). Physisorption of gases, with special reference to the evaluation of surface area and pore size distribution (IUPAC Technical Report). Pure and Applied Chemistry, 87(9–10), 1051–1069. https://doi.org/10.1515/pac-2014-1117

Trojanová, K., Veľková, V., & Kačík, F. (2025). Volatile Organic Compounds Arising from Wood Polymers on Thermal Loading of Spruce Wood. Polymers, 17(7), 875. https://doi.org/10.3390/polym17070875

U.S. National Recycling Goal | US EPA. (2023, April 14). US EPA. https://www.epa.gov/circulareconomy/us-national-recycling-goal

Uner, G., Karakus, G., & Can, H. (2022). Design, fabrication and characterization of silane tailored surface of halloysite based polymer nanocomposites. Polymer

Composites. https://doi.org/10.1002/pc.27172

Urooj, T., Mishra, M., & Pandey, S. (2024). Unlocking environmental solutions: a review of cyclodextrins in pollutant removal. Discover Environment, 2(1). https://doi.org/10.1007/s44274-024-00090-w

Väisänen, T., Laitinen, K., Tomppo, L., Joutsensaari, J., Raatikainen, O., Lappalainen, R., & Yli-Pirilä, P. (2016). A rapid technique for monitoring volatile organic compound emissions from wood–plastic composites. Indoor and Built Environment, 27(2), 194–204. https://doi.org/10.1177/1420326x16669976

Wadi, V. S., Jena, K. K., Halique, K., & Alhassan, S. M. (2020). Enhanced mechanical toughness of isotactic polypropylene using bulk molybdenum disulfide. ACS Omega, 5(20), 11394–11401. https://doi.org/10.1021/acsomega.0c00419

Wang, B., & Huang, H. (2013). Effects of halloysite nanotube orientation on crystallization and thermal stability of polypropylene nanocomposites. Polymer Degradation and Stability, 98(9), 1601–1608. https://doi.org/10.1016/j.polymdegradstab.2013.06.022

Wang, H., Wang, G., Hu, L., Ge, B., Yu, X., & Deng, J. (2023). Porous polymer materials for CO2 capture and electrocatalytic reduction. Materials, 16(4), 1630. https://doi.org/10.3390/ma16041630

Wang, S., & Zhang, A. (2007). Chemical characterization of smoke from the production process of wood-plastic composites. Forestry Studies in China, 9(1), 57–62. https://doi.org/10.1007/s11632-007-0010-6

Wieczorek, M., Tatarchuk, T., Skórczewska, K., Szulc, J., & Tomaszewska, J. (2024). The effect of silanized halloysite nanotubes on the structure of polyethylene–based composite. Materials, 17(13), 3260. https://doi.org/10.3390/ma17133260

Wolcott M.P., Adcock T., 2000. New advances in wood fiber-polymer formulations. In: Proc wood–plastic conference plastics technology magazine and polymer process, Communications, 107–14.

Wolfsgruber, N., Tanda, A., Archodoulaki, V., & Burgstaller, C. (2023). Influence of filler type and content on thermal conductivity and mechanical properties of thermoplastic compounds. Polymer Engineering and Science, 63(4), 1094–1105. https://doi.org/10.1002/pen.26266

Wong, L. W., Goh, C. B. S., Pasbakhsh, P., & Tan, J. B. L. (2022). Natural hollow clay nanotubes and their applications as polymer nanocomposites in tissue engineering. Journal of Science Advanced Materials and Devices, 7(2), 100431. https://doi.org/10.1016/j.jsamd.2022.100431

Wunderlich, B. (1990). Athas table of thermal properties of linear macromolecules. Thermal Analysis, London, UK: Academic Press Limited, 417-431. https://doi.org/10.1016/b978-0-12-765605-2.50012-1

Yang, F., Pan, L., Du, H., Ma, Z., & Li, Y. (2020). Effect of olefin-based compatibilizers on the formation of cocontinuous structure in immiscible HDPE/IPP blends. Chinese Journal of Polymer Science, 38(11), 1248–1257.

https://doi.org/10.1007/s10118-020-2433-7

Yang, Y., Chen, Y., Leng, F., Huang, L., Wang, Z., & Tian, W. (2017). Recent advances on surface modification of halloysite nanotubes for multifunctional applications. Applied Sciences, 7(12), 1215. https://doi.org/10.3390/app7121215

Yin, X., Wang, L., Li, S., He, G., & Yang, Z. (2017). Effects of surface modification of halloysite nanotubes on the morphology and the thermal and rheological properties of polypropylene/halloysite composites. Journal of Polymer Engineering, 38(2), 119–127. https://doi.org/10.1515/polyeng-2017-0025

You, J., Teng, Y., Zhang, B., & Fang, Z. (2021). Electrospun nanofiber membranes of β-cyclodextrin for VOC removal: Adsorption performance and mechanisms. Separation and Purification Technology, 259, 118145. https://doi.org/10.1016/j.seppur.2020.118145

Yu, L., Dean, K., Li, L. (2006). Polymer blends and composites from renewable resources.Progress in Polymer Science, 31(6), 576–602. https://doi.org/10.1016/j.progpolymsci.2006.03.002

Yuan, P., Tan, D., & Annabi-Bergaya, F. (2015). Properties and applications of halloysite nanotubes: recent research advances and future prospects. Applied Clay Science, 112–113, 75–93. https://doi.org/10.1016/j.clay.2015.05.001

Zeng, S., Zeng, Y., Guo, P., Hu, C., & Wang, Z. (2023). Characterization of odors and volatile organic compounds changes to recycled high-density polyethylene through mechanical recycling. Polymer Degradation and Stability, 208, 110263. https://doi.org/10.1016/j.polymdegradstab.2023.110263

Zhang, Q., Chen, B., Yan, T., Li, L., Jin, J., Fang, S., et al. (2024). Efficient VOC Suppression in Polypropylene Composites Using APTES-Modified Halloysite Nanotubes. Polymers, 16(23), 3332. https://doi.org/10.3390/polym16233332

Zhang, X., Gao, B., Creamer, A. E., Cao, C., & Li, Y. (2017). Adsorption of VOCs onto engineered carbon materials: A review. Journal of Hazardous Materials, 338, 102–123. https://doi.org/10.1016/j.jhazmat.2017.05.013

Zhao, W., Shi, B., & Hu, C. (2007). Adsorption Properties of β-Cyclodextrin for Adsorbing Aromatic Hydrocarbons from the Gas Phase and Water. Journal of Macromolecular Science Part B, 47(1), 211–216. https://doi.org/10.1080/00222340701748792

Zou, W., Gao, B., Ok, Y. S., & Dong, L. (2018). Integrated adsorption and photocatalytic degradation of volatile organic compounds (VOCs) using carbon-based nanocomposites: A critical review. Chemosphere, 218, 845–859. https://doi.org/10.1016/j.chemosphere.2018.11.175